Disentangling the complex gene interaction networks between rice and the blast fungus identifies a new pathogen effector

Yu Sugihara[1,2,3], Yoshiko Abe[1], Hiroki Takagi[1,#a], Akira Abe[1], Motoki Shimizu[1], Kazue Ito[1], Eiko Kanzaki[1], Kaori Oikawa[1], Jiorgos Kourelis[3], Thorsten Langner[3], Joe Win[3], Aleksandra Białas[3], Daniel Lüdke[3], Mauricio P. Contreras[3], Izumi Chuma[4], Hiromasa Saitoh[1,#b], Michie Kobayashi[1,#c], Shuan Zheng[1,2], Yukio Tosa[5], Mark J. Banfield[6], Sophien Kamoun[3]*, Ryohei Terauchi[1,2]*, Koki Fujisaki[1]*

[1] Iwate Biotechnology Research Center, Kitakami, Iwate, 024-0003, Japan
[2] Crop Evolution Laboratory, Kyoto University, Mozume, Muko, Kyoto, 617-0001, Japan
[3] The Sainsbury Laboratory, University of East Anglia, Norwich, NR4 7UH, United Kingdom
[4] Obihiro University of Agriculture and Veterinary Medicine, Obihiro, 080-8555, Japan
[5] Graduate School of Agricultural Science, Kobe University, Kobe, 657-8501, Japan
[6] Department of Biochemistry and Metabolism, John Innes Centre, Norwich Research Park, Norwich, NR4 7UH, United Kingdom
[#a] Current Address: Faculty of Bioresources and Environmental Sciences, Ishikawa Prefectural University, Nonoichi 921-8836, Japan
[#b] Current Address: Department of Molecular Microbiology, Tokyo University of Agriculture, Setagaya-ku, Tokyo 156-8502, Japan
[#c] Current Address: Institute of Agrobiological Sciences, National Agriculture and Food Research Organization (NARO), Kannondai 2-1-2, Tsukuba, Ibaraki 305-8602, Japan

*Corresponding authors
E-mail: sophien.kamoun@tsl.ac.uk (SK); terauchi@ibrc.or.jp (RT); k-fujisaki@ibrc.or.jp (KF)

Abstract

Studies focused solely on single organisms can fail to identify the networks underlying host–pathogen gene-for-gene interactions. Here, we integrate genetic analyses of rice (*Oryza sativa*, host) and rice blast fungus (*Magnaporthe oryzae*, pathogen) and uncover a new pathogen recognition specificity of the rice nucleotide-binding domain and leucine-rich repeat protein (NLR) immune receptor Pik, which mediates resistance to *M. oryzae* expressing the avirulence effector gene *AVR-Pik*. Rice Piks-1, encoded by an allele of *Pik-1*, recognizes a previously unidentified effector encoded by the *M. oryzae* avirulence gene *AVR-Mgk1*, which is found on a mini-chromosome. *AVR-Mgk1* has no sequence similarity to known *AVR-Pik* effectors, and is prone to deletion from the mini-chromosome mediated by repeated *Inago2* retrotransposon sequences. AVR-Mgk1 is detected by Piks-1 and by other Pik-1 alleles known to recognize AVR-Pik effectors; recognition is mediated by AVR-Mgk1 binding to the integrated heavy metal-associated (HMA) domain of Piks-1 and other Pik-1 alleles. Our findings highlight how complex gene-for-gene interaction networks can be

disentangled by applying forward genetics approaches simultaneously to the host and pathogen. We demonstrate dynamic co-evolution between an NLR integrated domain and multiple families of effector proteins.

Introduction

Immune recognition between plant hosts and pathogens is often mediated by gene-for-gene interactions [1]. In this classical genetic model, a match between a single plant disease resistance (*R*) gene and a single pathogen avirulence effector (*AVR*) gene leads to pathogen recognition and induces plant immunity [1]. This model is the foundation for understanding *R–AVR* interactions, leading to molecular cloning of numerous *R* and *AVR* genes. However, recent studies revealed there can be a higher level of complexity that expanded the gene-for-gene model [2–5]. In a given plant–pathogen combination, immune recognition frequently involves multiple tangled *R–AVR* interactions. In this case, knockout or knock-in of single host or pathogen genes does not alter the phenotype, hampering attempts to identify genes involved in the interaction. To overcome this problem, we need host and pathogen lines that allow dissection of a single of *R–AVR* interactions. Lines containing only a single *R* or *AVR* locus can be selected from recombinant lines derived from a cross between genetically distant parents. Such materials have been used to analyse the host or pathogen, but have not been simultaneously applied to both the host and pathogen. In this study, we employed integrated genetics approaches on the host and pathogen to unravel complex interactions between rice (*Oryza sativa*) and the rice blast fungus *Magnaporthe oryzae* (syn. *Pyricularia oryzae*).

Studies on the *M. oryzae*–host pathosystem benefited from examining gene-for-gene interactions. The filamentous ascomycete fungus *M. oryzae* causes blast disease in cereal crops, such as rice, wheat (*Triticum aestivum*), and foxtail millet (*Setaria italica*) [6–8]. *M. oryzae* consists of genetic subgroups that have infection specificities for particular host genera [7]. This host specificity is often determined by a repertoire of lineage-specific genes [9–12]. The gain and loss of these lineage-specific genes sometimes results in host jump and specialization [11,12]. Therefore, identifying host *R* genes with corresponding pathogen *AVR* genes is crucial to understanding host specificities.

Pathogen effectors modulate host cell physiology to promote susceptibility [13]. In *M. oryzae*, at least 15 effector genes have been identified as *AVR* genes [12,14–26]. The protein structures of AVR-Pik, AVR-Pia, AVR1-CO39, AvrPiz-t, AvrPib, and AVR-Pii have been experimentally determined [27–31]. All of their protein structures, except for the zinc-finger fold of AVR-Pii [31], share a similar six-stranded β-sandwich structure called the MAX (*Magnaporthe* Avrs and ToxB-like) fold [28,32]. This sequence-unrelated MAX effector superfamily has expanded in *M. oryzae* and *M. grisea*, probably through diversifying selection and adaptation to the host environment [28,33,34]. Recent advances in protein structure prediction enabled secretome-wide structure prediction to annotate MAX effectors and other effector families in *M. oryzae*

[34,35]. Nonetheless, most MAX effectors remain functionally uncharacterized, including their ability to activate plant immunity.

Similar to other plant pathogenic fungi [36–41], some *M. oryzae* strains contain supernumerary chromosomes called mini-chromosomes (syn. B-, accessory-, or conditionally dispensable chromosomes) in addition to the essential core chromosomes [42–44]. *M. oryzae* mini-chromosomes are smaller than core chromosomes, are rich in transposable elements, and have a lower gene density [45,46]. *M. oryzae* mini-chromosomes can be hypervariable with frequent inter-chromosomal translocations between core chromosomes and mini-chromosomes [46,47]. Since mini-chromosomes often carry virulence-related genes, such as *AVR-Pita* [16,47], *AVR-Pik* [18,46,48,49], a polyketide synthase *Avirulence Conferring Enzyme 1* (*ACE1*) [46,50], *PWL2* [15,45], *Biotrophy-associated secreted1* (*BAS1*) [45,51], and *AvrPib* [23,45], they are thought to contribute to host adaptation, although the precise mechanisms remain unclear [45–49,52].

To detect invading pathogens, plants evolved disease-resistance genes [53]. Nucleotide-binding domain and leucine-rich repeat protein (NLR) receptors constitute the predominant class of plant intracellular *R* genes [53–55]. The typical domain architecture of plant NLRs is characterized by the central NB-ARC (nucleotide-binding adaptor shared by Apaf-1, certain *R* genes and CED-4) domain and the C-terminal leucine-rich repeat (LRR) domain [56]. The N-terminus contains a TIR (Toll/interleukin 1 receptor), CC (Rx-type coiled-coil), or CC_R (RPW8-type CC) domain [57–59]. NLR genes are often clustered [60], and may consist of a genetically linked pair of NLRs in head-to-head orientation [61–65]. In the prevailing model, NLR pairs consist of functionally specialized sensor and helper NLRs [2,54,65]. Sensor NLRs directly or indirectly recognize pathogen effectors, while helper NLRs are required by sensor NLRs to activate defence signalling. Some sensor NLRs contain non-canonical integrated domains that act as baits for pathogen effectors [66,67].

In rice, three CC-type NLR pairs, *Pik* (Pik-1/Pik-2), *Pia* (Pia-2/Pia-1, also known as RGA5/RGA4), and *Pii* (Pii-2/Pii-1), have been characterized [61,64,68]. These NLR pairs are genetically linked in head-to-head orientation, and their sensor NLRs (Pik-1, Pia-2, and Pii-2, respectively) have non-canonical integrated domains that mediate pathogen detection. Pik-1 and Pia-2 have a heavy metal-associated (HMA, also known as RATX) domain as the integrated domain [29,64,69]. For Pik-1, the integrated HMA domain, located between the CC and NB-ARC domains, directly binds the *M. oryzae* effectors AVR-PikD, E, and A, and this binding is required to trigger the immune response [29,70–73]. By contrast, the Pia-2 integrated HMA domain C-terminal to the LRR [64] directly binds the two *M. oryzae* effectors AVR-Pia and AVR1-CO39, which have unrelated sequences [69,74,75]. AVR-Pik and AVR-Pik like (APikL) proteins bind members of the host HMA domain family, called small HMA (sHMA) proteins, which may act as susceptibility factors during pathogen infection [33,76–78]. Therefore, the HMA domains of Pik-1 and Pia-2 are considered to act as baits to trap pathogen effectors [66,67]. Lastly, Pii-2 has an integrated nitrate (NO_3)-induced (NOI) domain after the LRR domain [79]. Pii-2 indirectly recognizes the *M. oryzae* effector AVR-Pii via a complex between rice EXO70 (a subunit of the exocyst complex) and the NOI domain of Pii-2 [31,79,80]. The

integrated domains of these rice sensor NLRs have been used for protein engineering to confer broad-spectrum resistance [81–89].

Since cloning of the NLR pair *Pikm* [61], at least five additional *Pik* alleles (*Pikp*, *Pik**, *Pikh*, *Pike*, and *Piks*) have been identified at the *Pik* locus [61,90–95]. This allelic diversification is likely driven by an arms race co-evolution with *M. oryzae AVR-Pik* effectors, where a few Pik amino acid polymorphisms often define their recognition specificity [70–73,96]. The *Pik* alleles, except for *Piks*, were genetically defined as producing resistance against specific isolates of the blast fungus [61,91–95]. However, no report is available for *Piks*-conferred resistance and its target *AVR* gene [96].

In this study, we aimed to uncover additional functions of the well-studied rice Pik immune receptors by integrating host and pathogen genetic analyses (**Fig 1**). This revealed a previously overlooked interaction between a Pik receptor and a *M. oryzae* effector. We found that Piks-1 detects the *M. oryzae* effector AVR-Mgk1, which is unrelated to the AVR-Pik family in sequence and is encoded on a *M. oryzae* mini-chromosome. The integrated HMA domain of Piks-1 binds AVR-Mgk1 but not AVR-PikD, whereas the HMA domains of other Pik-1 alleles bind AVR-PikD and AVR-Mgk1. This study illustrates the potential of integrated host and pathogen genetic analyses to unravel complex gene-for-gene interactions.

Fig 1. Integrated host and pathogen genetic analyses reveal a previously overlooked gene-for-gene interaction. (A) Rice recombinant inbred lines (RILs) generated to genetically dissect rice resistance to different *M. oryzae* isolates. We generated RILs through self-pollination after the F_1 generation to reduce heterozygosity. (B) Rice genetics identifies a locus contributing to rice resistance (*R*) to a *M. oryzae* isolate. (C) *Magnaporthe* genetics identifies a locus contributing to avirulence (*AVR*) of a *M. oryzae* isolate to a rice cultivar. (D) Mechanistic studies confirm the gene-for-gene interaction between the identified *R* and *AVR* genes.

Results

Piks contributes to resistance against *M. oryzae* isolate O23

The *japonica*-type rice cultivar Hitomebore is resistant to the *M. oryzae* isolates TH3o and O23, which originate from Thailand and Indonesia, respectively (**Fig 2A**). In contrast, the *japonica*-type rice cultivar Moukoto is susceptible to these isolates (**Fig 2A**). To determine the loci contributing to the resistance of Hitomebore against TH3o and O23, we produced rice recombinant inbred lines (RILs) derived from a cross between Hitomebore and Moukoto, resulting in 249 RILs that were subsequently subjected to whole-genome sequencing (**S1 Table**). We used 156,503 single nucleotide polymorphism (SNP) markers, designed from the parental genomes, for genetic association analysis on 226 RILs (**S2 Table**). This analysis identified a

locus strongly associated with resistance to TH3o on chromosome 1 (**Fig 2B**), and loci associated with resistance to O23 on chromosomes 1 and 11 (**Fig 2C**). The chromosome 1 locus, associated with resistance to both TH3o and O23, contained the NLR gene *Pish*, which confers moderate resistance to *M. oryzae* [97]. In contrast, the locus on chromosome 11 was associated with resistance to O23 only (**Fig 2C**), and contained the NLR gene *Piks*, an allele of *Pik*. A subset of the RILs, including RIL #58, contained the Moukoto-type *Pish* allele and the Hitomebore-type *Piks* allele and was susceptible to TH3o but resistant to O23 (**Fig 2A**), suggesting a role of *Piks* in resistance against O23.

Fig 2. Rice recombinant inbred lines (RILs) untangle the genetics of rice cultivar Hitomebore for resistance to *M. oryzae* isolates TH3o and O23. (A) Punch inoculation assays using *M. oryzae* isolates TH3o and O23 on rice cultivars Hitomebore and Moukoto. Hitomebore is resistant (*R*) to TH3o and O23, while Moukoto is susceptible (*S*) to these isolates. RIL #58, one of the RILs produced from the cross between Hitomebore and Moukoto, is susceptible to TH3o but resistant to O23. (B) Genetic association analysis of rice RIL susceptibility to TH3o identified a locus containing the rice NLR resistance gene *Pish*. (C) Genetic association analysis of rice RIL susceptibility to O23 identified loci containing the rice NLR resistance genes *Pish* and *Piks*. We used 156,503 single nucleotide polymorphism (SNP) markers, designed from the parental genomes, for genetic association analysis on 226 RILs. The vertical axis indicates $-\log_{10}(p)$, where the *p*-value is how likely the marker shows association with a trait due to random chance. The dashed line shows the *p*-value corresponding to a false discovery rate of 0.05. (D) Punch inoculation assays of RNAi-mediated knockdown lines of *Piks-1* and *Piks-2* with the isolates TH3o and O23. We used RIL #58 (*Pish* -, *Piks* +) as the genetic background for the RNAi lines. For each *Pik* gene, we prepared two independent RNAi constructs targeting different regions on the gene (Piks-1A and Piks-1B for *Piks-1*, and Piks-2A and Piks-2B for *Piks-2*, **S1 Fig**). We performed punch inoculation assays using isolates TH3o and O23 with two RNAi lines per construct, along with RIL #58 as a control. The lesion size was quantified. Asterisks indicate statistically significant differences between TH3o and O23 (two-sided Welch's t-test). The data underlying **Fig 2B**–**D** can be found in **S1 Data**.

All known *Pik* alleles function as paired NLR genes, consisting of *Pik-1* (sensor NLR) and *Pik-2* (helper NLR), which cooperate to trigger an immune response [61,98]. Therefore, we performed RNA interference (RNAi)-mediated knockdown of *Piks-1* and *Piks-2* in the RIL #58 (*Pish* -, *Piks* +) background to test their roles in resistance to O23. For both *Piks-1* and *Piks-2*, we targeted two different regions of the open reading frame (**S1 Fig**) and isolated two independent lines per RNAi construct. We used reverse transcription quantitative PCR (RT-qPCR) to analyse *Piks-1* and *Piks-2* expression in these lines (**S2 Fig**). Subsequently, we inoculated the RNAi lines and RIL #58 as a control with the TH3o and O23 isolates (**Fig 2D**). The *Piks-1* and *Piks-2* knockdown lines were susceptible to O23, indicating that *Piks* is involved in resistance to O23.

Although *Pik* is a well-studied NLR gene, the *Piks* allele has not been functionally characterized. Therefore, we investigated the evolutionary relationship of *Piks* and other *Pik* alleles by reconstructing a phylogenetic

tree focusing on the *Pik-1* sensor NLRs (**Fig 3A**), which showed that *Piks-1* is most closely related to *Pikm-1*. Comparing amino acid sequences between Piks and Pikm revealed only two amino acid replacements. These two residues were located in the HMA domain of Pik-1 (**Fig 3B**, **S3 Fig**). The HMA domain of Pikm (Pikm-HMA) was crystalized in complex with the *M. oryzae* effector protein AVR-PikD [71]; the two amino acids differentiating Piks-HMA from Pikm-HMA were located at the interface of Pikm-HMA and AVR-PikD (**Fig 3C**), suggesting that these amino acid replacements may affect Pik-1 binding to the AVR-Pik effector. Amino acid sequences of the helper NLRs, Piks-2 and Pikm-2, were identical (**Fig 3B**).

Fig 3. Two amino acid replacements differentiate Piks-1 from Pikm-1. (A) Phylogenetic trees of *Pik* resistance gene alleles are shown together with the experimentally validated protein interactions between Pik and AVR-Pik allelic products. The phylogenetic trees of *Pik-1* and *Pik-2* were drawn based on nucleotide sequences and show the closest genetic relationship between *Piks* and *Pikm.* **(**B) Schematic representations of the gene locations and domain architectures of the NLR pair genes *Pik-1* and *Pik-2*. The genetically linked Pik-1 and Pik-2 share a common promoter region. Pik-1 has a non-canonical integrated HMA domain that binds *M. oryzae* AVR-Pik allelic products. Piks and Pikm differ by two amino acid replacements located at the integrated HMA domain of Pik-1. These polymorphisms, E229Q and A261V, are located at the binding interface 2 and 3 for AVR-PikD, respectively [71]. We calculated the sequence identities between Piks and Pikm based on amino acid sequences. (C) Structure of Pikm-HMA (PDB ID: 6FU9 chain A) in complex with AVR-PikD (PDB ID: 6FU9 chain B) [71]. The two amino acids differing between Piks-HMA and Pikm-HMA are exposed to the AVR-PikD-interaction site. The colors correspond to the colors of the alignment in (B).

Magnaporthe genetics reveals an avirulence effector gene *AVR-Mgk1* encoded on a mini-chromosome

To identify the *AVR* gene of *M. oryzae* isolate O23 that encodes the effector recognized by Piks, we crossed TH3o and O23 (**Fig 1** and **4A**). We first assembled the genome sequence of O23 into 11 contigs with a total size of 43 Mbp using long sequence reads from Oxford Nanopore Technologies (**S3 Table**). The Benchmarking Universal Single-Copy Orthologs (BUSCOs) value of the assembled genome [99] was 98.2% for the complete BUSCOs using the *Sordariomyceta* odb9 dataset (**S3 Table**). Comparing the O23 assembled contigs with the reference genome version MG8 of *M. oryzae* isolate 70-15 [100] by dot plot analysis revealed that the O23 genome was assembled almost completely end-to-end (**S4 Fig**). Compared to *M. oryzae* isolate 70-15, the O23 genome contained a large rearrangement between chromosome 1 and 6, which has been reported in other *M. oryzae* isolates [45,101–103].

Fig 4. *M. oryzae* genetic analysis identifies an *AVR* gene, *AVR-Mgk1*, encoded on a mini-chromosome. (A) Schematic representations of the F_1 progeny generated after a cross between *M. oryzae* isolates TH3o and O23. We subjected all F_1 progeny to whole-genome sequencing. O23 possesses a mini-chromosome [47]. (B) Genetic association of the TH3o x O23 F_1 progeny using infection lesion size on RIL #58 (*Pish* -,

Piks +) rice plants as a trait. The vertical axis indicates -$\log_{10}(p)$, where the *p*-value is how likely the marker shows association with a trait due to random chance. The dashed line shows the *p*-value corresponding to a false discovery rate of 0.05. The association analysis based on the O23 reference genome identified *AVR-Mgk1*, encoded on the mini-chromosome sequence O23_contig_1, as an *AVR* gene. O23_contig_1 was not present in the TH3o genome and was unique to the O23 genome. We used 7,867 SNP markers for chromosomes 1–7 and 265 presence/absence markers for the other contigs. (C) *p*-values for O23_contig_1 with annotated *AVR*s. We also detected *AVR-Pita* and *AVR-PikD* in O23_contig_1. *AVR-PikD* in O23_contig_1 contains a frameshift mutation, so we named this variant *AVR-PikD_O23*. The region encoding two *AVR-Mgk1* genes and showing lower *p*-values is highlighted in green. Nucleotide sequences of the two *AVR-Mgk1* genes, arranged in a head-to-head orientation, are identical. (D) Results of punch inoculation assays using *M. oryzae* isolate Sasa2 transformed with *AVR-PikD* or *AVR-Mgk1*. Wild-type Sasa2 infected all the cultivars tested in this study. The Sasa2 transformant expressing *AVR-PikD* infected RIL #58 (*Piks*), but that expressing *AVR-Mgk1* did not infect RIL #58 (*Piks*) or Tsuyuake (*Pikm*) rice plants. (E) Quantification of the lesion size in (D). Asterisks indicate statistically significant differences ($p < 0.001$, two-sided Welch's t-test). The data underlying **Fig 4B**, **C**, and **E** can be found in **S1 Data**.

A study using contour-clamped homogeneous electric field (CHEF) gel electrophoresis identified a mini-chromosome in O23 and reconstructed the sequence of the mini-chromosome region containing the *AVR-Pita* effector [47]. To identify the contigs corresponding to the mini-chromosome in our O23 assembly, we used AVR-Pita as an anchor using the alignment tool Exonerate [104]. AVR-Pita matched the 824-kbp contig named O23_contig_1, which was separately assembled from the core chromosomes (chromosomes 1–7). The presence of the telomeric repetitive sequence TTAGGG [105] in both ends suggested that this contig is a complete mini-chromosome. AVR-Pita was located close to the telomere of the O23_contig_1 as previously reported [47], suggesting that O23_contig_1 likely represents the O23 mini-chromosome [47]. The entire sequence of the O23_contig_1 was absent from the TH3o genome (**S5B Fig**).

We obtained 144 F_1 progeny from a cross between TH3o and O23 and subjected them to whole-genome sequencing (**S4 Table**). We then compared the TH3o and O23 genome sequences and extracted 7,867 SNP markers for the core chromosomes (chromosomes 1–7) and 265 presence/absence markers for other contigs, including O23_contig_1. Next, we inoculated RIL #58 (*Pish* -, *Piks* +) with each of the *M. oryzae* F_1 progeny and recorded the lesion size (**S5 Table**, **S6 Fig**). There was a strong association between lesion size and the DNA marker on the mini-chromosome sequence O23_contig_1 (**Fig 4B**). The *p*-values of the DNA markers showing higher levels of association were almost constant across O23_contig_1 (**Fig 4C**), except for position 755–785 kbp with lower *p*-values. This suggested that the candidate *AVR* gene is located on this mini-chromosome region.

To identify the genes expressed within the candidate region, we performed RNA sequencing (RNA-seq) of O23 and TH3o inoculated on barley (*Hordeum vulgare*) cv. Nigrate. Two genes were specifically expressed

from the candidate region of O23. These two genes had an identical nucleotide sequence and were arranged in a head-to-head orientation. We named these genes *AVR-Mgk1* (*Magnaporthe* gene recognized by *Pik*). Sequences similar to *AVR-Mgk1* were not detected in the TH3o genome. These results suggest that AVR-Mgk1 may encode the *M. oryzae* effector recognized by Piks.

To confirm the recognition of AVR-Mgk1 by Piks, we performed a punch inoculation assay using the *M. oryzae* isolate Sasa2, which is compatible with all the cultivars tested in this study, transformed with *AVR-PikD* or *AVR-Mgk1* (**Fig 4D** and **4E**, **S7** and **S8 Figs**). Sasa2 transformants expressing *AVR-PikD* infected RIL #58 (*Piks*) rice plants, but the transformants expressing *AVR-Mgk1* could not (**Fig 4D** and **4E**, **S7 Fig**), indicating that Piks recognizes AVR-Mgk1. Furthermore, Sasa2 transformants expressing *AVR-Mgk1* triggered resistance in the rice cultivar Tsuyuake (*Pikm*). To investigate the recognition specificity of the proteins encoded by other rice *Pik* alleles for AVR-Mgk1, we performed punch inoculation assays with K60 (*Pikp*) and Kanto51 (*Pik**) rice plants (**S9 Fig**). Sasa2 transformants expressing *AVR-Mgk1* were recognized by K60 (*Pikp*) and Kanto51 (*Pik**), showing that the proteins encoded by *Pikm*, *Pikp*, and *Pik** also detect AVR-Mgk1 (**S9 Fig**). These results indicate that AVR-Mgk1 is broadly recognized by Pik proteins.

In addition to *AVR-Mgk1*, we identified a sequence similar to *AVR-PikD* in O23_contig_1 (**Fig 4C**). This *AVR-PikD*-like gene carries a frameshift mutation, and thus encodes a protein with additional amino acids at the C-terminus (**S10A Fig**). We named it *AVR-PikD_O23*. To investigate whether Piks recognizes AVR-PikD_O23, we inoculated RIL #58 (*Piks*) and Tsuyuake (*Pikm*) with Sasa2 transformants expressing *AVR-PikD_O23* (**S10B Fig**). The transformants expressing *AVR-PikD_O23* infected RIL #58 (*Piks*), but not Tsuyuake (*Pikm*) (**S10B Fig**), indicating that AVR-PikD_O23 is not recognized by Piks but is recognized by Pikm, which is consistent with the *AVR* activity of the known *AVR-PikD* gene.

Retrotransposon repeat sequence-mediated deletion of *AVR-Mgk1* re-establishes virulence

The lower *p*-values of association around the *AVR-Mgk1* genes compared with the rest of the mini-chromosome (**Fig 4C**) facilitated their identification. To identify the F_1 progeny contributing to the lower *p*-values, we checked the presence/absence of genetic markers on the mini-chromosome in all F_1 progeny. One F_1 progeny, named d44a, lacked some markers around the *AVR-Mgk1* genes, suggesting that d44a inherited the mini-chromosome sequence from O23, but lacked the *AVR-Mgk1* genes.

To elucidate the mini-chromosome structure in the d44a isolate, we sequenced the d44a genome using Oxford Nanopore Technologies (**S3 Table**) and compared it with the O23 genome (**Fig 5A**, **S4 Fig**). Two tandemly duplicated sequences of the retrotransposon *Inago2* flanked the *AVR-Mgk1* coding regions in O23. However, in d44a, the *Inago2* sequences were directly associated without the *AVR-Mgk1* coding regions (**Fig 5A**). This suggests that an *Inago2* sequence repeat–mediated deletion of *AVR-Mgk1* occurred in d44a. This deletion was approximately 30 kbp long and the sequence carrying this deletion was assembled

separately from the core chromosomes in d44a. This suggests that the deletion was not caused by an inter-chromosome rearrangement between mini- and core chromosomes but by an intra-chromosome rearrangement within or between mini-chromosomes associated with the *Inago2* sequence repeats.

Fig 5. *Inago2* retrotransposon repeat sequence-mediated deletion of *AVR-Mgk1* re-establishes virulence. (A) Comparison of the genomic structures around the *AVR-Mgk1* genes between *M. oryzae* isolates O23 and d44a; d44a is an F_1 progeny of TH3o x O23. d44a lost the two *AVR-Mgk1* genes. Sequences of transposable elements around *AVR-Mgk1* genes (*Pot2*, *Pot3*, *Inago1*, *Inago2*, and *MGLR-3*) are indicated by color-coded rectangles. Long terminal repeats (LTRs) of retrotransposons are shown in triangles. (B) d44a is virulent against RIL #58 rice plants. We performed punch inoculation assays using O23, TH3o, and d44a on RIL #58 (*Piks*) plants. (C) Quantification of the lesion size in (B). Statistically significant differences are indicated ($p < 0.01$, two-sided Welch's t-test). The data underlying **Fig 5C** can be found in **S1 Data**.

To investigate the virulence of the d44a isolate on RIL #58 (*Piks*), we performed a punch inoculation assay using O23 and TH3o as controls (**Fig 5B** and **5C**). Consistent with the loss of the two *AVR-Mgk1* genes from the d44a mini-chromosome (**Fig 5A**), d44a infected RIL #58 (*Piks*) plants (**Fig 5B** and **5C**). Since d44a still carries *AVR-PikD_O23* on its mini-chromosome, this result supports that AVR-PikD_O23 is not recognized by Piks.

AVR-Mgk1 is predicted to be a MAX fold protein that belongs to a distinct family from AVR-Pik effectors

To determine whether AVR-Mgk1 (**Fig 6A**) is related to the AVR-Pik effectors in amino acid sequence, we performed a global alignment between AVR-Mgk1 and AVR-PikD, which revealed a sequence identity of only ~10% (**S11 Fig**). Therefore, we conclude that these proteins are not related in terms of amino acid sequences.

Fig 6. AVR-Mgk1 is predicted to be a MAX fold protein that belongs to a distinct family from AVR-Pik effectors. (A) Domain architecture and amino acid sequence of AVR-Mgk1. We used SignalP v6.0 [106] to predict signal peptide (SP) sequences in AVR-Mgk1. AVR-Mgk1 has the two cysteine residues (Cys27 and Cys67, indicated by black arrowheads) conserved in the MAX effector superfamily. (B) Clustering of putative *M. oryzae* AVR protein sequences using TRIBE-MCL [107]. Tribe-MCL assigned AVR-Mgk1 and AVR-PikD into different tribes. If a tribe includes an experimentally characterized protein, it is shown to represent the tribe. If a tribe includes an experimentally validated MAX effector protein or AVR-Mgk1, the tribe is shown in orange. Tribes having only one protein are not shown. (C) AVR-Mgk1 protein structure predicted by AlphaFold2 [108]. AVR-Mgk1 has antiparallel β sheets, characteristic of the MAX effector superfamily. (D) Protein structure of AVR-PikD (PDB ID: 6FU9 chain B) [71]. (E) Structure-based protein alignment between AVR-Mgk1 and AVR-PikD. TM-align [109] revealed significant structural

similarity between AVR-Mgk1 and AVR-PikD, while the regions highlighted in pink structurally differ (C, D). This structural difference involves the highly polymorphic residues (His46-Pro47-Gly48) of AVR-Pik effectors that determine Pik-1 HMA domain binding and are probably modulated by arms race co-evolution [70,96]. The data underlying **Fig 6B** and **E** can be found in **S1 Data**.

To further investigate the relationship between AVR-Mgk1 and AVR-Pik effectors, we applied TRIBE-MCL clustering algorithm [107] to a dataset of putative *M. oryzae* effector proteins [32], amended with AVR-Mgk1. TRIBE-MCL assigned AVR-Mgk1 and AVR-PikD (**Fig 6B**) into different tribes. This indicates that AVR-Mgk1 belongs to a distinct protein family from AVR-Pik effectors.

Although AVR-Mgk1 has little primary sequence similarity to the AVR-Pik family, AlphaFold2 [108] predicted the protein structure of AVR-Mgk1 as antiparallel β sheets, characteristic of the MAX effector superfamily (**Fig 6C**) [28]. To further evaluate the structural similarity between AVR-Mgk1 and AVR-PikD, we aligned the structures of AVR-Mgk1 (**Fig 6C**) and AVR-PikD (**Fig 6D**) in complex with the HMA domain of Pikm [71] using the structure-based aligner TM-align [109]. TM-align revealed significant structural similarity between the AVR-Mgk1 predicted model and AVR-PikD (**Fig 6E**) with a TM-score >0.5, indicating that they share a similar fold [110]. In addition, AVR-Mgk1 contains the two cysteine residues (Cys27 and Cys67, indicated by black arrowheads, **Fig 6A** and **6E**) conserved in the MAX effector superfamily [28]. Overall, these results indicate that AVR-Mgk1 and AVR-PikD are MAX fold effector proteins that belong to distinct families.

AVR-Mgk1 **occurs with low frequency in** ***M. oryzae***

Given that Piks has a narrow recognition spectrum against *M. oryzae* [96], we investigated the distribution of *AVR-Mgk1* in sequenced genomes of the blast fungus. To this end, we performed BLASTN and BLASTP searches against a non-redundant NCBI database using AVR-Mgk1 sequences as query (**S6 Table**). While the BLASTN search failed to find any relevant hits for sequences from the non-redundant nucleotide collection, the BLASTP search found one sequence in the *M. oryzae* isolate Y34 [111] with a sequence identity of ~52%.

We also performed a BLASTN search against whole-genome shotgun contigs of *Magnaporthe* deposited in NCBI (**S6 Table**). We found sequences identical to *AVR-Mgk1* in the *M. oryzae* isolates 10100 [112] and v86010 [113]. We also found two sequences with ~91% identity to *AVR-Mgk1* in *M. grisea Digitaria* isolate DS9461 [114], which is a sister species of *M. oryzae* but is genetically markedly different from *M. oryzae* [114,115]. These results indicate that *AVR-Mgk1* occurs with low frequency in *M. oryzae* and may derive from *M. grisea*.

The Pik-1 integrated HMA domain binds AVR-Mgk1

The integrated HMA domains of Pia and Pik sensor NLRs (Pia-2 and Pik-1) bind multiple *M. oryzae* MAX effectors [69,75,116]. Therefore, we hypothesized that AVR-Mgk1 binds the integrated HMA domain of Pik-1. To investigate this, we performed yeast two-hybrid assays and *in vitro* co-immunoprecipitation (co-IP) experiments (**Fig 7A** and **7B**). The integrated HMA domain of Pikm-1 bound AVR-Mgk1 and AVR-PikD, whereas the HMA domain of Piks-1 bound only AVR-Mgk1 (**Fig 7A** and **7B**). These results indicate that the Pik-1 integrated HMA domain directly binds AVR-Mgk1, and that one or both of the amino acid changes in Piks-HMA hinder its binding to AVR-PikD (**Fig 3**).

Fig 7. Piks specifically responds to AVR-Mgk1 but not to AVR-PikD. (A) Yeast two-hybrid assays between the Pik integrated HMA domains and AVRs. We used Myc-tagged HMA domains and HA-tagged AVRs as bait and prey, respectively. Empty vector was used as a negative control. Left side: basal medium lacking leucine (L) and tryptophan (W) for growth control. Right side: basal medium lacking leucine (L), tryptophan (W), adenine (A), and histidine (H) and containing X-α-gal and 10 mM 3AT for selection. (B) *In vitro* co-immunoprecipitation (co-IP) experiments between the Pik integrated HMA domains and AVRs. We used N-terminally tagged HA:HMA and FLAG:AVR in the experiments, and the protein complexes were pulled down by HA:HMA using Anti-HA affinity gel. Empty vector was used as a negative control. The large subunit of ribulose bisphosphate carboxylase (RuBisCO) stained by Coomassie brilliant blue is shown as a loading control. (C) Representative images of hypersensitive response (HR) cell death assay after transient co-expression of the AVRs with Pik-1 and Pik-2 in *N. benthamiana*. Pikm and Piks were tested on the left and right sides of the leaf, respectively. The empty vector only expressing p19 was used as a negative control. The leaves were photographed 5–6 days after infiltration under daylight (left) and UV light (right). (D) The HR in (C) was quantified. Statistically significant differences are indicated (Mann-Whitney U rank test). Each column represents an independent experiment. The data underlying **Fig 7D** can be found in **S1 Data**.

To investigate protein-protein interactions between AVR-Mgk1 and the HMA domains of other Pik proteins (Pikp and Pik*), we performed yeast two-hybrid assays and *in vitro* co-IP experiments for Pikp and Pik* (**S12**–**S16 Figs**). The integrated HMA domains of Pikp and Pik* bound AVR-Mgk1 and AVR-PikD, although Pikp bound AVR-Mgk1 with a lower apparent affinity than the other Pik proteins (**S14** and **S16 Figs**). Taken together, these results demonstrated that the HMA domains of all Pik proteins tested bind AVR-Mgk1, which are consistent with the results of the inoculation assay (**S9 Fig**).

Piks specifically responds to AVR-Mgk1 in a *Nicotiana benthamiana* transient expression assay

The AVR-Pik-elicited hypersensitive response (HR) cell death mediated by Pik NLR pairs has been recapitulated in *Nicotiana benthamiana* transient expression assays [29,71,98]. To investigate whether the HR cell death can be recapitulated with AVR-Mgk1, we performed HR cell death assays in *N. benthamiana*

by transiently co-expressing *AVR-Mgk1* or *AVR-PikD* with *Piks* (*Piks-1*/*Piks-2*) or *Pikm* (*Pikm-1*/*Pikm-2*). While Pikm responded to AVR-Mgk1 and AVR-PikD, Piks responded only to AVR-Mgk1 (**Fig 7C** and **7D**). AVR-Mgk1 and AVR-PikD alone did not trigger the HR in *N. benthamiana* (**S17 Fig**). These results are consistent with the protein-protein interaction results (**Fig 7A** and **7B**) and indicate that Piks has a narrower effector recognition range than Pikm.

Two polymorphisms, E229Q and A261V, between Piks and Pikm quantitatively affect the response to AVR-Pik

We investigated if the amino acid polymorphisms between Piks-1 and Pikm-1 (**Fig 3**) contribute to the differential response to AVR-PikD. We produced single-amino acid mutants of Piks-1 (Piks-1^{E229Q} and Piks-1^{A261V}, **Fig 8A**) and performed HR cell death assays in *N. benthamiana* by transiently co-expressing *Piks* (*Piks-1*/*Piks-2*), *Piks*^{E229Q} (*Piks-1*^{E229Q}/*Piks-2*), *Piks*^{A261V} (*Piks-1*^{A261V}/*Piks-2*), or *Pikm* (*Pikm-1*/*Pikm-2*) with *AVR-PikD* or *AVR-Mgk1* (**Fig 8B**–**D**). The helper NLRs Piks-2 and Pikm-2 have an identical amino acid sequence (**Fig 3B**). Both polymorphisms (E229Q and A261V) quantitatively affected the response to AVR-PikD (**Fig 8B**). Neither Piks-1^{E229Q} nor Piks-1^{A261V} achieved the same response level as Pikm; however, Piks-1^{A261V} was slightly more responsive to AVR-PikD than Piks-1^{E229Q} (**Fig 8B**–**D**). The E229Q and A261V mutations did not affect the response to AVR-Mgk1 (**Fig 8C** and **8D**). These results demonstrated that the Q229 and V261 residues of the HMA domain of Pikm are essential for the full response to AVR-PikD.

Fig 8. The polymorphisms (E229Q and A261V) between Piks and Pikm quantitatively affect the response to AVR-PikD. (A) Schematic representations of single amino acid mutants (Piks^{E229Q} and Piks^{A261V}) used in the HR cell death assay in *N. benthamiana* with AVR-PikD. (B) We quantified HR scores of Piks (Piks-1/Piks-2), Piks^{E229Q} (Piks-1^{E229Q}/Piks-2), Piks^{A261V} (Piks-1^{A261V}/Piks-2), or Pikm (Pikm-1/Pikm-2) with AVR-PikD 5–6 days after agroinfiltration and statistically significant differences are indicated (Mann-Whitney U rank test). Piks-2 and Pikm-2 are identical. (C) HR cell death assay with Piks^{E229Q} and AVRs. (D) HR cell death assay with Piks^{A261V} and AVRs. The leaves were photographed 5–6 days after infiltration under daylight (left) and UV light (right). We quantified the HR at 5–6 days after agroinfiltration and statistically significant differences are indicated (Mann-Whitney U rank test). Each column represents an independent experiment. The data underlying **Fig 8B**–**D** can be found in **S1 Data**.

To confirm the effects of E229Q and A261V mutations in the HMA domain of Piks-1 on the interaction with AVR-PikD and AVR-Mgk1, we performed yeast two-hybrid assays. The yeast two-hybrid assay showed that both Piks^{E229Q}-HMA and Piks^{A261V}-HMA as bait bound AVR-PikD as prey to similar levels compared to Pikm-HMA binding with AVR-PikD (**Fig 9A**, **S18 Fig**). This result is consistent with the result of yeast two-hybrid assay in a recent study [117]. On the other hand, we found that Piks^{E229Q}-HMA and Piks^{A261V}-HMA as prey weakly bound AVR-PikD as bait, compared to Pikm-HMA binding with AVR-PikD (**Fig 9B**, **S19 Fig**). The E229Q and A261V mutations in the HMA domain of Piks-1 did not affect the binding to

AVR-Mgk1 (**Fig 9**, **S18** and **S19 Figs**). These results support our findings in HR cell death assay showing that both E229Q and A261V quantitatively affect the response to AVR-PikD but not to AVR-Mgk1 (**Fig 8**). A recent study independently showed the quantitative binding affinity of Piks-HMA mutants (Pikm-HMA > Piks^{A261V}-HMA > Piks^{E229Q}-HMA > Piks-HMA) to AVR-PikD by analytical gel filtration [117]. Overall, both Q229 and V261 residues of the HMA domain of Pikm are essential for the full binding to AVR-PikD (**Fig 8** and **9**).

Fig 9. Yeast two-hybrid assay shows that the polymorphisms (E229Q and A261V) between Piks-HMA and Pikm-HMA quantitatively affect their binding to AVR-PikD. (A) HA-tagged AVRs as prey and Myc-tagged HMA domains as bait. (B) Myc-tagged AVRs as bait and HA-tagged HMA domains as prey. Empty vector was used as a negative control. Left side: basal medium lacking leucine (L) and tryptophan (W) for growth control. Right side: basal medium lacking leucine (L), tryptophan (W), adenine (A), and histidine (H) and containing X-α-gal for selection.

Discussion

In this study, we revealed a gene-for-gene interaction between the well-studied rice *Pik* resistance gene and *M. oryzae* effector genes. We discovered that the *Pik* allele *Piks* encodes a protein that detects the *M. oryzae* effector AVR-Mgk1, a secreted protein that does not belong to the AVR-Pik effector family. Piks specifically detects and responds to AVR-Mgk1, but other Pik proteins detects AVR-Mgk1 and AVR-Pik, indicating a complex network of gene-for-gene interactions (**Fig 10**, **S7 Table**). The response of Pik-1 to AVR-Mgk1 was previously overlooked; this illustrates the challenge of unravelling complex gene-for-gene interactions using classical genetic approaches and highlights the dynamic nature of the co-evolution between an NLR integrated domain and multiple families of effector proteins. As illustrated in **Fig 10**, our understanding of the interactions between *M. oryzae AVR* effectors and rice disease resistance genes has gone beyond Flor's single gene-for-gene model and involves network-type complexity at multiple levels [2–5].

Fig 10. Beyond the gene-for-gene model: complex interactions between MAX effectors and rice NLR pairs. The NLR pairs Pik (Pik-1/Pik-2) and Pia (Pia-2/Pia-1, also known as RGA5/RGA4) have an integrated HMA domain (grey) in their sensor NLRs (Pik-1 and Pia-2). The Pia-2 HMA domain binds the sequence-unrelated MAX effectors AVR-Pia and AVR1-CO39 [69]. The Pikp-1 HMA domain weakly binds AVR-Pia, while that of Pikm-1 cannot [116]. The AVR-Mgk1 effector is detected by several Pik proteins, including Piks, which does not respond to AVR-PikD. Complex interactions also occur between sensor and helper NLRs forming homo- and hetero-complexes [98,118]. An allelic mismatch of a receptor pair leads to autoimmunity (Pikp-1/Pikm-2) or reduced response (Pikm-1/Pikp-2) due to allelic specialization [119].The structures of AVR-Mgk1 predicted by AlphaFold2 [108], AVR-PikD (PDB ID: 6FU9 chain B) [71], AVR-Pia (PDB ID: 6Q76 chain B) [116], and AVR1-CO39 (PDB ID: 5ZNG chain C) [75] were visualised by ChimeraX [120].

Why was the response of Pik-1 to AVR-Mgk1 previously overlooked?

Despite its recognition by multiple Pik proteins, AVR-Mgk1 had not been discovered by previous studies. This is mainly because *AVR-Mgk1* sequences are rare among the available *M. oryzae* genome sequences (**S6 Table**). In addition, the mini-chromosome encoding *AVR-Mgk1* appears to be absent from many isolates, and thus has no homologous chromosome sequence to recombine with. Our TH3o x O23 cross resulted in constantly similar significant *p*-values in the genetic association analysis (**Fig 4C**). The mini-chromosome is also affected by segregation distortion, resulting in a lower-than-expected frequency of *AVR-Mgk1* inheritance in the F_1 progeny (**S5A Fig**). Lastly, the mini-chromosome of the O23 isolate carries two distinct *AVR* genes, *AVR-Mgk1* (two copies) and *AVR-PikD_O23*, which are both recognized by a single *Pik-1* resistance gene (**Fig 4C**, **S10 Fig**). *AVR-Mgk1* and *AVR-PikD_O23* mask each other's activities and are tightly linked on the mini-chromosome, which is unfavourable for identification using classical genetic approaches.

Another challenge for identifying *AVR-Mgk1* was that the rice *Pish* locus, which confers resistance to O23 and TH3o, is also present in the rice cultivar Hitomebore (which contains *Piks*) (**Fig 2B** and **2C**). Thus, this network of gene-for-gene interactions was complicated by mutually masking *AVR* genes as well as by stacked and paired rice resistance genes. Disentangling the overlapping contributions of these resistance loci required rice RILs lacking the *Pish* locus (**Fig 2**). Therefore, unravelling complex networks of gene-for-gene interactions requires multiple-organism genetic approaches. This also demonstrates that to fully exploit genetic resistance, we need to go beyond the 'blind' approach of breeding and deploying *R* genes in agricultural crops without knowledge of the identity and population structure of the *AVR* genes encoding the effectors they are potentially sensing.

The *AVR-Mgk1* genes are flanked by retrotransposon sequences

We observed deletion of *AVR-Mgk1* genes in one out of 144 sexual recombinants in just one generation. This event was mediated by the tandemly duplicated *Inago2* retrotransposon sequences that flank the *AVR-Mgk1* genes (**Fig 5A**). We hypothesize that this type of repeat sequence-mediated deletion of *AVR* genes might occur frequently in nature. The *M. oryzae* effector gene *AVR-Pita*, which occurs on the same mini-chromosome as *AVR-Mgk1* and *AVR-PikD_O23*, is also flanked by the solo long terminal repeats (solo-LTRs) of the retrotransposons *Inago1* and *Inago2* near the telomeric end of the chromosome [47] opposite of *AVR-Mgk1* and *AVR-PikD_O23* (**Fig 4C**). Chuma et al. proposed that the linkage of *AVR-Pita* to retrotransposons is associated with translocation between different *M. oryzae* isolates, and therefore, may facilitate horizontal gene transfer and recovery, particularly in asexual lineages [47]. This effector gene–retrotransposon linkage could enable persistence of the effector gene in the fungal population despite repeated deletions, and is a potential mechanism underpinning the two-speed genome concept [121–123]. In

the case of *AVR-Mgk1*, *Inago2* and dense solo-LTRs located between the two *AVR-Mgk1* copies (**Fig 5A**) appear to contribute to the effector gene's genetic instability and may explain its low frequency in *M. oryzae* populations.

AVR-Mgk1 is predicted to adopt a MAX fold structure

Despite the primary sequence dissimilarity between AVR-Mgk1 and AVR-Pik, AlphaFold2 [108] predicted that AVR-Mgk1 adopts a MAX fold structure (**Fig 6C**) similar to AVR-Pik and several other *M. oryzae* effectors [27–30,35,124]. However, the region that includes the highly polymorphic residues of AVR-Pik effectors, which determine their binding to the HMA domain of Pik-1 and are modulated by arms race co-evolution [70,71,96], differs structurally in AVR-Mgk1 (**Fig 6C**–**E**). This suggests that the HMA domain may bind AVR-Mgk1 at different interacting residues (or a subset of different interacting residues) from AVR-Pik as demonstrated for other MAX effectors [72,74,75,116]. This is supported by the observation that the Piks polymorphisms, which alter binding to AVR-PikD, do not affect the interaction with AVR-Mgk1 (**Fig 8** and **9**). It is remarkable that *M. oryzae* effectors may have evolved to bind the HMA domain through multiple interfaces, which necessitates additional structural studies of effector–HMA complexes.

Identification of AVR-Mgk1 highlights flexible and complex host–pathogen recognition by an integrated domain

The identification of AVR-Mgk1 expands our understanding of the interaction between the integrated HMA domains of rice NLR receptors and MAX effectors (**Fig 10**). Pik proteins Pikm, Pik*, and Pikp detect and bind AVR-Mgk1 and AVR-PikD via the Pik-1 integrated HMA domain (**S9** and **S12**–**16 Figs**). The recognition of multiple MAX effectors by an NLR receptor was reported in the rice NLR pair Pia [69]. The sensor NLR Pia-2 (RGA5) also contains the HMA domain, which binds the sequence-unrelated MAX effectors AVR-Pia and AVR1-CO39 [69,74,75]. The presence of the HMA domain in Pik proteins also enables Pikp to weakly respond to AVR-Pia, while this response is not observed with the combination of Pikm and AVR-Pia [116]. These reports indicate that an integrated domain can flexibly recognize multiple pathogen effectors. Our findings further extend the knowledge of HMA-mediated MAX effector recognition in that the recognition specificity of AVR-Mgk1 is different from that of previously identified MAX effectors, such as AVR-PikD, AVR-Pia, and AVR1-CO39 (**Fig 10**). The AVR-Mgk1- and AVR-PikD-interacting residues (or a subset of interacting residues) of the Pik HMA domain likely differ (**Fig 6**, **8**, and **9**). These different modes of interactions would enable an HMA domain to target multiple effectors, and therefore contribute to a broad recognition spectrum for pathogen effectors.

In the interactions between Pik proteins and AVR-Pik effectors, only a few polymorphisms dynamically change the recognition spectrum and determine the recognition specificity [70–73,96]. Here, we demonstrated that Piks binds and responds to AVR-Mgk1, but not to AVR-PikD (**Fig 7**). This unique recognition spectrum of Piks among other Pik family proteins (**Fig 10**) is caused by two amino acid changes

(E229Q and A261V) relative to its quasi-identical protein Pikm (**Fig 8** and **9**). We could not unambiguously reconstruct the ancestral state and evolutionary trajectory of these two key polymorphisms because they are recurrently polymorphic among Pik-1 proteins. However, considering that these polymorphisms between Piks-1 and Pikm-1 have arisen among cultivated rice, Piks-1 may have lost the capacity to respond to AVR-PikD as a trade-off between Pik immunity and rice yield, as reported for another rice resistance gene, *Pigm* [125].

Collectively, our findings imply the potential of integrated HMA domains to flexibly recognize pathogen effectors. In parallel, arms race co-evolution with *M. oryzae* and agricultural selection generate HMA domain variants with different recognition specificities, which results in a network of tangled gene-for-gene interactions between integrated HMA domains and MAX effectors (**Fig 10**). HMA–effector interactions can be a model to understand the flexible and complex mechanisms of host–pathogen recognition established during their co-evolution.

Materials and Methods

Magnaporthe oryzae isolates O23 and TH3o and their genetic cross

The *Magnaporthe oryzae* isolates used in this study were imported to Japan with permission from the Ministry of Agriculture, Forest and Fishery (MAFF), Japan and are maintained at Iwate Biotechnology Research Center under the license numbers “TH3: MAFF directive 12 yokoshoku 1139” and “O23: MAFF directive 51 yokoshoku 2502”. Genetic crosses of the *M. oryzae* isolates TH3o (subculture of TH3) and O23 (O-23IN [PO12-7301-2]) [47] were performed as previously described [126]. Briefly, perithecia were formed at the intersection of mycelial colonies of TH3o and O23 on oatmeal agar medium (20 g oatmeal, 10 g agar, and 2.5 g sucrose in 500 ml water) in a Petri dish during 3–4 weeks of incubation at 22°C under continuous fluorescent illumination. Mature perithecia were crushed to release asci, which were transferred to a water agar medium (10 g of agar in 500 ml of water) with a pipette. Each ascus was separated with a fine sterilized glass needle under a micromanipulator. After 24 h incubation, germinated asci were transferred to potato dextrose agar (PDA) slants. After two weeks incubation, the resulting mycelial colonies were used for spore induction, and the spore solution was diluted and spread on PDA medium. After a 1-week incubation, a mycelial colony derived from a single spore was transferred and used as an F_1 progeny of TH3o and O23. For long-term storage, the F_1 progeny was grown on sterilized barley (*Hordeum vulgare*) seeds in vials at 25°C for one month and kept in a case with silica gel at 10°C.

M. oryzae infection assays

For infection assay, rice plants one month after sowing were used. *M. oryzae* isolates TH3o, O23, and their F_1 progeny were grown on oatmeal agar medium [40% oatmeal (w/v), 5% sucrose (w/v), and 20% agar

(w/v)] for two weeks at 25°C. Then aerial mycelia were washed off by rubbing mycelial surfaces with plastic tube, and the colonies were incubated under black light (FL15BLB; Toshiba) for 3 to 5 days to induce conidiation. Resulting conidia were suspended in distilled water, and adjusted to the concentration of 5×10^5 spores per ml. The conidial suspension was inoculated onto the press-injured sites on rice leaves. The inoculated plants were incubated under dark at 28°C for 20 h, and then transferred to a growth chamber at 28°C with a 16-h light/8-h dark photoperiod. Disease lesions were photographed 10–12 days after inoculation. The vertical lesion length was measured. The lesion sizes were plotted by the "barplot" and "swarmplot" functions in the "seaborn" python library v0.11.2. The confidence interval was calculated by the default parameters of the "barplot" function. Two-sided Welch's t-test was conducted by the "ttest_ind" function in the "SciPy" python library v1.7.2 with the option "equal_var: False, alternative: two-sided".

Sequencing of rice cultivars Hitomebore and Moukoto and RILs derived from their cross

We re-sequenced rice (*Oryza sativa*) lines Hitomebore and Moukoto and 249 RILs from their cross. First, genomic DNA was extracted from fresh leaves using Agencourt Chloropure Kit (Beckman Coulter, Inc, CA, USA). Then, DNA was quantified using Invitrogen Quant-iT PicoGreen dsDNA Assay Kits (Thermo Fisher Scientific, MA, USA). For Hitomebore and Moukoto, library construction was performed using TruSeq DNA PCR-Free Library Prep Kit (Illumina, CA, USA). These two libraries were sequenced using the Illumina NextSeq, HiSeq, and MiSeq platforms (Illumina, CA, USA) for 75-bp, 150-bp, and 250/300-bp paired-end reads, respectively (**S1 Table**). For the 249 RILs, library construction was performed using house-made sequencing adapters and indices. These libraries were sequenced using the Illumina NextSeq platform for 75 bp paired-end reads (**S1 Table**). First, we removed adapter sequences using FaQCs v2.08 [127]. Then, we used PRINSEQ lite v0.20.4 [128] to remove low-quality bases with the option "-trim_left 5 -trim_qual_right 20 -min_qual_mean 20 -min_len 50." In addition, 300-bp reads were trimmed to 200 bp by adding an option "-trim_to_len 200."

SNP calling for the rice RIL population

The quality-trimmed short reads of the two parents and 249 RILs were aligned to the reference genome of Os-Nipponbare-Reference-IRGSP-1.0 [129] using bwa mem command in BWA v0.7.17 [130] with default parameters. Using SAMtools v1.10 [131], duplicated reads were marked, and the alignments were sorted in positional order. These BAM files were subjected to variant calling. First, we performed valiant calling for the parent cultivars Hitomebore and Moukoto according to the "GATK Best Practices for Germline short variant discovery" [132] (https://gatk.broadinstitute.org/), which contains a BQSR step, two variant calling steps with HaplotypeCaller in GVCF mode and GenotypeGVCFs commands, and a filter valiant step with VariantFiltration command with the option "QD < 2.0 || FS > 60.0 || MQ < 40.0 || MQRankSum < -12.5 || ReadPosRankSum < -8.0 || SOR > 4.0." In the resulting VCF file, we only retained biallelic SNPs where: 1) both parental cultivars had homozygous alleles, 2) the genotypes were different between Hitomebore and

Moukoto, and 3) both parental cultivars had a depth (DP) of eight or higher. As a result, 156,503 SNP markers were extracted, and the position of these SNPs was converted to a bed file (position.bed) using the BCFtools query command. For SNP genotyping of the 249 RILs, the VCF file was generated as follows: 1) BCFtools v1.10.2 [133] mpileup command with the option "-t DP,AD,SP -A -B -Q 18 -C 50 -uv -l position.bed"; 2) BCFtools call command with the option "-P 0 -A -c -f GQ"; 3) BCFtools filter command with the option "-v snps -i 'INFO/MQ>=0 & INFO/MQ0F<=1 & AVG(GQ)>=0"; 4) BCFtools norm command with the option "-m+both. " Finally, we imputed the variants based on Hitomebore and Moukoto genotypes using LB-impute [134].

De novo assembly of the Hitomebore genome

To reconstruct the *Pish* and *Pik* regions in Hitomebore, we performed a *de novo* assembly using Nanopore long reads and Illumina short reads. To extract high-molecular-weight DNA from leaf tissue for nanopore sequencing, we used the NucleoBond high-molecular-weight DNA kit (MACHEREY-NAGEL, Germany). After DNA extraction, low-molecular-weight DNA was eliminated using the Short Read Eliminator Kit XL (Circulomics, Inc, MD, USA). Then, following the manufacturer's instructions, sequencing was performed using Nanopore PromethION (Oxford Nanopore Technologies [ONT], UK). First, base-calling of the Nanopore long reads was performed for FAST5 files using Guppy 3.4.5 (ONT, UK), converted to FASTQ format (**S1 Table**). The lambda phage genome was removed from the generated raw reads with NanoLyse v1.1.0 [135]. We then trimmed the first 50 bp of each read and filtered out reads with an average read quality score of less than seven and reads shorter than 3,000 bases with NanoFilt v2.7.1 [135]. Next, the Nanopore long reads were assembled using NECAT v0.0.1 [136] setting the genome size to 380 Mbp. To further improve the accuracy of assembly, Racon v1.4.20 [137] was used twice for error correction, and Medaka v1.4.1 (https://github.com/nanoporetech/medaka) was subsequently used to correct mis-assembly. Following this, two rounds of consensus correction were performed using bwa-mem v0.7.17 [130] and HyPo v1.0.3 [138] with Illumina short reads. We subsequently removed haplotigs using purge-haplotigs v1.1.1 [139], resulting in a 374.8 Mbp *de novo* assembly comprising 77 contigs. This assembly was further scaffolded with RagTag v1.1.0 [140], with some manual corrections, using the Os-Nipponbare-Reference-IRGSP-1.0 as a reference genome. The resulting Hitomebore genome sequence was deposited on Zenodo (https://doi.org/10.5281/zenodo.7317319).

RNAi-mediated knockdown of *Piks-1* and *Piks-2* in rice

To prepare *Piks-1* and *Piks-2* knockdown vectors, the cDNA fragments Piks-1A (nt 618–1011) and Piks-1B (nt 1132–1651) for *Piks-1*, and Piks-2A (nt 121–524) and Piks-2B (nt 2317–2726) for *Piks-2* were amplified using primer sets (KF852f/KF853r, KF854f/KF855r, KF848f/KF849r, and KF801f/KF802r, respectively, **S8 Table**). The resulting PCR products were cloned into the Gateway vector pENTR-D-TOPO (Invitrogen, Carlsbad, CA, USA), and transferred into the pANDA vector [141] using LR clonase (Invitrogen), resulting

in pANDA-Piks-1A, pANDA-Piks-1B, pANDA-Piks-2A, and pANDA-Piks-2B. Plasmids were transformed into *Agrobacterium tumefaciens* (EHA105) and used for stable transformation of rice RIL #58 (*Piks* +) by *Agrobacterium*-mediated transformation. Transformation and regeneration of rice plants were performed according to Hiei et al. [142].

To determine *Piks-1* and *Piks-2* expression in the transgenic lines, reverse transcription quantitative PCR (RT-qPCR) was performed. Total RNA was isolated from transformant leaves using the Qiagen RNeasy plant mini kit (Qiagen, Venlo, the Netherlands). cDNA was synthesized with the ReverTra Ace kit (TOYOBO, http://www.toyobo.co.jp) and used as a template for quantitative PCR (qPCR) using primer sets (YS29f/YS30r for *Piks-1*, YS35f/YS36r for *Piks-2*, Actin-RTf/Actin-RTr for rice *Actin*, **S8 Table**). qPCR was performed using the Luna Universal qPCR Master Mix (New England Biolabs Japan, Tokyo, Japan) on a QuantStudio 3 Real-Time PCR System (Thermo Fisher Scientific, MA, USA). The relative expression levels of *Piks*-1 and *Piks*-2 were calculated via normalization with rice *Actin*. The relative expression levels were plotted by the "barplot" and "swarmplot" functions in the "seaborn" python library v0.11.2. The confidence interval was calculated by the default parameters of the "barplot" function. A two-sided Welch's t-test was conducted by the "ttest_ind" function in the "SciPy" python library v1.7.2 with the option "equal_var: False, alternative: two-sided".

Phylogenetic analysis of Pik alleles

The sequences of *Pik-1* (*Pikh-1* [AET36549.1], *Pikp-1* [ADV58352.1], *Pik*-1* [ADZ48537.1], *Pikm-1* [AB462324.1], and *Piks-1* [AET36547.1]) and *Pik-2* (*Pikh-2* [AET36550.1], *Pikp-2* [ADV58351.1], *Pik*-2* [ADZ48538.1], *Pikm-2* [AB462325.1], and *Piks-2* [AET36548.1]) were aligned using MAFFT v7.490 [143] with the option "--globalpair --maxiterate 1000". The phylogenetic trees of *Piks-1* and *Piks-2* were separately drawn based on nucleotide sequences with IQ-TREE v2.0.3 [144] using 1,000 ultrafast bootstrap replicates [145]. The models for reconstructing trees were automatically selected by ModelFinder [146] in IQ-TREE. ModelFinder selected "HKY+F" for *Pik-1* and "F81+F" for *Pik-2* as the best-fit models according to the Bayesian information criterion (BIC). Finally, the midpoint rooted trees were drawn with FigTree v1.4.4 (http://tree.bio.ed.ac.uk/software/figtree/).

Sequencing of *M. oryzae* isolates O23 and TH3o and their F_1 progeny

For long-read sequencing, O23 and d44a genomic DNA was extracted from liquid-cultured aerial hyphae using the NucleoBond high-molecular-weight DNA kit (MACHEREY-NAGEL, Germany). The genomic DNA was processed through the short-read eliminator kit XL (Circulomics). The filtered genomic DNA (2 µg) was used to construct a library for Nanopore sequencing using the ligation sequencing kit SQK-LSK109 (ONT, UK). Sequencing was performed using the MinION system with a FLO-MIN106D (R9.4) flow cell (ONT, UK).

TH3o genomic DNA was extracted using the cetyl trimethyl ammonium bromide (CTAB) method. The extracted DNA was purified using Genomic-tip (Qiagen, Germany) according to the manufacturer's protocol. Sequencing was performed by Macrogen, Inc., Seoul, Korea, using the PacBio RS II sequencer (Pacific Biosciences of California, Inc., Menlo Park, CA, USA).

For short-read sequencing of O23, TH3o, and their F_1 progeny, genomic DNA was extracted from aerial hyphae using the NucleoSpin Plant II Kit (Macherey Nagel). Libraries for paired-end short reads were constructed using an Illumina TruSeq DNA LT Sample Prep Kit (Illumina, CA, USA). The paired-end library was sequenced by the Illumina NextSeq platform (Illumina, CA, USA). We also sequenced O23 genomic DNA using the MiSeq platform to polish the *de novo* O23 assembly.

The adapters of short-reads were trimmed by FaQCs v2.08 [127]. In this step, we also filtered the reads and discarded reads shorter than 50 bases and those with an average read quality below 20.

***De novo* assembly of O23, TH3o, and d44a genomes**

First, base-calling of the Nanopore long reads was performed for FAST5 files of O23 and d44a with Guppy 3.4.4 (ONT, UK). The lambda phage genome was removed from the generated raw reads with NanoLyse v1.1.0 [135]. We then trimmed the first 50 bp of each read and filtered out reads with an average read quality score of less than 7 and reads shorter than 3,000 bases with NanoFilt v2.7.1 [135]. The quality-trimmed Nanopore long reads of O23 and d44a were assembled with NECAT v0.0.1 [136] setting the genome size to 42 Mbp. The assembled contigs were then polished with medaka v0.12.1 (https://github.com/nanoporetech/medaka) and with Hypo v1.0.3 [138]. In Hypo, we used MiSeq and NextSeq short-reads for O23 and d44a, respectively, in addition to quality-trimmed Nanopore long reads.

For the *de novo* assembly of TH3o, we trimmed the first 50 bp of each read and filtered out reads with an average read quality score of less than 7 and reads shorter than 2,000 bases with NanoFilt v2.7.1 [135]. The quality-trimmed PacBio long reads of TH3o were assembled with MECAT v2 [147] setting the genome size to 42 Mbp. The assembled contigs were polished with Hypo v1.0.3 [138] using NextSeq short-reads and PacBio long reads of TH3o.

To evaluate the completeness of the gene set in the assembled contigs, we applied BUSCO analysis v3.1.0 [99]. For BUSCO analysis, we set "genome" as the assessment mode, and *Magnaporthe grisea* was used as the species in AUGUSTUS [148]. *Sordariomyceta* odb9 was used as the dataset.

The genome sequences of the *M. oryzae* isolates 70-15 (MG8 genome assembly in https://fungi.ensembl.org/Magnaporthe_oryzae/Info/Index) [100], O23, TH3o, and d44a were compared by

dot plot analysis of D-GENIES [149]. The chromosome sequences of O23 and d44a were numbered and ordered based on those of 70-15.

Variant calling for the *M. oryzae* F_1 progeny derived from a cross between O23 and TH3o

Quality-trimmed short-reads were aligned to the O23 reference genome using the bwa mem command in BWA v0.7.17 with default parameters [130]. Using SAMtools v1.10 [131], duplicated reads were marked and the alignments were sorted to positional order. Only properly paired and uniquely mapped reads were retained using SAMtools [131]. For SNP markers on core chromosomes (chromosomes 1–7), the VCF file was generated as follows: 1) BCFtools v1.10.2 [133] mpileup command with the option "-a AD,ADF,ADR -B -q 40 -Q 18 -C 50"; 2) BCFtools call command with the option "-vm -f GQ,GP --ploidy 1"; 3) BCFtools filter command with the option "-i "INFO/MQ>=40". In the VCF file, biallelic SNPs were retained only where: 1) O23 had the same genotype as the O23 reference genome, 2) both parental isolates, O23 and TH3o, had a depth (DP) of four or higher, 3) the average genotype quality (GQ) across all the samples was 100 or higher, 4) the number of missing genotypes among the 144 F_1 progeny was less than 15, and 5) the allele frequency was between 0.05 and 0.95. As a result, 7,867 SNP markers were extracted from the core chromosomes. For presence/absence markers on the remaining contigs, we selected candidate presence/absence regions on the parental genomes, O23 and TH3o. First, the BCFtools mpileup command was used only for the BAM files of O23 and TH3o with the option "-a DP -B -q 40 -Q 18 -C 50". Second, BCFtools view command was used with the option "-g miss -V indels" to extract the positions where either O23 or TH3o was missing. Third, only the positions where O23 had a depth of eight or higher and TH3o had a depth of zero were retained. These positions were concatenated using the bedtools v2.29.2 [150] merge command with the option "-d 10". Only candidate regions larger than or equal to 50 bp were retained. Using the SAMtools bedcov command with the option "-Q 0", the number of alignments of each F_1 progeny on these candidate regions was counted. If an F_1 progeny had at least one alignment on a candidate region, the F_1 progeny was considered to have a presence-type marker for that region. On the other hand, if an F_1 progeny had no alignment on a candidate region, the F_1 progeny was considered to have an absence-type maker for that region. Finally, only the presence/absence markers that 1) had an average depth of four or higher for O23 regions, and one or less for TH3o regions, and 2) had an allele frequency between 0.05 and 0.95 were retained. As a result, 265 presence/absence markers were extracted for the remaining contigs.

Annotation of the O23 reference genome

The segregation distortion of each marker was tested by a two-sided binomial test (p = 0.5). O23-specific regions were annotated by aligning TH3o contigs to the O23 reference genome with Minimap2 [151] using the option "-x asm5". Transposable elements were annotated by EDTA v1.9.0 [152] with the option "--anno 1 --species others --step all". Coding sequences of the genome assembly version MG8 of the *M. oryzae* isolate 70-15 [100] and the library of transposable elements curated in Chuma et al. [47] were also provided

as input to EDTA. We only retained the annotations from the provided transposable elements. LTRs of retrotransposons were also annotated by EDTA, independently. The genes on the O23 reference genome were annotated by aligning the coding sequences of the genome assembly version MG8 of 70-15 using Spaln2 v2.3.3 [153]. The sequence similarity of the mini-chromosome sequence O23_contig_1 was analysed against the O23 core chromosomes using Minimap2 [151] with the option "-x asm5". We filtered out the alignments shorter than 1 kbp or with a mapping quality less than 40. Finally, these sequence similarities were plotted by Circos v0.69.8 (http://circos.ca/) including other genomic features. For gene density, the overlapped gene annotations were regarded as a single gene annotation. The plotted figure does not include contigs smaller than O23_contig_1.

Association analysis between genetic markers and phenotype

The association between the genetic markers and the phenotype was evaluated using the R package rrBLUP [154]. To correct the threshold of *p*-values for multiple testing, false discovery rate was used for the rice RILs and *M. oryzae* F_1 progeny. For false discovery rate, the "multipletests" function in the "statsmodels" python library was used with the option "method: fdr_bh, alpha: 0.05".

RNA-seq to identify *AVR-Mgk1*

Total RNA of TH3o and O23 was extracted at different stages (24 and 48 h) of barley infection using the SV Total RNA Isolation System (Promega, WI, USA). One microgram of total RNA was used to prepare each sequencing library with the NEBNext Ultra II Directional RNA library prep kit (New England Biolabs Japan, Tokyo, Japan) following the manufacturer's protocol. The library was sequenced by paired-end mode using the Illumina Hiseq X platform (Illumina, CA, USA).

For quality control, the reads were filtered and reads shorter than 50 bases and those with an average read quality below 20 and trimmed poly(A) sequences were discarded with FaQCs v2.08 [127]. The quality-trimmed reads were aligned to the O23 reference genome with HISAT2 v2.1 [155] with the options "--no-mixed --no-discordant --dta". BAM files were sorted and indexed with SAMtools v1.10 [131], and transcript alignments were assembled with StringTie v2.0 [156] separately for each BAM file.

Transformation of *M. oryzae* isolate Sasa2 with *AVR-Mgk1* and *AVR-PikD_O23*

To construct the *pCB1531-pex22p-AVR-Mgk1* expression vector, *AVR-Mgk1* was amplified by PCR using primer sets XbaI_O23_48h.1149.1-F and BamHI_O23_48h.1149.1-R (**S8 Table**) from cDNA of *M. oryzae* O23-infected barley leaf material. The PCR product was digested with *Xba*I and *Bam*HI and ligated into the *pCB1531-pex22p-EGFP* vector [18] using the *Xba*I and *Bam*HI sites to be exchanged with EGFP tag. To construct the *pCB1531-pex22p-AVR-PikD'*(*AVR-Pik-D_O23*) expression vector, a 0.3-kb fragment

containing *AVR-PikD'* (*AVR-Pik-D_O23*) was amplified by PCR using the primers Xba1_kozak_pex31_U1 [18] and KF792r (**S8 Table**) from *M. oryzae* O23 genomic DNA. The PCR product and *pCB1531-pex22p-EGFP* expression vector were digested with *Xba*I and *Eco*RI to ligate *AVR-PikD_O23* into the position of the EGFP tag, generating *pCB1531-pex22p-AVR-PikD'*(*AVR-Pik-D_O23*). The resulting vectors were used to transform *M. oryzae* Sasa2 following a previously described method [157].

To confirm *AVR-Mgk1* expression in infected rice leaves, Sasa2 transformants were punch inoculated on rice cultivar Moukoto. We reverse transcribed cDNA from RNA extracted from the infected rice leaves and amplified *AVR-Mgk1* via PCR using primer sets listed in **S8 Table**. Rice and *M. oryzae Actin* were used as controls.

Protein sequence alignment between AVR-Mgk1 and AVR-PikD

NCBI BLAST (https://blast.ncbi.nlm.nih.gov/Blast.cgi) was used to align the AVR-Mgk1 and AVR-PikD protein sequences using the Needleman-Wunsch algorithm [158] for pairwise global alignment using default parameters.

Clustering of putative *M. oryzae* AVR protein sequences using TRIBE-MCL

A dataset of the putative *M. oryzae* effector proteins [32] amended with AVR-Mgk1 was clustered by TRIBE-MCL [107] using "1e-10" for an E-value cut-off of BLASTP [159] and "1.4" for the inflation parameter "-I" in mcl. The other parameters were default. The sequence set used in this analysis was deposited in Zenodo (https://doi.org/10.5281/zenodo.7317319).

AVR-Mgk1 structure prediction

The AVR-Mgk1 structure was predicted using AlphaFold2 [108]. The signal peptide sequence in AVR-Mgk1 was predicted by SignalP v6.0 (https://services.healthtech.dtu.dk/service.php?SignalP) [106]. The amino acid sequence without the signal peptide (Arg25-Trp85) was used as an input for AlphaFold2 [108], available on the Colab notebook. The best model generated by AlphaFold2 was visualised by ChimeraX v1.2.5 [120] together with the protein structures of AVR-PikD (PDB ID: 6FU9 chain B) [71], AVR-Pia (PDB ID: 6Q76 chain B) [116], and AVR1-CO39 (PDB ID: 5ZNG chain C) [75]. The protein structures of AVR-Mgk1 and AVR-PikD were aligned by structure-based alignment using TM-align (https://zhanggroup.org/TM-align) [109]. The AVR-Mgk1 structure predicted by AlphaFold2 is deposited on Zenodo (https://doi.org/10.5281/zenodo.7317319).

BLAST search of AVR-Mgk1 to the NCBI database

To find sequences related to AVR-Mgk1, BLASTN and BLASTP searches were run against the non-redundant NCBI database. A BLASTN search was also run against the whole-genome shotgun contigs of *Magnaporthe* (taxid: 148303). For all analyses, default parameters were used.

Assays for protein-protein interactions

For the yeast two-hybrid assay, In-Fusion HD Cloning Kit (Takara Bio USA) was used to insert the *AVR-Mgk1* fragment (Arg25-Trp85) into pGADT7 (prey) and pGBKT7 (bait). DNA sequences of the fragments of AVR-PikD (Glu22-Phe113) and the Pik HMA domains (Piks-HMA [Gly186-Asp264], Pikp-HMA [Gly186-Asp263], Pik*-HMA [Gly186-Asp264], Pikm-HMA [Gly186-Asp264], Piks^{E229Q}-HMA [Gly186-Asp264], and Piks^{A261V}-HMA [Gly186-Asp264], defined in De la Concepcion et al. [71]) were ligated into pGADT7 and pGBKT7 as described previously [70]. The primer sets used for PCR amplification of the fragments are listed in **S8 Table**. Yeast two-hybrid assays were performed as described previously [70] using a basal medium lacking leucine (L), tryptophan (W), adenine (A), and histidine (H) and containing 5-Bromo-4-Chloro-3-Indolyl α-D-galactopyranoside (X-α-gal) (Clontech) to detect interactions. The basal medium also contained 10 mM 3-amino-1,2,4-triazole (3AT) (Sigma) for selection, except for **Fig 9**.

Co-IP experiments of transiently expressed proteins in *Nicotiana benthamiana* were performed as described previously [70]. The protein regions used in the co-IP experiment were the same as those used in the yeast two-hybrid assay. We used N-terminally tagged FLAG:AVR and HA:HMA. The lysates of AVRs and HMA domains were diluted to compare the results at the same concentration and mixed (1:4, 1:2, or 1:1 ratio) *in vitro* to assemble the protein complex. For co-IP of HA-tagged proteins, Anti-HA affinity gel (Sigma) was used, and proteins were eluted by using 0.25 mg/ml HA peptide (Roche). HA- and FLAG-tagged proteins were immunologically detected using HRP-conjugated anti-HA 3F10 (Roche) and anti-FLAG M2 (Sigma), respectively. The primer sets used in this experiment are listed in **S8 Table**.

Hypersensitive response cell death assay in *N. benthamiana*

Transient gene expression in *N. benthamiana* was performed by agroinfiltration according to methods described by van der Hoorn et al. [160]. Briefly, *A. tumefaciens* strain GV3101 pMP90 carrying binary vectors was inoculated from glycerol stock in liquid LB supplemented with 30 µg/ml rifampicin, 20 µg/ml gentamycin, and 50 µg/ml kanamycin and grown overnight at 28°C with shaking until saturation. Cells were harvested by centrifugation at 2000 × g at room temperature for 5 min. Cells were resuspended in infiltration buffer (10 mM $MgCl_2$, 10 mM MES-KOH pH 5.6, 200 µM acetosyringone) and diluted to the appropriate OD_{600} (**S9 Table** and also see [82,161]) in the stated combinations and left to incubate in the dark for 2 hours at room temperature prior to infiltration into 5-week-old *N. benthamiana* leaves. Hypersensitive cell death phenotypes were scored from 0 to 6 according to the scale in Maqbool et al. [29].

Data Availability Statement

All the sequence data used in this study was deposited at European Nucleotide Archive (ENA, https://www.ebi.ac.uk/ena/browser/home) and the DNA Data Bank of Japan (DDBJ, https://www.ddbj.nig.ac.jp/index-e.html) with the study accessions PRJEB53625 and PRJDB13864, respectively. The datasets used in this study are available at Github repository (https://github.com/YuSugihara/Sugihara_et_al_2022) archived in Zenodo (https://doi.org/10.5281/zenodo.7317319).

Funding

This study was supported by JSPS KAKENHI 15H05779, 20H05681 to RT, the Royal Society UK-Japan International exchange grants JPJSBP120215702 and IEC\R3\203081 to RT, SK and MB, the Gatsby Charitable Foundation (https://www.gatsby.org.uk/), the UK Research and Innovation Biotechnology and Biological Sciences Research Council (UKRI-BBSRC) grants BB/P012574, BBS/E/J/000PR9797, BBS/E/J/000PR9798 BB/R01356X/1, and the European Research Council (ERC) BLASTOFF grant 743165.

Acknowledgements

We thank Hiroe Utsushi, Akiko Hirabuchi, Yukie Hiraka, and Mari Iwai at Iwate Biotechnology Research Center, Japan, for technical support, and Phil Robinson at The Sainsbury Laboratory, UK for photography. We also thank Jeff Ellis for his comments on the preprint.

S1 Fig. Schematic representations of the RNAi-mediated *Pik-1* and *Pik-2* knockdown experiment. For each *Pik* gene, we prepared two independent RNAi constructs targeting different regions on the gene (Piks-1A and Piks-1B for *Piks-1*, and Piks-2A and Piks-2B for *Piks-2*).

S2 Fig. *Piks-1* and *Piks-2* expression in RNAi-mediated knockdown lines. We analyzed *Piks-1* and *Piks-2* expression in RNAi-mediated knockdown lines using RT-qPCR. RIL #58 (*Pish* -, *Piks* +) was used as the genetic background for the mutant lines. Rice *Actin* was used for normalization. [a] indicates statistically significant differences compared to RIL #58 ($p < 0.01$, two-sided Welch's t-test). The data underlying this figure can be found in **S1 Data**.

S3 Fig. Amino acid sequence alignment of the HMA domains of Pik proteins. The sequences are visualized by the software AliView [162].

S4 Fig. Pairwise dot plot analyses among the *de novo*-assembled genome sequences of *M. oryzae* isolates 70-15, O23, TH3o, and d44a. We compared the *de novo*-assembled genome sequences of O23, TH3o, and d44a with the previously assembled reference genome (MG8 genome assembly) of the isolate 70-15 [100], using D-GENIES [149]. The chromosome sequences of O23 and d44a are numbered and ordered based on those of 70-15. The data underlying this figure can be found in **S1 Data**.

S5 Fig. Genomic features of a *M. oryzae* mini-chromosome O23_contig_1. (A) Segregation distortion in TH3o x O23 F_1 progeny. Grey markers are statistically neutral ($p \geq 0.05$). (B) O23-specific regions (black) where TH3o contigs could not be aligned. (C) Density of transposable elements. (D) Gene density. (E) GC contents (0.45–0.55). (F) Sequence similarity between the O23 mini-chromosome and core chromosomes (chromosomes 1–7). The data underlying this figure can be found in **S1 Data**.

S6 Fig. Histogram of the lesion size of F_1 progeny in the rice inoculation assays to Moukoto and RIL #58. (A) Lesion size (mm) of F_1 progeny on Moukoto. (B) Lesion size (mm) of F_1 progeny on RIL #58. The percentiles (25%, 50%, and 75%) are indicated by the red lines. The data underlying this figure can be found in **S1 Data**.

S7 Fig. Sasa2 transformants expressing *AVR-Mgk1* cannot infect RIL #58 rice plants containing *Piks*. We produced four independent *M. oryzae* Sasa2 transformants expressing *AVR-Mgk1* and performed punch inoculation assays using wild-type Sasa2 and Sasa2 transformants on rice lines Moukoto (*Piks* -) and RIL #58 (*Piks* +). The lesion size was quantified. Statistically significant differences between rice lines are indicated by asterisks ($p < 0.05$, two-sided Welch's t-test). The transformant Sasa2-AVR-Mgk1 #4 was used for the punch inoculation assay in **Fig 4D** and **4E** and **S9 Fig**. The data underlying this figure can be found in **S1 Data**.

S8 Fig. *AVR-Mgk1* expression in infected rice leaves. We punch inoculated independent *M. oryzae* Sasa2 transformants expressing *AVR-Mgk1* on rice cultivar Moukoto. We reverse transcribed cDNA from RNA extracted from the infected rice leaves and amplified *AVR-Mgk1* via PCR. Rice and *M. oryzae Actin* were used as controls.

S9 Fig. Punch inoculation assays using Sasa2 transformants expressing *AVR-Mgk1* show the broad recognition of AVR-Mgk1 by Pik proteins. (A) We performed punch inoculation assays using wild-type Sasa2 and transformants expressing *AVR-PikD* and *AVR-Mgk1* on rice plants carrying different *Pik* alleles (*Piks*, *Pikp*, *Pik**, and *Pikm*). A subset of this picture was used in **Fig 4D**. (B) The lesion size in (A) was quantified. Statistically significant differences between isolates are indicated by asterisks (two-sided Welch's t-test). A subset of this data was used in **Fig 4E**. The data underlying **S9B Fig** can be found in **S1 Data**.

S10 Fig. The protein product of *AVR-PikD_O23*, carrying a frameshift mutation, is detected by Pikm but not by Piks. (A) *AVR-PikD* on the O23 mini-chromosome carries a frameshift mutation near the C-terminus that extends the amino acid sequence compared to previously described AVR-PikD. We named this variant *AVR-PikD_O23*. (B) Punch inoculation assays using Sasa2 and its transformant expressing *AVR-PikD_O23*. Sasa2 transformants expressing *AVR-PikD_O23* could not infect Tsuyuake (*Pikm*) but infected RIL #58 (*Piks*).

S11 Fig. Global sequence alignment reveals that AVR-Mgk1 and AVR-PikD are unrelated in amino acid sequence. We aligned the AVR-Mgk1 and AVR-PikD amino acid sequences using the Needleman-Wunsch global sequence alignment algorithm [158]. Twelve amino acids (red) are identical between AVR-Mgk1 and AVR-PikD. The two cysteine residues conserved in the MAX effector superfamily [28] are indicated by black arrowheads.

S12 Fig. Yeast two-hybrid assay shows that the HMA domains of Pik proteins (bait) bind AVR-Mgk1 (prey). We used HA-tagged AVRs as prey and Myc-tagged HMA domains as bait. Empty vector was used as a negative control. Left side: basal medium lacking leucine (L) and tryptophan (W) for growth control. Right side: basal medium lacking leucine (L), tryptophan (W), adenine (A), and histidine (H) and containing X-α-gal and 10 mM 3AT for selection.

S13 Fig. Accumulation of AVRs (prey) and HMA domains (bait) in yeast cells as confirmed by immunoblot analysis. To confirm protein accumulation for the yeast two-hybrid assay, we detected HA-tagged AVRs (prey) by anti-HA antibody and Myc-tagged HMA domains (bait) by anti-Myc antibody. Total proteins of yeast cells detected by Coomassie brilliant blue staining are shown in the bottom as a loading control.

S14 Fig. Yeast two-hybrid assay shows that the HMA domains of Pik proteins (prey) bind AVR-Mgk1 (bait). We used Myc-tagged AVRs as bait and HA-tagged HMA domains as prey. Empty vector was used as a negative control. Left side: basal medium lacking leucine (L) and tryptophan (W) for growth control. Right side: basal medium lacking leucine (L), tryptophan (W), adenine (A), and histidine (H) and containing X-α-gal and 10 mM 3AT for selection.

S15 Fig. Accumulation of AVRs (bait) and HMA domains (prey) in yeast cells as confirmed by immunoblot analysis. To confirm protein accumulation for the yeast two-hybrid assay, we detected Myc-tagged AVRs (bait) by anti-Myc antibody and HA-tagged HMA domains (prey) by anti-HA antibody. Total proteins of yeast cells detected by Coomassie brilliant blue staining are shown in the bottom as a loading control.

S16 Fig. AVR-Mgk1 interacts with the HMA domains of Pik proteins in an *in vitro* co-IP experiment. (A) *In vitro* co-IP experiment between AVR-Mgk1 or AVR-PikD and the HMA domains of Piks (Piks-HMA), Pikm (Pikm-HMA), or Pik* (Pik*-HMA) (1:4 mixed ratio). (B) *In vitro* co-IP experiment between AVR-Mgk1 or AVR-PikD and the HMA domain of Pikp (Pikp-HMA) (1:4 mixed ratio). (C) *In vitro* co-IP experiment between AVR-Mgk1 and Pikp-HMA (1:2 or 1:1 mixed ratios). N-terminally tagged FLAG:AVRs and HA:HMA were expressed in *N. benthamiana*. Empty vector was used as a negative control. We diluted the lysates of AVRs and HMA domains to compare the results at the same concentration and mixed them (1:4, 1:2, or 1:1 ratio) *in vitro* to assemble the protein complex. The protein complexes were pulled down by HA:HMA using Anti-HA affinity gel. *In vitro* co-IP experiments between AVR-Mgk1 and Pikp-HMA (1:2 or 1:1 mixed ratios) were photographed in long-exposure time. The large subunit of ribulose bisphosphate carboxylase (RuBisCO) stained by Coomassie brilliant blue is shown as a loading control.

S17 Fig. AVR-Mgk1 and AVR-PikD alone do not trigger the HR in *N. benthamiana*. (A) Representative images 5–6 days after transiently co-expressing AVR-Mgk1 and AVR-PikD, either with an empty vector control only expressing p19 or with Pikm, respectively, in *N. benthamiana*. The leaves were photographed under daylight (left) and UV light (right). (B) We quantified the HR in (A) and statistically significant differences are indicated (Mann-Whitney U rank test). Each column shows an independent experiment. The data underlying **S17B Fig** can be found in **S1 Data**.

S18 Fig. Accumulation of AVRs (prey) and Piks-HMA mutants (bait) in yeast cells as confirmed by immunoblot analysis. To confirm protein accumulation for the yeast two-hybrid assay (**Fig 9A**), we detected HA-tagged AVRs (prey) by anti-HA antibody and Myc-tagged HMA domains (bait) by anti-Myc antibody. Total proteins of yeast cells detected by Coomassie brilliant blue staining are shown in the bottom as a loading control.

S19 Fig. Accumulation of AVRs (bait) and Piks-HMA mutants (prey) in yeast cells as confirmed by immunoblot analysis. To confirm protein accumulation for the yeast two-hybrid assay (**Fig 9B**), we detected Myc-tagged AVRs (bait) by anti-Myc antibody and HA-tagged HMA domains (prey) by anti-HA antibody. Total proteins of yeast cells detected by Coomassie brilliant blue staining are shown in the bottom as a loading control.

S1 Table. Summary of sequences of rice cultivars Hitomebore and Moukoto and their RILs.

S2 Table. Summary of phenotypes of rice RILs derived from a cross between Hitomebore and Moukoto. The scores 0, 1, and 2 indicate resistant, intermediate, and susceptible phenotypes, respectively. We used these scores as a trait in the genetic association analyses (**Fig 2B** and **C**).

S3 Table. Summary of *de novo* assemblies of the *M. oryzae* isolates TH3, O23, and d44a. We sequenced TH3o using PacBio and Illumina DNA sequencers, and O23 and the F_1 progeny d44a using Oxford Nanopore Technologies (ONT) and Illumina DNA sequencers. The *Sordariomyceta* odb9 dataset was used in BUSCO analysis [99].

S4 Table. Summary of sequences of *M. oryzae* isolates TH3o and O23 and their F_1 progeny.

S5 Table. Summary of infectivity of the TH3o x O23 F_1 progeny on RIL #58 and Moukoto rice plants.

S6 Table. BLAST search results using AVR-Mgk1 as query. We used different NCBI databases and algorithms to find sequences related to AVR-Mgk1. We did not find hits in the non-redundant (nr) nucleotide collection using BLASTN search, but found one sequence in the non-redundant (nr) protein collection using BLASTP search. We found other sequences related to AVR-Mgk1 in whole-genome shotgun contigs (wgs) of *Magnaporthe* (taxid: 148303) using BLASTN search. All the BLAST searches were performed using default parameters.

S7 Table. Summary of the various interactions and phenotypes between Pik NLRs and AVRs in this study. +++ indicates strong, ++ indicates medium, and + indicates weak interactions or phenotypes, while "-" indicates no interactions or phenotypes for the respective experiments performed.

S8 Table. Primer sequences used in this study.

S9 Table. Cloning details of constructs used for the hypersensitive response cell death assays.

S1 Data. Underlying numerical data for Figs 2B, 2C, 2D, 4B, 4C, 4E, 5C, 6B, 6E, 7D, 8B, 8C, and 8D, and S2, S4, S5, S6, S7, S9B, and S17B Figs.

S1 Raw images. Raw images for Fig 7B and S8, S13, S15, S16, S18, and S19 Figs.

1. Flor HH. Current Status of the Gene-For-Gene Concept. Annu Rev Phytopathol. 1971;9: 275–296. doi:10.1146/annurev.py.09.090171.001423

2. Wu C-H, Derevnina L, Kamoun S. Receptor networks underpin plant immunity. Science. 2018;360: 1300–1301. doi:10.1126/science.aat2623

3. Derevnina L, Contreras MP, Adachi H, Upson J, Cruces AV, Xie R, et al. Plant pathogens convergently evolved to counteract redundant nodes of an NLR immune receptor network. PLOS Biol. 2021;19: e3001136. doi:10.1371/journal.pbio.3001136

4. Petit-Houdenot Y, Fudal I. Complex Interactions between Fungal Avirulence Genes and Their Corresponding Plant Resistance Genes and Consequences for Disease Resistance Management. Front Plant Sci. 2017;8. doi:10.3389/fpls.2017.01072

5. Bourras S, McNally KE, Müller MC, Wicker T, Keller B. Avirulence Genes in Cereal Powdery Mildews: The Gene-for-Gene Hypothesis 2.0. Front Plant Sci. 2016;7. doi:10.3389/fpls.2016.00241

6. Dean R, Van Kan J a. L, Pretorius ZA, Hammond-Kosack KE, Di Pietro A, Spanu PD, et al. The Top 10 fungal pathogens in molecular plant pathology. Mol Plant Pathol. 2012;13: 414–430. doi:10.1111/j.1364-3703.2011.00783.x

7. Gladieux P, Condon B, Ravel S, Soanes D, Maciel JLN, Nhani A, et al. Gene Flow between Divergent Cereal- and Grass-Specific Lineages of the Rice Blast Fungus Magnaporthe oryzae. Taylor JW, editor. mBio. 2018;9: e01219-17. doi:10.1128/mBio.01219-17

8. Barragan AC, Latorre SM, Mock PG, Harant A, Win J, Malmgren A, et al. Wild grass isolates of Magnaporthe (Syn. Pyricularia) spp. from Germany can cause blast disease on cereal crops. bioRxiv; 2022. p. 2022.08.29.505667. doi:10.1101/2022.08.29.505667

9. Tosa Y, Osue J, Eto Y, Oh H-S, Nakayashiki H, Mayama S, et al. Evolution of an Avirulence Gene, AVR1-CO39, Concomitant with the Evolution and Differentiation of Magnaporthe oryzae. Mol Plant-Microbe Interactions. 2005;18: 1148–1160. doi:10.1094/MPMI-18-1148

10. Chiapello H, Mallet L, Guérin C, Aguileta G, Amselem J, Kroj T, et al. Deciphering Genome Content and Evolutionary Relationships of Isolates from the Fungus Magnaporthe oryzae Attacking Different Host Plants. Genome Biol Evol. 2015;7: 2896–2912. doi:10.1093/gbe/evv187

11. Yoshida K, Saunders DGO, Mitsuoka C, Natsume S, Kosugi S, Saitoh H, et al. Host specialization of the blast fungus Magnaporthe oryzae is associated with dynamic gain and loss of genes linked to transposable elements. BMC Genomics. 2016;17: 370. doi:10.1186/s12864-016-2690-6

12. Inoue Y, Vy TTP, Yoshida K, Asano H, Mitsuoka C, Asuke S, et al. Evolution of the wheat blast fungus through functional losses in a host specificity determinant. Science. 2017;357: 80–83. doi:10.1126/science.aam9654

13. Franceschetti M, Maqbool A, Jiménez-Dalmaroni MJ, Pennington HG, Kamoun S, Banfield MJ. Effectors of Filamentous Plant Pathogens: Commonalities amid Diversity. Microbiol Mol Biol Rev. 2017;81: e00066-16. doi:10.1128/MMBR.00066-16

14. Kang S, Sweigard JA, Valent B. The PWL host specificity gene family in the blast fungus Magnaporthe grisea. Mol Plant-Microbe Interactions. 1995;8: 939–948.

15. Sweigard JA, Carroll AM, Kang S, Farrall L, Chumley FG, Valent B. Identification, cloning, and characterization of PWL2, a gene for host species specificity in the rice blast fungus. Plant Cell. 1995;7: 1221–1233.

16. Orbach MJ, Farrall L, Sweigard JA, Chumley FG, Valent B. A Telomeric Avirulence Gene Determines Efficacy for the Rice Blast Resistance Gene Pi-ta. Plant Cell. 2000;12: 2019–2032. doi:10.1105/tpc.12.11.2019

17. Miki S, Matsui K, Kito H, Otsuka K, Ashizawa T, Yasuda N, et al. Molecular cloning and characterization of the AVR-Pia locus from a Japanese field isolate of Magnaporthe oryzae. Mol Plant Pathol. 2009;10: 361–374. doi:10.1111/j.1364-3703.2009.00534.x

18. Yoshida K, Saitoh H, Fujisawa S, Kanzaki H, Matsumura H, Yoshida K, et al. Association Genetics Reveals Three Novel Avirulence Genes from the Rice Blast Fungal Pathogen Magnaporthe oryzae. Plant Cell. 2009;21: 1573–1591. doi:10.1105/tpc.109.066324

19. Farman ML, Leong SA. Chromosome Walking to the AVR1-CO39 Avirulence Gene of Magnaporthe grisea: Discrepancy Between the Physical and Genetic Maps. Genetics. 1998;150: 1049–1058. doi:10.1093/genetics/150.3.1049

20. Ribot C, Césari S, Abidi I, Chalvon V, Bournaud C, Vallet J, et al. The Magnaporthe oryzae effector AVR1–CO39 is translocated into rice cells independently of a fungal-derived machinery. Plant J. 2013;74: 1–12. doi:10.1111/tpj.12099

21. Li W, Wang B, Wu J, Lu G, Hu Y, Zhang X, et al. The Magnaporthe oryzae Avirulence Gene AvrPiz-t Encodes a Predicted Secreted Protein That Triggers the Immunity in Rice Mediated by the Blast Resistance Gene Piz-t. Mol Plant-Microbe Interactions. 2009;22: 411–420. doi:10.1094/MPMI-22-4-0411

22. Wu J, Kou Y, Bao J, Li Y, Tang M, Zhu X, et al. Comparative genomics identifies the Magnaporthe oryzae avirulence effector AvrPi9 that triggers Pi9-mediated blast resistance in rice. New Phytol. 2015;206: 1463–1475. doi:10.1111/nph.13310

23. Zhang S, Wang L, Wu W, He L, Yang X, Pan Q. Function and evolution of Magnaporthe oryzae avirulence gene AvrPib responding to the rice blast resistance gene Pib. Sci Rep. 2015;5: 11642. doi:10.1038/srep11642

24. Ray S, Singh PK, Gupta DK, Mahato AK, Sarkar C, Rathour R, et al. Analysis of Magnaporthe oryzae Genome Reveals a Fungal Effector, Which Is Able to Induce Resistance Response in Transgenic Rice Line Containing Resistance Gene, Pi54. Front Plant Sci. 2016;7: 1140. doi:10.3389/fpls.2016.01140

25. Anh VL, Inoue Y, Asuke S, Vy TTP, Anh NT, Wang S, et al. Rmg8 and Rmg7, wheat genes for resistance to the wheat blast fungus, recognize the same avirulence gene AVR-Rmg8. Mol Plant Pathol. 2018;19: 1252–1256. doi:10.1111/mpp.12609

26. Shimizu M, Hirabuchi A, Sugihara Y, Abe A, Takeda T, Kobayashi M, et al. A genetically linked pair of NLR immune receptors shows contrasting patterns of evolution. Proc Natl Acad Sci. 2022;119: e2116896119. doi:10.1073/pnas.2116896119

27. Zhang Z-M, Zhang X, Zhou Z-R, Hu H-Y, Liu M, Zhou B, et al. Solution structure of the Magnaporthe oryzae avirulence protein AvrPiz-t. J Biomol NMR. 2013;55: 219–223. doi:10.1007/s10858-012-9695-5

28. de Guillen K, Ortiz-Vallejo D, Gracy J, Fournier E, Kroj T, Padilla A. Structure Analysis Uncovers a Highly Diverse but Structurally Conserved Effector Family in Phytopathogenic Fungi. PLOS Pathog. 2015;11: e1005228. doi:10.1371/journal.ppat.1005228

29. Maqbool A, Saitoh H, Franceschetti M, Stevenson C, Uemura A, Kanzaki H, et al. Structural basis of pathogen recognition by an integrated HMA domain in a plant NLR immune receptor. Nürnberger T, editor. eLife. 2015;4: e08709. doi:10.7554/eLife.08709

30. Zhang X, He D, Zhao Y, Cheng X, Zhao W, Taylor IA, et al. A positive-charged patch and stabilized hydrophobic core are essential for avirulence function of AvrPib in the rice blast fungus. Plant J. 2018;96: 133–146. doi:10.1111/tpj.14023

31. De la Concepcion JC, Fujisaki K, Bentham AR, Cruz Mireles N, Sanchez de Medina Hernandez V, Shimizu M, et al. A blast fungus zinc-finger fold effector binds to a hydrophobic pocket in host Exo70 proteins to modulate immune recognition in rice. Proc Natl Acad Sci. 2022;119: e2210559119. doi:10.1073/pnas.2210559119

32. Petit-Houdenot Y, Langner T, Harant A, Win J, Kamoun S. A Clone Resource of Magnaporthe oryzae Effectors That Share Sequence and Structural Similarities Across Host-Specific Lineages. Mol Plant-Microbe Interactions. 2020;33: 1032–1035. doi:10.1094/MPMI-03-20-0052-A

33. Bentham AR, Petit-Houdenot Y, Win J, Chuma I, Terauchi R, Banfield MJ, et al. A single amino acid polymorphism in a conserved effector of the multihost blast fungus pathogen expands host-target binding spectrum. PLOS Pathog. 2021;17: e1009957. doi:10.1371/journal.ppat.1009957

34. Seong K, Krasileva K. Comparative computational structural genomics highlights divergent evolution of fungal effectors. bioRxiv; 2022. p. 2022.05.02.490317. doi:10.1101/2022.05.02.490317

35. Seong K, Krasileva KV. Computational Structural Genomics Unravels Common Folds and Novel Families in the Secretome of Fungal Phytopathogen Magnaporthe oryzae. Mol Plant-Microbe Interactions. 2021;34: 1267–1280. doi:10.1094/MPMI-03-21-0071-R

36. Ma L-J, van der Does HC, Borkovich KA, Coleman JJ, Daboussi M-J, Di Pietro A, et al. Comparative genomics reveals mobile pathogenicity chromosomes in Fusarium. Nature. 2010;464: 367–373. doi:10.1038/nature08850

37. Stukenbrock EH, Jørgensen FG, Zala M, Hansen TT, McDonald BA, Schierup MH. Whole-Genome and Chromosome Evolution Associated with Host Adaptation and Speciation of the Wheat Pathogen Mycosphaerella graminicola. PLOS Genet. 2010;6: e1001189. doi:10.1371/journal.pgen.1001189

38. Goodwin SB, M'Barek SB, Dhillon B, Wittenberg AHJ, Crane CF, Hane JK, et al. Finished Genome of the Fungal Wheat Pathogen Mycosphaerella graminicola Reveals Dispensome Structure, Chromosome Plasticity, and Stealth Pathogenesis. PLOS Genet. 2011;7: e1002070. doi:10.1371/journal.pgen.1002070

39. Croll D, Zala M, McDonald BA. Breakage-fusion-bridge Cycles and Large Insertions Contribute to the Rapid Evolution of Accessory Chromosomes in a Fungal Pathogen. PLOS Genet. 2013;9: e1003567. doi:10.1371/journal.pgen.1003567

40. Croll D, McDonald BA. The Accessory Genome as a Cradle for Adaptive Evolution in Pathogens. PLOS Pathog. 2012;8: e1002608. doi:10.1371/journal.ppat.1002608

41. Jones N. New species with B chromosomes discovered since 1980. The Nucleus. 2017;60: 263–281. doi:10.1007/s13237-017-0215-6

42. Talbot NJ, Salch YP, Ma M, Hamer JE. Karyotypic Variation within Clonal Lineages of the Rice Blast Fungus, Magnaporthe grisea. Appl Environ Microbiol. 1993;59: 585–593. doi:10.1128/aem.59.2.585-593.1993

43. Orbach MJ, Chumley FG, Valent B. Electrophoretic karyotypes of Magnaporthe grisea pathogens of diverse grasses. Mol Plant-Microbe Interactions. 1996;9: 261–271.

44. Mills D, McCluskey K. Electrophoretic karyotypes of fungi: the new cytology. Mol Plant Microbe Interact. 1990;3: 351–357.

45. Peng Z, Oliveira-Garcia E, Lin G, Hu Y, Dalby M, Migeon P, et al. Effector gene reshuffling involves dispensable mini-chromosomes in the wheat blast fungus. PLOS Genet. 2019;15: e1008272. doi:10.1371/journal.pgen.1008272

46. Langner T, Harant A, Gomez-Luciano LB, Shrestha RK, Malmgren A, Latorre SM, et al. Genomic rearrangements generate hypervariable mini-chromosomes in host-specific isolates of the blast fungus. PLOS Genet. 2021;17: e1009386. doi:10.1371/journal.pgen.1009386

47. Chuma I, Isobe C, Hotta Y, Ibaragi K, Futamata N, Kusaba M, et al. Multiple Translocation of the AVR-Pita Effector Gene among Chromosomes of the Rice Blast Fungus Magnaporthe oryzae and Related Species. PLOS Pathog. 2011;7: e1002147. doi:10.1371/journal.ppat.1002147

48. Luo C-X, Yin L-F, Ohtaka K, Kusaba M. The 1.6Mb chromosome carrying the avirulence gene AvrPik in Magnaporthe oryzae isolate 84R-62B is a chimera containing chromosome 1 sequences. Mycol Res. 2007;111: 232–239. doi:10.1016/j.mycres.2006.10.008

49. Kusaba M, Mochida T, Naridomi T, Fujita Y, Chuma I, Tosa Y. Loss of a 1.6 Mb chromosome in Pyricularia oryzae harboring two alleles of AvrPik leads to acquisition of virulence to rice cultivars containing resistance alleles at the Pik locus. Curr Genet. 2014;60: 315–325. doi:10.1007/s00294-014-0437-y

50. Böhnert HU, Fudal I, Dioh W, Tharreau D, Notteghem J-L, Lebrun M-H. A Putative Polyketide Synthase/Peptide Synthetase from Magnaporthe grisea Signals Pathogen Attack to Resistant Rice. Plant Cell. 2004;16: 2499–2513. doi:10.1105/tpc.104.022715

51. Mosquera G, Giraldo MC, Khang CH, Coughlan S, Valent B. Interaction Transcriptome Analysis Identifies Magnaporthe oryzae BAS1-4 as Biotrophy-Associated Secreted Proteins in Rice Blast Disease. Plant Cell. 2009;21: 1273–1290. doi:10.1105/tpc.107.055228

52. Ma L-J, Xu J-R. Shuffling effector genes through mini-chromosomes. PLOS Genet. 2019;15: e1008345. doi:10.1371/journal.pgen.1008345

53. Kourelis J, van der Hoorn RAL. Defended to the Nines: 25 Years of Resistance Gene Cloning Identifies Nine Mechanisms for R Protein Function. Plant Cell. 2018;30: 285–299. doi:10.1105/tpc.17.00579

54. Adachi H, Derevnina L, Kamoun S. NLR singletons, pairs, and networks: evolution, assembly, and regulation of the intracellular immunoreceptor circuitry of plants. Curr Opin Plant Biol. 2019;50: 121–131. doi:10.1016/j.pbi.2019.04.007

55. Araújo AC de, Fonseca FCDA, Cotta MG, Alves GSC, Miller RNG. Plant NLR receptor proteins and their potential in the development of durable genetic resistance to biotic stresses. Biotechnol Res Innov. 2019;3: 80–94. doi:10.1016/j.biori.2020.01.002

56. Takken FL, Goverse A. How to build a pathogen detector: structural basis of NB-LRR function. Curr Opin Plant Biol. 2012;15: 375–384. doi:10.1016/j.pbi.2012.05.001

57. Shao Z-Q, Xue J-Y, Wu P, Zhang Y-M, Wu Y, Hang Y-Y, et al. Large-Scale Analyses of Angiosperm Nucleotide-Binding Site-Leucine-Rich Repeat Genes Reveal Three Anciently Diverged Classes with Distinct Evolutionary Patterns. Plant Physiol. 2016;170: 2095–2109. doi:10.1104/pp.15.01487

58. Shao Z-Q, Xue J-Y, Wang Q, Wang B, Chen J-Q. Revisiting the Origin of Plant NBS-LRR Genes. Trends Plant Sci. 2019;24: 9–12. doi:10.1016/j.tplants.2018.10.015

59. Kourelis J, Sakai T, Adachi H, Kamoun S. RefPlantNLR is a comprehensive collection of experimentally validated plant disease resistance proteins from the NLR family. PLOS Biol. 2021;19: e3001124. doi:10.1371/journal.pbio.3001124

60. Barragan AC, Weigel D. Plant NLR diversity: the known unknowns of pan-NLRomes. Plant Cell. 2021;33: 814–831. doi:10.1093/plcell/koaa002

61. Ashikawa I, Hayashi N, Yamane H, Kanamori H, Wu J, Matsumoto T, et al. Two Adjacent Nucleotide-Binding Site–Leucine-Rich Repeat Class Genes Are Required to Confer Pikm-Specific Rice Blast Resistance. Genetics. 2008;180: 2267–2276. doi:10.1534/genetics.108.095034

62. Lee S-K, Song M-Y, Seo Y-S, Kim H-K, Ko S, Cao P-J, et al. Rice Pi5-Mediated Resistance to Magnaporthe oryzae Requires the Presence of Two Coiled-Coil–Nucleotide-Binding–Leucine-Rich Repeat Genes. Genetics. 2009;181: 1627–1638. doi:10.1534/genetics.108.099226

63. Narusaka M, Shirasu K, Noutoshi Y, Kubo Y, Shiraishi T, Iwabuchi M, et al. RRS1 and RPS4 provide a dual Resistance-gene system against fungal and bacterial pathogens. Plant J. 2009;60: 218–226. doi:10.1111/j.1365-313X.2009.03949.x

64. Okuyama Y, Kanzaki H, Abe A, Yoshida K, Tamiru M, Saitoh H, et al. A multifaceted genomics approach allows the isolation of the rice Pia-blast resistance gene consisting of two adjacent NBS-LRR protein genes. Plant J. 2011;66: 467–479. doi:10.1111/j.1365-313X.2011.04502.x

65. Białas A, Zess EK, De la Concepcion JC, Franceschetti M, Pennington HG, Yoshida K, et al. Lessons in Effector and NLR Biology of Plant-Microbe Systems. Mol Plant-Microbe Interactions. 2018;31: 34–45. doi:10.1094/MPMI-08-17-0196-FI

66. Césari S, Bernoux M, Moncuquet P, Kroj T, Dodds P. A novel conserved mechanism for plant NLR protein pairs: the 'integrated decoy' hypothesis. Front Plant Sci. 2014;5. doi:10.3389/fpls.2014.00606

67. Cesari S. Multiple strategies for pathogen perception by plant immune receptors. New Phytol. 2018;219: 17–24. doi:10.1111/nph.14877

68. Takagi H, Uemura A, Yaegashi H, Tamiru M, Abe A, Mitsuoka C, et al. MutMap-Gap: whole-genome resequencing of mutant F2 progeny bulk combined with de novo assembly of gap regions identifies the rice blast resistance gene Pii. New Phytol. 2013;200: 276–283. doi:10.1111/nph.12369

69. Cesari S, Thilliez G, Ribot C, Chalvon V, Michel C, Jauneau A, et al. The Rice Resistance Protein Pair RGA4/RGA5 Recognizes the Magnaporthe oryzae Effectors AVR-Pia and AVR1-CO39 by Direct Binding. Plant Cell. 2013;25: 1463–1481. doi:10.1105/tpc.112.107201

70. Kanzaki H, Yoshida K, Saitoh H, Fujisaki K, Hirabuchi A, Alaux L, et al. Arms race co-evolution of Magnaporthe oryzae AVR-Pik and rice Pik genes driven by their physical interactions. Plant J. 2012;72: 894–907. doi:10.1111/j.1365-313X.2012.05110.x

71. De la Concepcion JC, Franceschetti M, Maqbool A, Saitoh H, Terauchi R, Kamoun S, et al. Polymorphic residues in rice NLRs expand binding and response to effectors of the blast pathogen. Nat Plants. 2018;4: 576–585. doi:10.1038/s41477-018-0194-x

72. Białas A, Langner T, Harant A, Contreras MP, Stevenson CE, Lawson DM, et al. Two NLR immune receptors acquired high-affinity binding to a fungal effector through convergent evolution of their integrated domain. Monaghan J, Kleine-Vehn J, Delaux P-M, editors. eLife. 2021;10: e66961. doi:10.7554/eLife.66961

73. De la Concepcion JC, Maidment JHR, Longya A, Xiao G, Franceschetti M, Banfield MJ. The allelic rice immune receptor Pikh confers extended resistance to strains of the blast fungus through a single polymorphism in the effector binding interface. Birch P, editor. PLOS Pathog. 2021;17: e1009368. doi:10.1371/journal.ppat.1009368

74. Ortiz D, de Guillen K, Cesari S, Chalvon V, Gracy J, Padilla A, et al. Recognition of the Magnaporthe oryzae Effector AVR-Pia by the Decoy Domain of the Rice NLR Immune Receptor RGA5. Plant Cell. 2017;29: 156–168. doi:10.1105/tpc.16.00435

75. Guo L, Cesari S, de Guillen K, Chalvon V, Mammri L, Ma M, et al. Specific recognition of two MAX effectors by integrated HMA domains in plant immune receptors involves distinct binding surfaces. Proc Natl Acad Sci. 2018;115: 11637–11642. doi:10.1073/pnas.1810705115

76. Oikawa K, Fujisaki K, Shimizu M, Takeda T, Saitoh H, Hirabuchi A, et al. The blast pathogen effector AVR-Pik binds and stabilizes rice heavy metal-associated (HMA) proteins to co-opt their function in immunity. bioRxiv; 2020. p. 2020.12.01.406389. doi:10.1101/2020.12.01.406389

77. Fukuoka S, Saka N, Koga H, Ono K, Shimizu T, Ebana K, et al. Loss of Function of a Proline-Containing Protein Confers Durable Disease Resistance in Rice. Science. 2009;325: 998–1001. doi:10.1126/science.1175550

78. Maidment JHR, Franceschetti M, Maqbool A, Saitoh H, Jantasuriyarat C, Kamoun S, et al. Multiple variants of the fungal effector AVR-Pik bind the HMA domain of the rice protein OsHIPP19, providing a foundation to engineer plant defense. J Biol Chem. 2021;296. doi:10.1016/j.jbc.2021.100371

79. Fujisaki K, Abe Y, Kanzaki E, Ito K, Utsushi H, Saitoh H, et al. An unconventional NOI/RIN4 domain of a rice NLR protein binds host EXO70 protein to confer fungal immunity. bioRxiv; 2017. p. 239400. doi:10.1101/239400

80. Fujisaki K, Abe Y, Ito A, Saitoh H, Yoshida K, Kanzaki H, et al. Rice Exo70 interacts with a fungal effector, AVR-Pii, and is required for AVR-Pii-triggered immunity. Plant J. 2015;83: 875–887. doi:10.1111/tpj.12934

81. De la Concepcion JC, Franceschetti M, MacLean D, Terauchi R, Kamoun S, Banfield MJ. Protein engineering expands the effector recognition profile of a rice NLR immune receptor. Nürnberger T, Weigel D, Nürnberger T, editors. eLife. 2019;8: e47713. doi:10.7554/eLife.47713

82. Kourelis J, Marchal C, Kamoun S. NLR immune receptor-nanobody fusions confer plant disease resistance. bioRxiv; 2021. doi:10.1101/2021.10.24.465418

83. Liu Y, Zhang X, Yuan G, Wang D, Zheng Y, Ma M, et al. A designer rice NLR immune receptor confers resistance to the rice blast fungus carrying noncorresponding avirulence effectors. Proc Natl Acad Sci. 2021;118: e2110751118. doi:10.1073/pnas.2110751118

84. Cesari S, Xi Y, Declerck N, Chalvon V, Mammri L, Pugnière M, et al. New recognition specificity in a plant immune receptor by molecular engineering of its integrated domain. Nat Commun. 2022;13: 1524. doi:10.1038/s41467-022-29196-6

85. Marchal C, Michalopoulou VA, Zou Z, Cevik V, Sarris PF. Show me your ID: NLR immune receptors with integrated domains in plants. Essays Biochem. 2022; EBC20210084. doi:10.1042/EBC20210084

86. Maidment JH, Shimizu M, Vera S, Franceschetti M, Longya A, Stevenson CE, et al. Effector target-guided engineering of an integrated domain expands the disease resistance profile of a rice NLR immune receptor. bioRxiv; 2022. p. 2022.06.14.496076. doi:10.1101/2022.06.14.496076

87. Zhang X, Liu Y, Yuan G, Wang D, Zhu T, Wu X, et al. The effector recognition by synthetic sensor NLR receptors requires the concerted action of multiple interfaces within and outside the integrated domain. bioRxiv; 2022. p. 2022.08.17.504349. doi:10.1101/2022.08.17.504349

88. Bentham AR, Concepcion JCD la, Benjumea JV, Jones S, Mendel M, Stubbs J, et al. Allelic compatibility in plant immune receptors facilitates engineering of new effector recognition specificities. bioRxiv; 2022. p. 2022.10.10.511592. doi:10.1101/2022.10.10.511592

89. Marchal C, Pai H, Kamoun S, Kourelis J. Emerging principles in the design of bioengineered made-to-order plant immune receptors. Curr Opin Plant Biol. 2022; 102311. doi:10.1016/j.pbi.2022.102311

90. Wang B, Ebbole DJ, Wang Z. The arms race between Magnaporthe oryzae and rice: Diversity and interaction of Avr and R genes. J Integr Agric. 2017;16: 2746–2760. doi:10.1016/S2095-3119(17)61746-5

91. Yuan B, Zhai C, Wang W, Zeng X, Xu X, Hu H, et al. The Pik-p resistance to Magnaporthe oryzae in rice is mediated by a pair of closely linked CC-NBS-LRR genes. Theor Appl Genet. 2011;122: 1017–1028. doi:10.1007/s00122-010-1506-3

92. Zhai C, Lin F, Dong Z, He X, Yuan B, Zeng X, et al. The isolation and characterization of Pik, a rice blast resistance gene which emerged after rice domestication. New Phytol. 2011;189: 321–334. doi:10.1111/j.1469-8137.2010.03462.x

93. Ashikawa I, Hayashi N, Abe F, Wu J, Matsumoto T. Characterization of the rice blast resistance gene Pik cloned from Kanto51. Mol Breed. 2012;30: 485–494. doi:10.1007/s11032-011-9638-y

94. Zhai C, Zhang Y, Yao N, Lin F, Liu Z, Dong Z, et al. Function and Interaction of the Coupled Genes Responsible for Pik-h Encoded Rice Blast Resistance. PLOS ONE. 2014;9: e98067. doi:10.1371/journal.pone.0098067

95. Chen J, Peng P, Tian J, He Y, Zhang L, Liu Z, et al. Pike, a rice blast resistance allele consisting of two adjacent NBS–LRR genes, was identified as a novel allele at the Pik locus. Mol Breed. 2015;35: 117. doi:10.1007/s11032-015-0305-6

96. Li J, Wang Q, Li C, Bi Y, Fu X, Wang R. Novel haplotypes and networks of AVR-Pik alleles in Magnaporthe oryzae. BMC Plant Biol. 2019;19: 204. doi:10.1186/s12870-019-1817-8

97. Takahashi A, Hayashi N, Miyao A, Hirochika H. Unique features of the rice blast resistance Pish locus revealed by large scale retrotransposon-tagging. BMC Plant Biol. 2010;10: 175. doi:10.1186/1471-2229-10-175

98. Zdrzałek R, Kamoun S, Terauchi R, Saitoh H, Banfield MJ. The rice NLR pair Pikp-1/Pikp-2 initiates cell death through receptor cooperation rather than negative regulation. PLOS ONE. 2020;15: e0238616. doi:10.1371/journal.pone.0238616

99. Simão FA, Waterhouse RM, Ioannidis P, Kriventseva EV, Zdobnov EM. BUSCO: assessing genome assembly and annotation completeness with single-copy orthologs. Bioinformatics. 2015;31: 3210–3212. doi:10.1093/bioinformatics/btv351

100. Dean RA, Talbot NJ, Ebbole DJ, Farman ML, Mitchell TK, Orbach MJ, et al. The genome sequence of the rice blast fungus Magnaporthe grisea. Nature. 2005;434: 980–986. doi:10.1038/nature03449

101. Bao J, Chen M, Zhong Z, Tang W, Lin L, Zhang X, et al. PacBio Sequencing Reveals Transposable Elements as a Key Contributor to Genomic Plasticity and Virulence Variation in Magnaporthe oryzae. Mol Plant. 2017;10: 1465–1468. doi:10.1016/j.molp.2017.08.008

102. Gómez Luciano LB, Tsai IJ, Chuma I, Tosa Y, Chen Y-H, Li J-Y, et al. Blast Fungal Genomes Show Frequent Chromosomal Changes, Gene Gains and Losses, and Effector Gene Turnover. Mol Biol Evol. 2019;36: 1148–1161. doi:10.1093/molbev/msz045

103. Win J, Harant A, Malmgren A, Langner T, Shrestha R-K, Latorre SM, et al. Large scale genome assemblies of Magnaporthe oryzae rice isolates from Italy. 2020 [cited 22 Mar 2022]. doi:10.5281/zenodo.4326823

104. Slater GSC, Birney E. Automated generation of heuristics for biological sequence comparison. BMC Bioinformatics. 2005;6: 31. doi:10.1186/1471-2105-6-31

105. Starnes JH, Thornbury DW, Novikova OS, Rehmeyer CJ, Farman ML. Telomere-Targeted Retrotransposons in the Rice Blast Fungus Magnaporthe oryzae: Agents of Telomere Instability. Genetics. 2012;191: 389–406. doi:10.1534/genetics.111.137950

106. Teufel F, Almagro Armenteros JJ, Johansen AR, Gíslason MH, Pihl SI, Tsirigos KD, et al. SignalP 6.0 predicts all five types of signal peptides using protein language models. Nat Biotechnol. 2022; 1–3. doi:10.1038/s41587-021-01156-3

107. Enright AJ, Van Dongen S, Ouzounis CA. An efficient algorithm for large-scale detection of protein families. Nucleic Acids Res. 2002;30: 1575–1584. doi:10.1093/nar/30.7.1575

108. Jumper J, Evans R, Pritzel A, Green T, Figurnov M, Ronneberger O, et al. Highly accurate protein structure prediction with AlphaFold. Nature. 2021;596: 583–589. doi:10.1038/s41586-021-03819-2

109. Zhang Y, Skolnick J. TM-align: a protein structure alignment algorithm based on the TM-score. Nucleic Acids Res. 2005;33: 2302–2309. doi:10.1093/nar/gki524

110. Xu J, Zhang Y. How significant is a protein structure similarity with TM-score = 0.5? Bioinformatics. 2010;26: 889–895. doi:10.1093/bioinformatics/btq066

111. Xue M, Yang J, Li Z, Hu S, Yao N, Dean RA, et al. Comparative Analysis of the Genomes of Two Field Isolates of the Rice Blast Fungus Magnaporthe oryzae. PLOS Genet. 2012;8: e1002869. doi:10.1371/journal.pgen.1002869

112. Longya A, Chaipanya C, Franceschetti M, Maidment JHR, Banfield MJ, Jantasuriyarat C. Gene Duplication and Mutation in the Emergence of a Novel Aggressive Allele of the AVR-Pik Effector in the Rice Blast Fungus. Mol Plant-Microbe Interactions. 2019;32: 740–749. doi:10.1094/MPMI-09-18-0245-R

113. Zhu K, Bao J, Zhang L, Yang X, Li Y, Zhu M, et al. Comparative analysis of the genome of the field isolate V86010 of the rice blast fungus Magnaporthe oryzae from Philippines. J Integr Agric. 2017;16: 2222–2230. doi:10.1016/S2095-3119(16)61607-6

114. Zhong Z, Norvienyeku J, Chen M, Bao J, Lin L, Chen L, et al. Directional Selection from Host Plants Is a Major Force Driving Host Specificity in Magnaporthe Species. Sci Rep. 2016;6: 25591. doi:10.1038/srep25591

115. Kim K-T, Ko J, Song H, Choi G, Kim H, Jeon J, et al. Evolution of the Genes Encoding Effector Candidates Within Multiple Pathotypes of Magnaporthe oryzae. Front Microbiol. 2019;10. doi:10.3389/fmicb.2019.02575

116. Varden FA, Saitoh H, Yoshino K, Franceschetti M, Kamoun S, Terauchi R, et al. Cross-reactivity of a rice NLR immune receptor to distinct effectors from the rice blast pathogen Magnaporthe oryzae provides partial disease resistance. J Biol Chem. 2019;294: 13006–13016. doi:10.1074/jbc.RA119.007730

117. Xiao G, Wang W, Liu M, Li Y, Liu J, Franceschetti M, et al. The Piks allele of the NLR immune receptor Pik breaks the recognition of AvrPik effectors of the rice blast fungus. J Integr Plant Biol. n/a. doi:10.1111/jipb.13375

118. Césari S, Kanzaki H, Fujiwara T, Bernoux M, Chalvon V, Kawano Y, et al. The NB-LRR proteins RGA4 and RGA5 interact functionally and physically to confer disease resistance. EMBO J. 2014;33: 1941–1959. doi:10.15252/embj.201487923

119. De la Concepcion JC, Vega Benjumea J, Bialas A, Terauchi R, Kamoun S, Banfield MJ. Functional diversification gave rise to allelic specialization in a rice NLR immune receptor pair. Zhou J-M, Kleine-Vehn J, Zhou J-M, Chae E, editors. eLife. 2021;10: e71662. doi:10.7554/eLife.71662

120. Pettersen EF, Goddard TD, Huang CC, Meng EC, Couch GS, Croll TI, et al. UCSF ChimeraX: Structure visualization for researchers, educators, and developers. Protein Sci. 2021;30: 70–82. doi:10.1002/pro.3943

121. Raffaele S, Farrer RA, Cano LM, Studholme DJ, MacLean D, Thines M, et al. Genome Evolution Following Host Jumps in the Irish Potato Famine Pathogen Lineage. Science. 2010;330: 1540–1543. doi:10.1126/science.1193070

122. Raffaele S, Kamoun S. Genome evolution in filamentous plant pathogens: why bigger can be better. Nat Rev Microbiol. 2012;10: 417–430. doi:10.1038/nrmicro2790

123. Dong S, Raffaele S, Kamoun S. The two-speed genomes of filamentous pathogens: waltz with plants. Curr Opin Genet Dev. 2015;35: 57–65. doi:10.1016/j.gde.2015.09.001

124. Brabham HJ, Cruz DGDL, Were V, Shimizu M, Saitoh H, Hernández-Pinzón I, et al. Barley MLA3 recognizes the host-specificity determinant PWL2 from rice blast (M. oryzae). bioRxiv; 2022. p. 2022.10.21.512921. doi:10.1101/2022.10.21.512921

125. Deng Y, Zhai K, Xie Z, Yang D, Zhu X, Liu J, et al. Epigenetic regulation of antagonistic receptors confers rice blast resistance with yield balance. Science. 2017;355: 962–965. doi:10.1126/science.aai8898

126. Murakami J, Tosa Y, Kataoka T, Tomita R, Kawasaki J, Chuma I, et al. Analysis of Host Species Specificity of Magnaporthe grisea Toward Wheat Using a Genetic Cross Between Isolates from Wheat and Foxtail Millet. Phytopathology. 2000;90: 1060–1067. doi:10.1094/PHYTO.2000.90.10.1060

127. Lo C-C, Chain PSG. Rapid evaluation and quality control of next generation sequencing data with FaQCs. BMC Bioinformatics. 2014;15: 366. doi:10.1186/s12859-014-0366-2

128. Schmieder R, Edwards R. Quality control and preprocessing of metagenomic datasets. Bioinformatics. 2011;27: 863–864. doi:10.1093/bioinformatics/btr026

129. Kawahara Y, de la Bastide M, Hamilton JP, Kanamori H, McCombie WR, Ouyang S, et al. Improvement of the Oryza sativa Nipponbare reference genome using next generation sequence and optical map data. Rice. 2013;6: 4. doi:10.1186/1939-8433-6-4

130. Li H, Durbin R. Fast and accurate short read alignment with Burrows-Wheeler transform. Bioinformatics. 2009;25: 1754–1760. doi:10.1093/bioinformatics/btp324

131. Li H, Handsaker B, Wysoker A, Fennell T, Ruan J, Homer N, et al. The Sequence Alignment/Map format and SAMtools. Bioinformatics. 2009;25: 2078–2079. doi:10.1093/bioinformatics/btp352

132. McKenna A, Hanna M, Banks E, Sivachenko A, Cibulskis K, Kernytsky A, et al. The Genome Analysis Toolkit: A MapReduce framework for analyzing next-generation DNA sequencing data. Genome Res. 2010;20: 1297–1303. doi:10.1101/gr.107524.110

133. Li H. A statistical framework for SNP calling, mutation discovery, association mapping and population genetical parameter estimation from sequencing data. Bioinformatics. 2011;27: 2987–2993. doi:10.1093/bioinformatics/btr509

134. Fragoso CA, Heffelfinger C, Zhao H, Dellaporta SL. Imputing Genotypes in Biallelic Populations from Low-Coverage Sequence Data. Genetics. 2016;202: 487–495. doi:10.1534/genetics.115.182071

135. De Coster W, D'Hert S, Schultz DT, Cruts M, Van Broeckhoven C. NanoPack: visualizing and processing long-read sequencing data. Bioinformatics. 2018;34: 2666–2669. doi:10.1093/bioinformatics/bty149

136. Chen Y, Nie F, Xie S-Q, Zheng Y-F, Dai Q, Bray T, et al. Efficient assembly of nanopore reads via highly accurate and intact error correction. Nat Commun. 2021;12: 60. doi:10.1038/s41467-020-20236-7

137. Vaser R, Sović I, Nagarajan N, Šikić M. Fast and accurate de novo genome assembly from long uncorrected reads. Genome Res. 2017;27: 737–746. doi:10.1101/gr.214270.116

138. Kundu R, Casey J, Sung W-K. HyPo: Super Fast & Accurate Polisher for Long Read Genome Assemblies. bioRxiv; 2019 Dec. doi:10.1101/2019.12.19.882506

139. Roach MJ, Schmidt SA, Borneman AR. Purge Haplotigs: allelic contig reassignment for third-gen diploid genome assemblies. BMC Bioinformatics. 2018;19: 460. doi:10.1186/s12859-018-2485-7

140. Alonge M, Lebeigle L, Kirsche M, Aganezov S, Wang X, Lippman ZB, et al. Automated assembly scaffolding elevates a new tomato system for high-throughput genome editing. bioRxiv; 2021 Nov. doi:10.1101/2021.11.18.469135

141. Miki D, Shimamoto K. Simple RNAi Vectors for Stable and Transient Suppression of Gene Function in Rice. Plant Cell Physiol. 2004;45: 490–495. doi:10.1093/pcp/pch048

142. Hiei Y, Ohta S, Komari T, Kumashiro T. Efficient transformation of rice (Oryza sativa L.) mediated by Agrobacterium and sequence analysis of the boundaries of the T-DNA. Plant J. 1994;6: 271–282. doi:10.1046/j.1365-313X.1994.6020271.x

143. Katoh K, Standley DM. MAFFT Multiple Sequence Alignment Software Version 7: Improvements in Performance and Usability. Mol Biol Evol. 2013;30: 772–780. doi:10.1093/molbev/mst010

144. Minh BQ, Schmidt HA, Chernomor O, Schrempf D, Woodhams MD, von Haeseler A, et al. IQ-TREE 2: New Models and Efficient Methods for Phylogenetic Inference in the Genomic Era. Mol Biol Evol. 2020;37: 1530–1534. doi:10.1093/molbev/msaa015

145. Hoang DT, Chernomor O, von Haeseler A, Minh BQ, Vinh LS. UFBoot2: Improving the Ultrafast Bootstrap Approximation. Mol Biol Evol. 2018;35: 518–522. doi:10.1093/molbev/msx281

146. Kalyaanamoorthy S, Minh BQ, Wong TKF, von Haeseler A, Jermiin LS. ModelFinder: fast model selection for accurate phylogenetic estimates. Nat Methods. 2017;14: 587–589. doi:10.1038/nmeth.4285

147. Xiao C-L, Chen Y, Xie S-Q, Chen K-N, Wang Y, Han Y, et al. MECAT: fast mapping, error correction, and de novo assembly for single-molecule sequencing reads. Nat Methods. 2017;14: 1072–1074. doi:10.1038/nmeth.4432

148. Stanke M, Diekhans M, Baertsch R, Haussler D. Using native and syntenically mapped cDNA alignments to improve de novo gene finding. Bioinformatics. 2008;24: 637–644. doi:10.1093/bioinformatics/btn013

149. Cabanettes F, Klopp C. D-GENIES: dot plot large genomes in an interactive, efficient and simple way. PeerJ. 2018;6: e4958. doi:10.7717/peerj.4958

150. Quinlan AR, Hall IM. BEDTools: a flexible suite of utilities for comparing genomic features. Bioinformatics. 2010;26: 841–842. doi:10.1093/bioinformatics/btq033

151. Li H. Minimap2: pairwise alignment for nucleotide sequences. Birol I, editor. Bioinformatics. 2018;34: 3094–3100. doi:10.1093/bioinformatics/bty191

152. Ou S, Su W, Liao Y, Chougule K, Agda JRA, Hellinga AJ, et al. Benchmarking transposable element annotation methods for creation of a streamlined, comprehensive pipeline. Genome Biol. 2019;20: 275. doi:10.1186/s13059-019-1905-y

153. Iwata H, Gotoh O. Benchmarking spliced alignment programs including Spaln2, an extended version of Spaln that incorporates additional species-specific features. Nucleic Acids Res. 2012;40: e161. doi:10.1093/nar/gks708

154. Endelman JB. Ridge Regression and Other Kernels for Genomic Selection with R Package rrBLUP. Plant Genome. 2011;4. doi:10.3835/plantgenome2011.08.0024

155. Kim D, Langmead B, Salzberg SL. HISAT: a fast spliced aligner with low memory requirements. Nat Methods. 2015;12: 357–360. doi:10.1038/nmeth.3317

156. Kovaka S, Zimin AV, Pertea GM, Razaghi R, Salzberg SL, Pertea M. Transcriptome assembly from long-read RNA-seq alignments with StringTie2. Genome Biol. 2019;20: 278. doi:10.1186/s13059-019-1910-1

157. Sweigard J, Chumley F, Carroll A, Farrall L, Valent B. A series of vectors for fungal transformation. Fungal Genet Rep. 1997;44: 52–53. doi:10.4148/1941-4765.1287

158. Needleman SB, Wunsch CD. A general method applicable to the search for similarities in the amino acid sequence of two proteins. J Mol Biol. 1970;48: 443–453. doi:10.1016/0022-2836(70)90057-4

159. Camacho C, Coulouris G, Avagyan V, Ma N, Papadopoulos J, Bealer K, et al. BLAST+: architecture and applications. BMC Bioinformatics. 2009;10: 421. doi:10.1186/1471-2105-10-421

160. Van der Hoorn RAL, Laurent F, Roth R, De Wit PJGM. Agroinfiltration Is a Versatile Tool That Facilitates Comparative Analyses of Avr9/Cf-9-Induced and Avr4/Cf-4-Induced Necrosis. Mol Plant-Microbe Interactions. 2000;13: 439–446. doi:10.1094/MPMI.2000.13.4.439

161. Kourelis J, Malik S, Mattinson O, Krauter S, Kahlon PS, Paulus JK, et al. Evolution of a guarded decoy protease and its receptor in solanaceous plants. Nat Commun. 2020;11: 4393. doi:10.1038/s41467-020-18069-5

162. Larsson A. AliView: a fast and lightweight alignment viewer and editor for large datasets. Bioinformatics. 2014;30: 3276–3278. doi:10.1093/bioinformatics/btu531

Fig 1

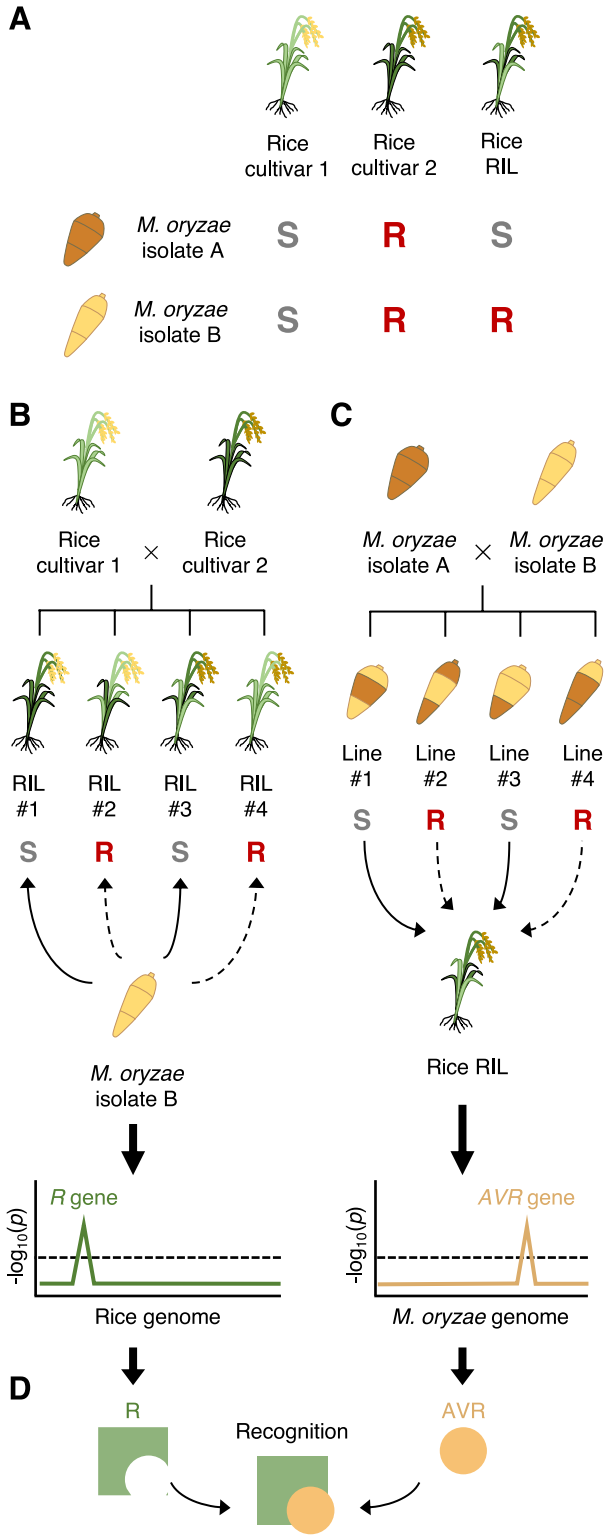
A
Rice cultivar 1
Rice cultivar 2
Rice RIL
M. oryzae isolate A
S
R
S
M. oryzae isolate B
S
R
R
B
Rice cultivar 1
×
Rice cultivar 2
RIL #1
RIL #2
RIL #3
RIL #4
S
R
S
R
M. oryzae isolate B
C
M. oryzae isolate A
×
M. oryzae isolate B
Line #1
Line #2
Line #3
Line #4
S
R
S
R
Rice RIL
R gene
-log10(p)
Rice genome
AVR gene
-log10(p)
M. oryzae genome
D
R
Recognition
AVR

Fig 2

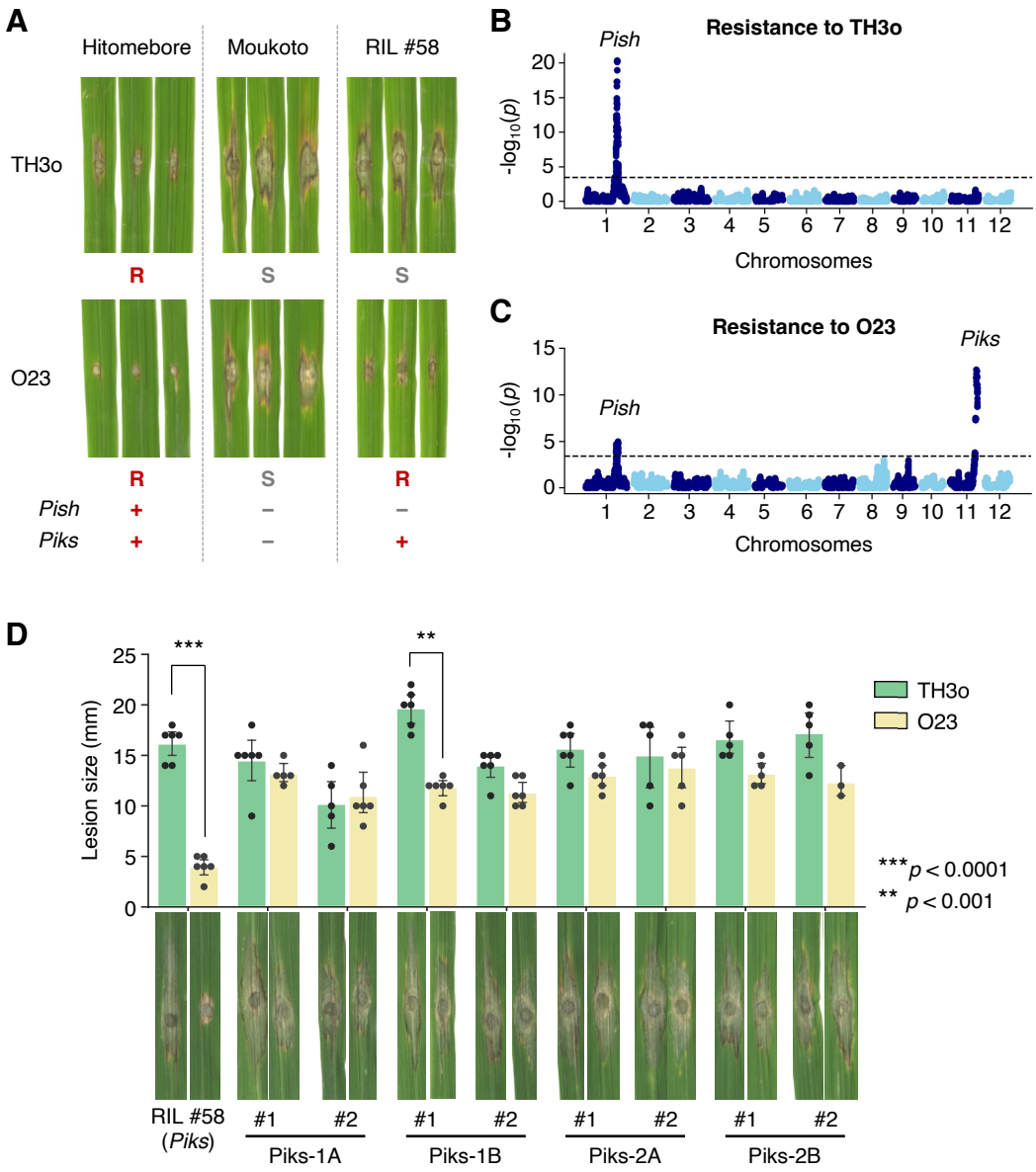
A
Hitomebore
Moukoto
RIL #58
TH3o
R
S
S
O23
R
S
R
Pish
+
–
–
Piks
+
–
+
B
Resistance to TH3o
Pish
-log10(p)
Chromosomes
C
Resistance to O23
Pish
Piks
-log10(p)
Chromosomes
D
Lesion size (mm)
***
**
TH3o
O23
***p < 0.0001
** p < 0.001
RIL #58
(Piks)
#1
#2
Piks-1A
Piks-1B
Piks-2A
Piks-2B

Fig 3

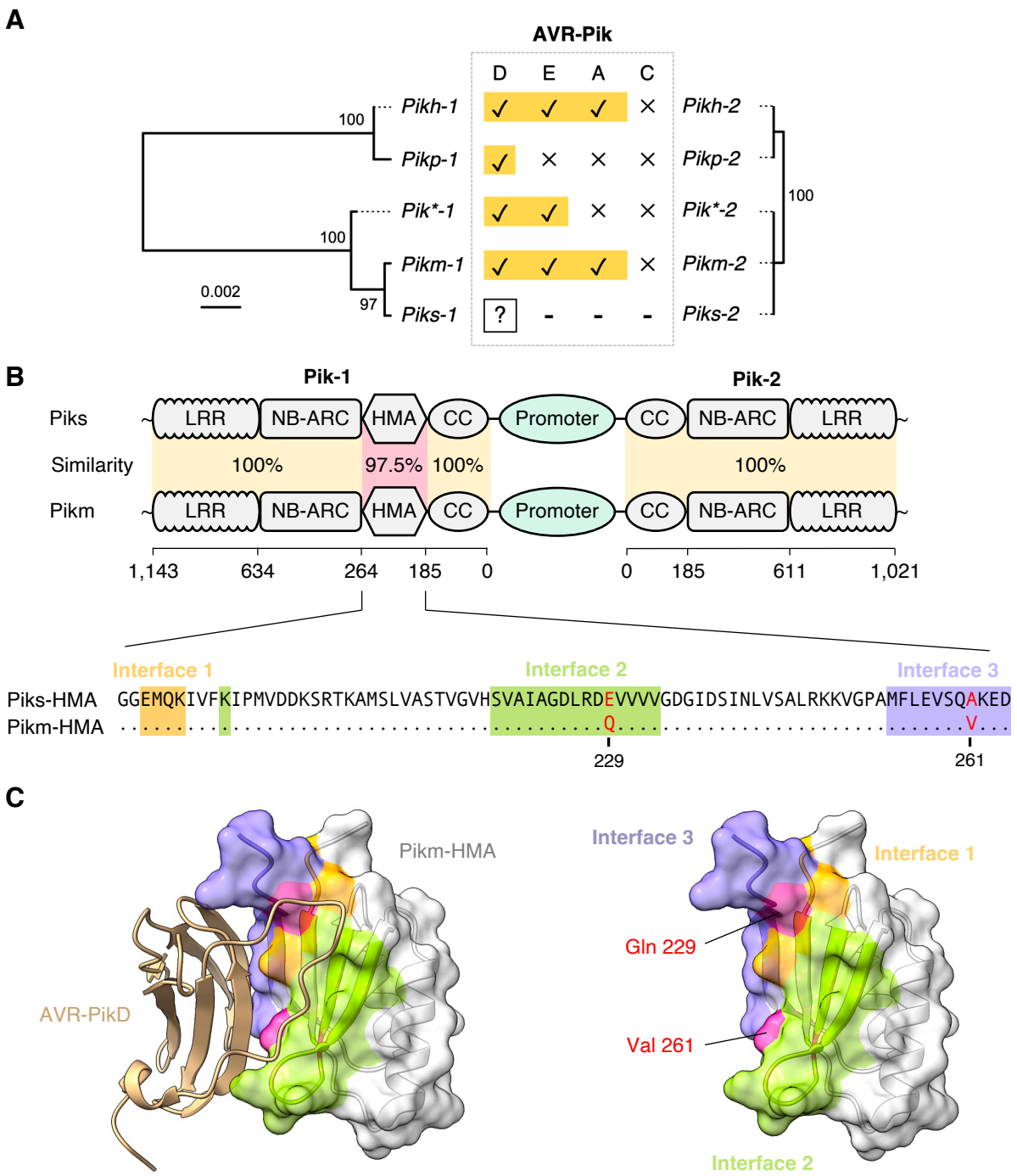
A
AVR-Pik
D E A C
Pikh-1
Pikp-1
Pik*-1
Pikm-1
Piks-1
Pikh-2
Pikp-2
Pik*-2
Pikm-2
Piks-2
100
100
100
97
0.002
B
Pik-1
Pik-2
Piks
Similarity
Pikm
LRR
NB-ARC
HMA
CC
Promoter
100%
97.5%
1,143
634
264
185
0
611
1,021
Interface 1
Interface 2
Interface 3
Piks-HMA GGEMQKIVFKIPMVDDKSRTKAMSLVASTVGVHSVAIAGDLRDEVVVVGDGIDSINLVSALRKKVGPAMFLEVSQAKED
Pikm-HMA
229
261
C
Pikm-HMA
AVR-PikD
Interface 3
Interface 1
Gln 229
Val 261
Interface 2

Fig 4

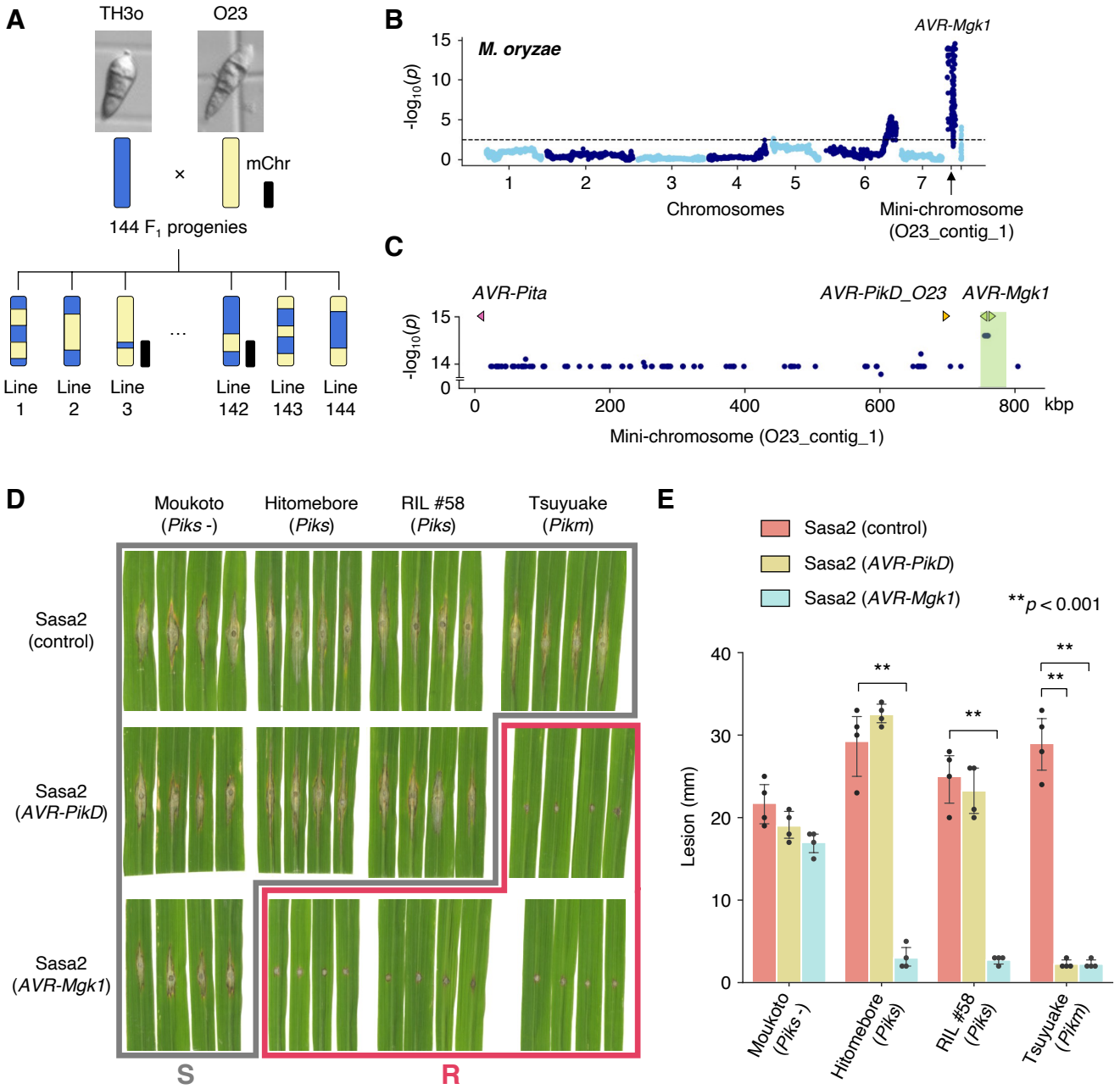
A
TH3o
O23
mChr
×
144 F1 progenies
Line 1
Line 2
Line 3
Line 142
Line 143
Line 144
B
M. oryzae
AVR-Mgk1
-log10(p)
Chromosomes
Mini-chromosome (O23_contig_1)
C
AVR-Pita
AVR-PikD_O23
AVR-Mgk1
-log10(p)
kbp
Mini-chromosome (O23_contig_1)
D
Moukoto (Piks -)
Hitomebore (Piks)
RIL #58 (Piks)
Tsuyuake (Pikm)
Sasa2 (control)
Sasa2 (AVR-PikD)
Sasa2 (AVR-Mgk1)
S
R
E
Sasa2 (control)
Sasa2 (AVR-PikD)
Sasa2 (AVR-Mgk1)
**p < 0.001
Lesion (mm)
Moukoto (Piks -)
Hitomebore (Piks)
RIL #58 (Piks)
Tsuyuake (Pikm)

Fig 5

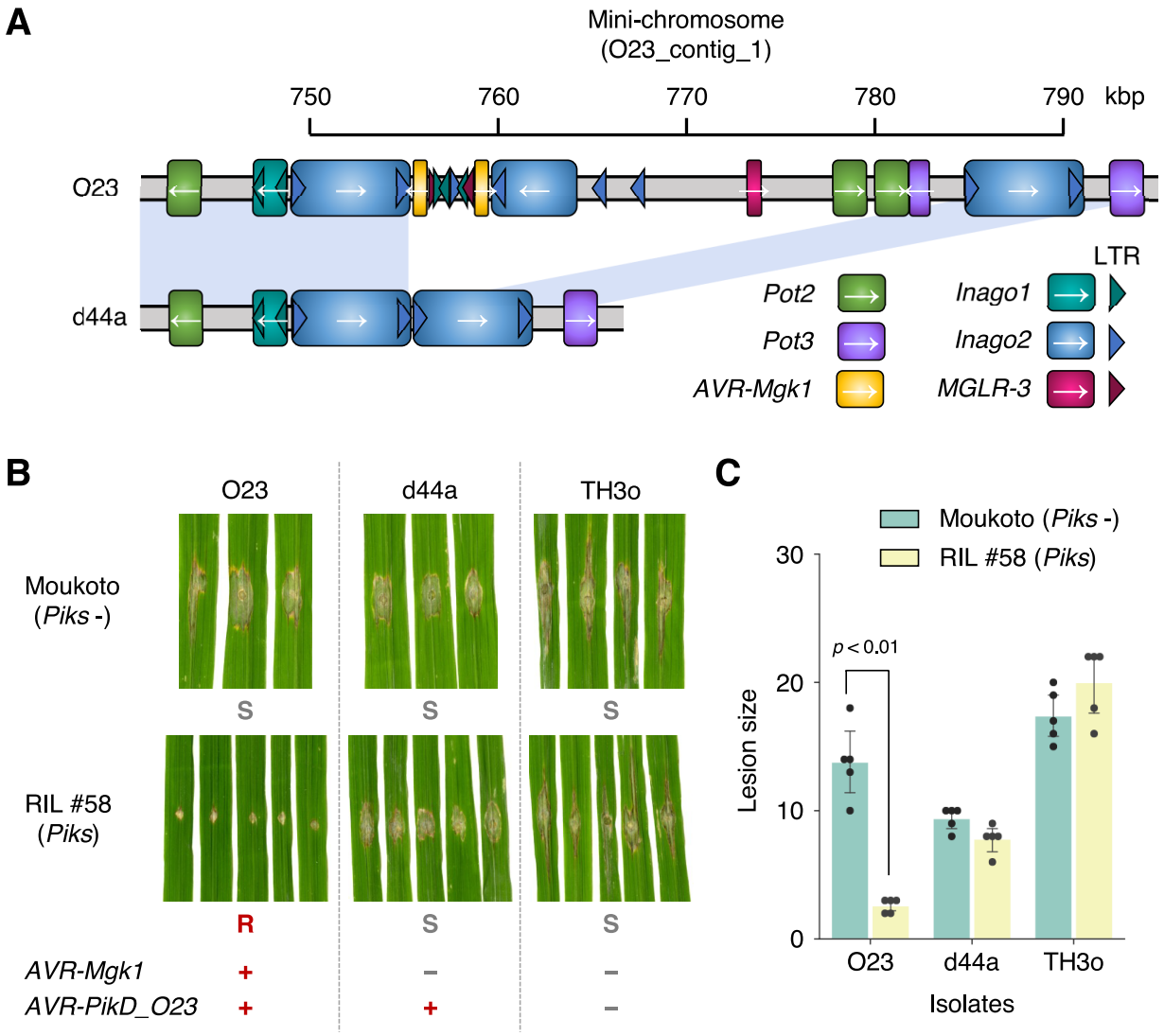
A
Mini-chromosome
(O23_contig_1)
750
760
770
780
790
kbp
O23
d44a
LTR
Pot2
Pot3
AVR-Mgk1
Inago1
Inago2
MGLR-3
B
O23
d44a
TH3o
Moukoto
(Piks -)
RIL #58
(Piks)
S
S
S
R
S
S
AVR-Mgk1
AVR-PikD_O23
+
+
–
+
–
–
C
Moukoto (Piks -)
RIL #58 (Piks)
p < 0.01
Lesion size
30
20
10
0
O23
d44a
TH3o
Isolates

Fig 6

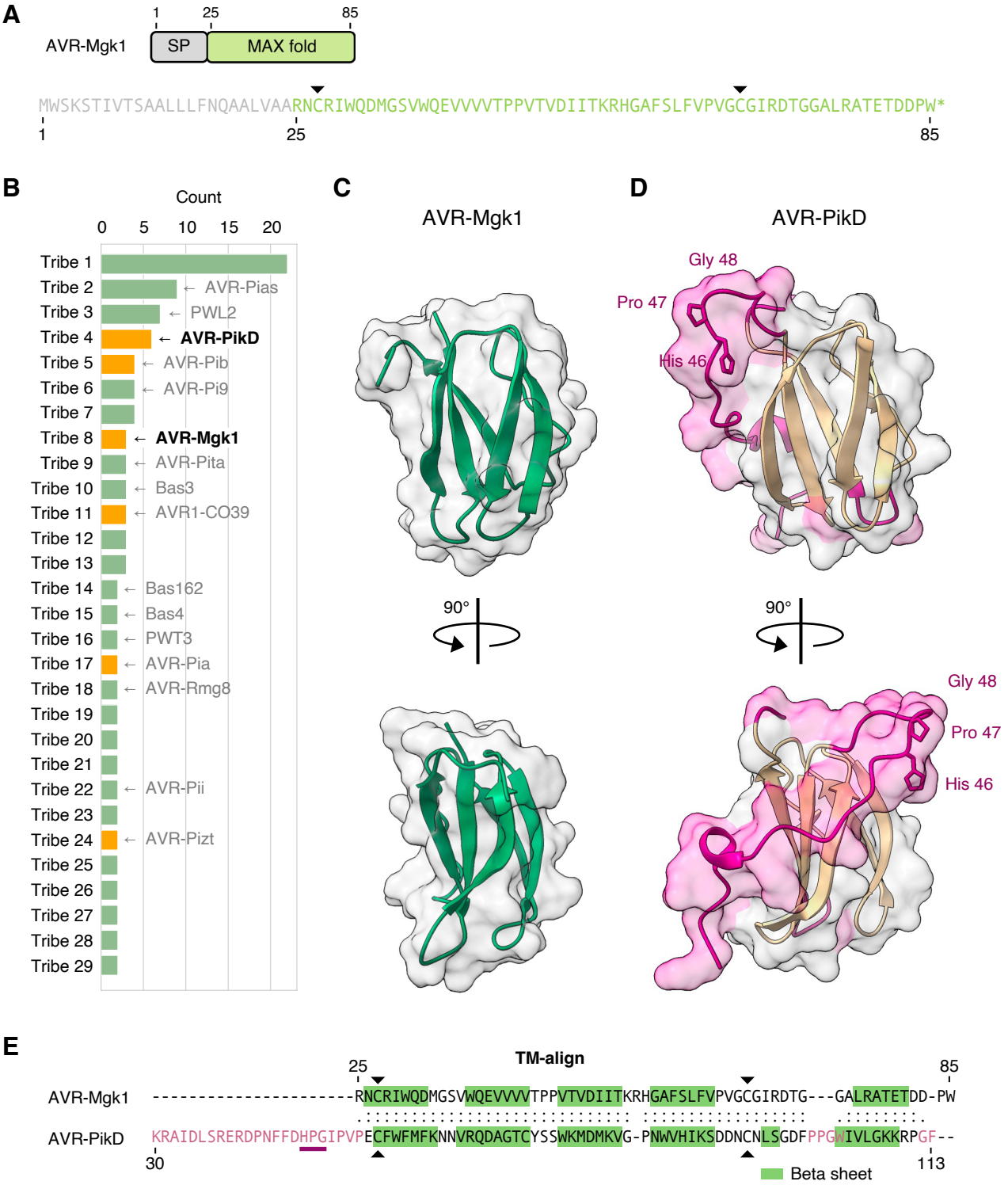
A
AVR-Mgk1
SP
MAX fold
1
25
85
MWSKSTIVTSAALLLFNQAALVAARNCRIWQDMGSVWQEVVVVTPPVTVDIITKRHGAFSLFVPVGCGIRDTGGALRATETDDPW*
B
Count
0 5 10 15 20
Tribe 1
Tribe 2 ← AVR-Pias
Tribe 3 ← PWL2
Tribe 4 ← AVR-PikD
Tribe 5 ← AVR-Pib
Tribe 6 ← AVR-Pi9
Tribe 7
Tribe 8 ← AVR-Mgk1
Tribe 9 ← AVR-Pita
Tribe 10 ← Bas3
Tribe 11 ← AVR1-CO39
Tribe 12
Tribe 13
Tribe 14 ← Bas162
Tribe 15 ← Bas4
Tribe 16 ← PWT3
Tribe 17 ← AVR-Pia
Tribe 18 ← AVR-Rmg8
Tribe 19
Tribe 20
Tribe 21
Tribe 22 ← AVR-Pii
Tribe 23
Tribe 24 ← AVR-Pizt
Tribe 25
Tribe 26
Tribe 27
Tribe 28
Tribe 29
C
AVR-Mgk1
90°
D
AVR-PikD
Gly 48
Pro 47
His 46
90°
Gly 48
Pro 47
His 46
E
TM-align
25
85
AVR-Mgk1 ----------RNCRIWQDMGSVWQEVVVVTPPVTVDIITKRHGAFSLFVPVGCGIRDTG---GALRATETDD-PW
AVR-PikD KRAIDLSRERDPNFFDHPGIPVPECFWFMFKNNVRQDAGTCYSSWKMDMKVG-PNWVHIKSDDNCNLSGDFPPGWIVLGKKRPGF--
30
113
Beta sheet

Fig 7

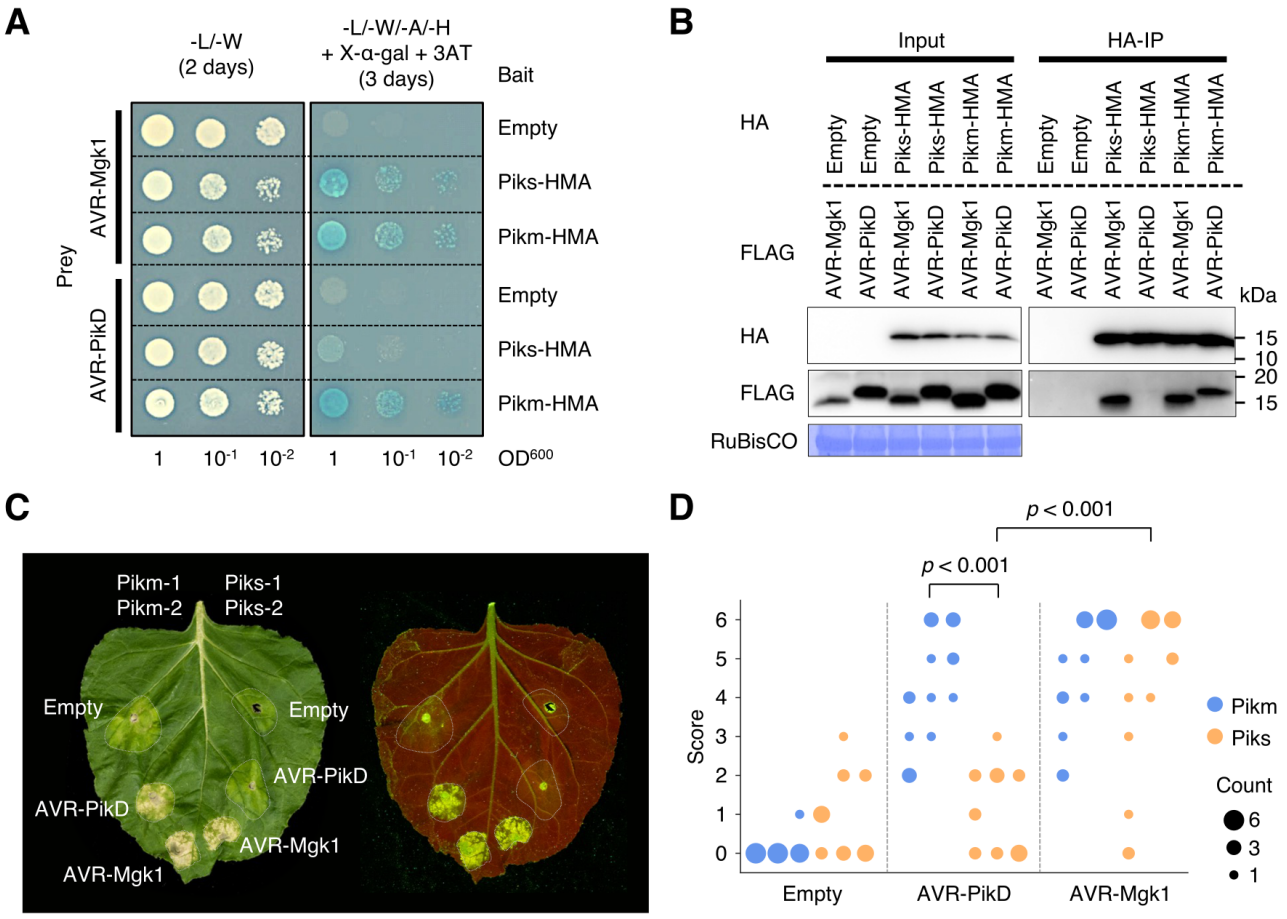
A
-L/-W
(2 days)
-L/-W/-A/-H
+ X-α-gal + 3AT
(3 days)
Bait
Prey
AVR-Mgk1
AVR-PikD
Empty
Piks-HMA
Pikm-HMA
Empty
Piks-HMA
Pikm-HMA
1
10-1
10-2
1
10-1
10-2
OD600
B
Input
HA-IP
HA
FLAG
RuBisCO
Empty
Empty
Piks-HMA
Piks-HMA
Pikm-HMA
Pikm-HMA
AVR-Mgk1
AVR-PikD
kDa
15
10
20
15
C
Pikm-1
Pikm-2
Piks-1
Piks-2
Empty
Empty
AVR-PikD
AVR-PikD
AVR-Mgk1
AVR-Mgk1
D
p < 0.001
p < 0.001
Score
Empty
AVR-PikD
AVR-Mgk1
Pikm
Piks
Count
6
3
1

Fig 8

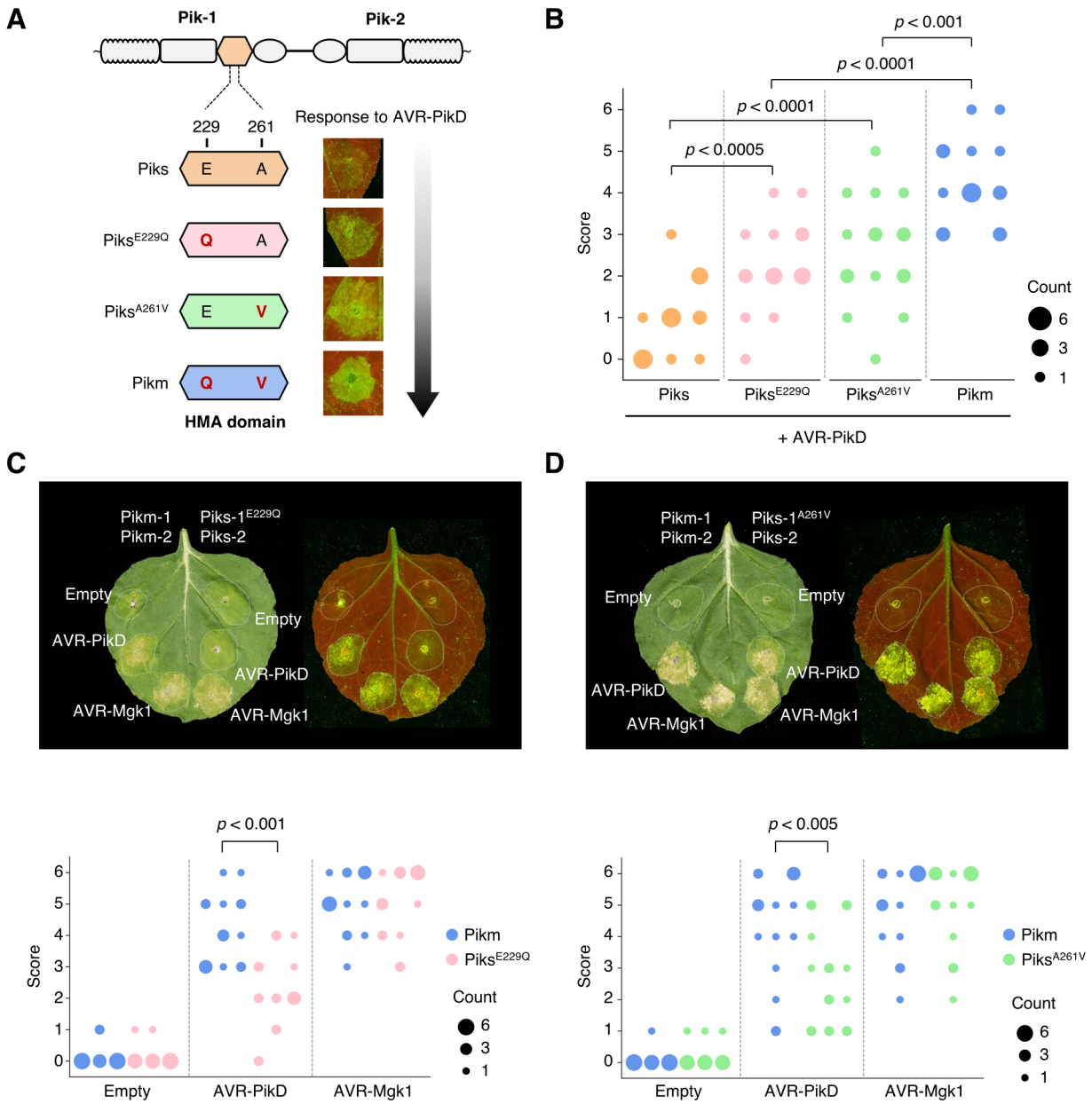
A
Pik-1
Pik-2
229
261
Response to AVR-PikD
Piks
E
A
Piks^E229Q
Q
A
Piks^A261V
E
V
Pikm
Q
V
HMA domain
B
p < 0.001
p < 0.0001
p < 0.0001
p < 0.0005
Score
Count
6
3
1
Piks
Piks^E229Q
Piks^A261V
Pikm
+ AVR-PikD
C
Pikm-1
Pikm-2
Piks-1^E229Q
Piks-2
Empty
Empty
AVR-PikD
AVR-PikD
AVR-Mgk1
AVR-Mgk1
D
Pikm-1
Pikm-2
Piks-1^A261V
Piks-2
Empty
Empty
AVR-PikD
AVR-PikD
AVR-Mgk1
AVR-Mgk1
p < 0.001
Score
Pikm
Piks^E229Q
Count
Empty
AVR-PikD
AVR-Mgk1
p < 0.005
Score
Pikm
Piks^A261V
Count
Empty
AVR-PikD
AVR-Mgk1

Fig 9

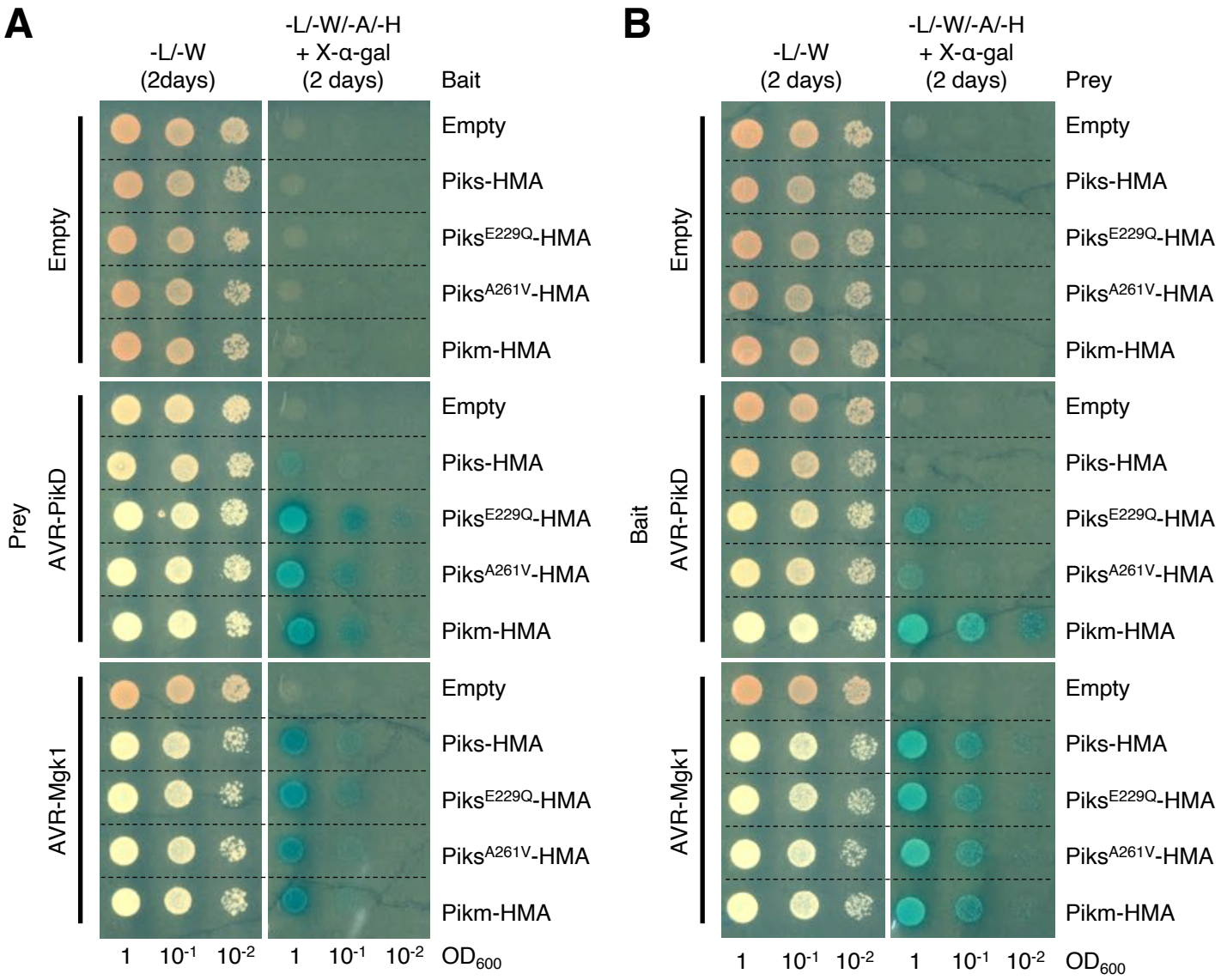
A
-L/-W
(2days)
-L/-W/-A/-H
+ X-α-gal
(2 days)
Bait
Prey
Empty
AVR-PikD
AVR-Mgk1
Empty
Piks-HMA
PiksE229Q-HMA
PiksA261V-HMA
Pikm-HMA
1
10-1
10-2
OD600
B
-L/-W
(2 days)
-L/-W/-A/-H
+ X-α-gal
(2 days)
Prey
Bait

Fig 10

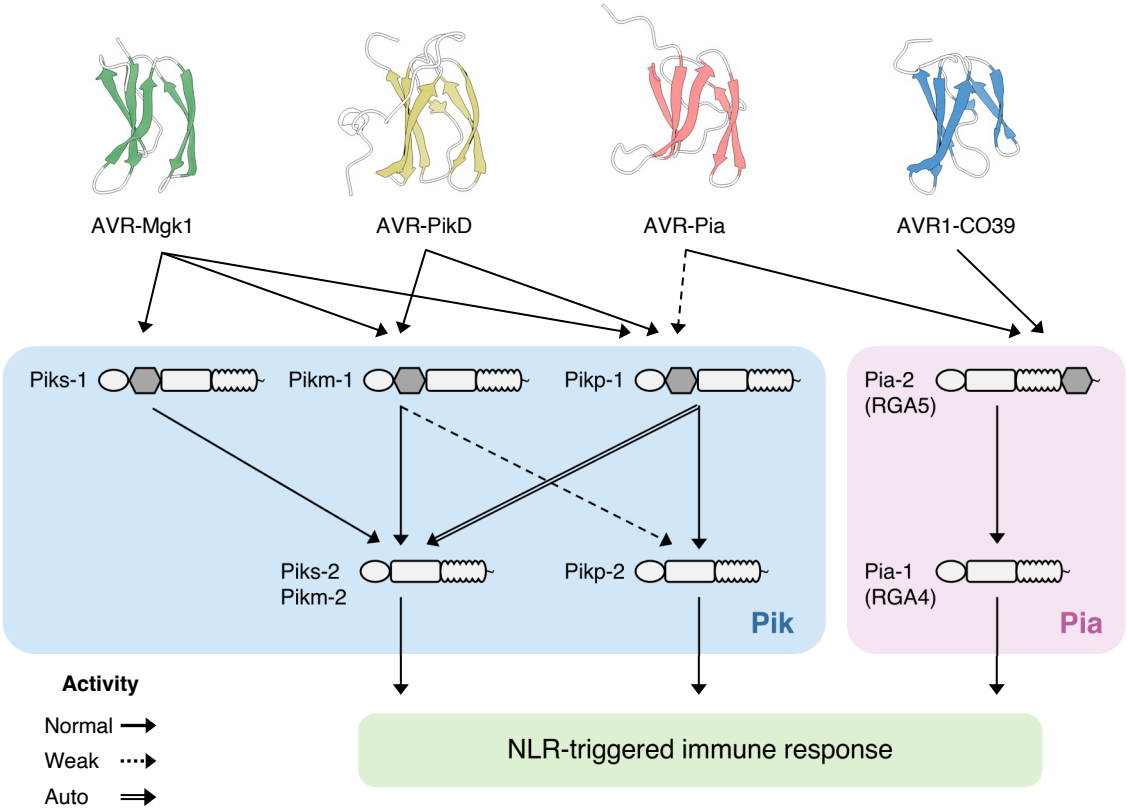
AVR-Mgk1
AVR-PikD
AVR-Pia
AVR1-CO39
Piks-1
Pikm-1
Pikp-1
Piks-2
Pikm-2
Pikp-2
Pik
Pia-2
(RGA5)
Pia-1
(RGA4)
Pia
Activity
Normal
Weak
Auto
NLR-triggered immune response

S1 Fig

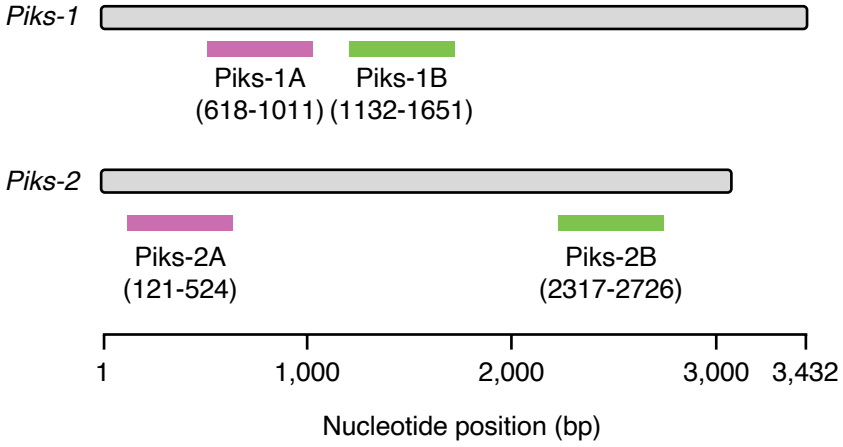
Piks-1
Piks-1A
(618-1011)
Piks-1B
(1132-1651)
Piks-2
Piks-2A
(121-524)
Piks-2B
(2317-2726)
1
1,000
2,000
3,000
3,432
Nucleotide position (bp)

S2 Fig

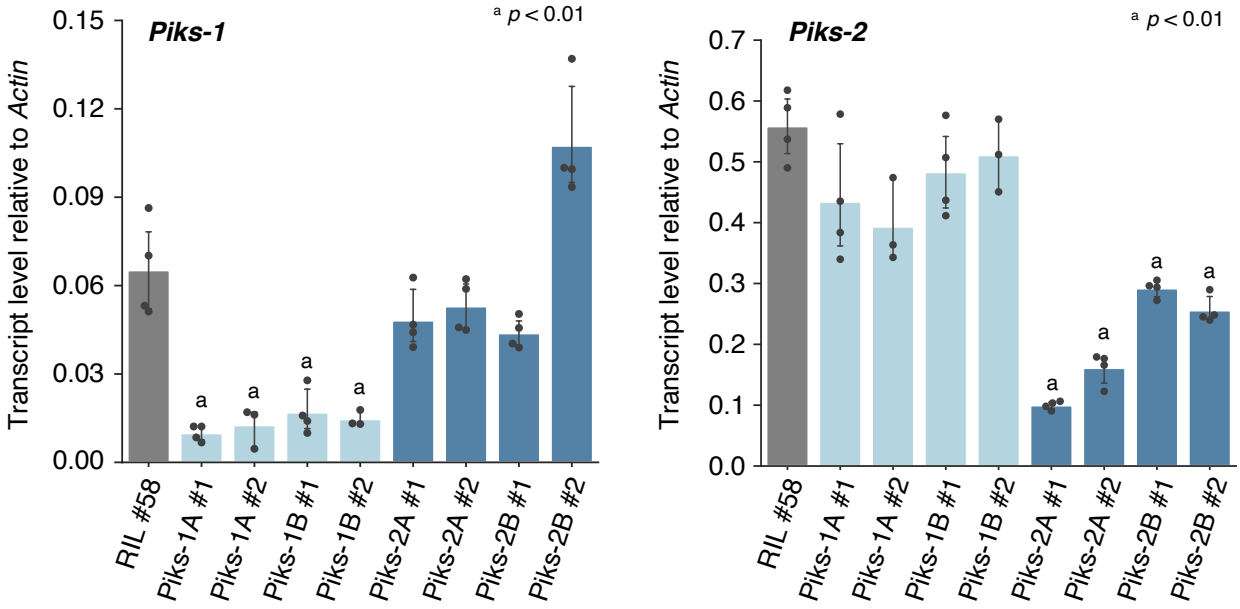
Piks-1
[a] p < 0.01
Transcript level relative to Actin
0.15
0.12
0.09
0.06
0.03
0.00
a
RIL #58
Piks-1A #1
Piks-1A #2
Piks-1B #1
Piks-1B #2
Piks-2A #1
Piks-2A #2
Piks-2B #1
Piks-2B #2
Piks-2
[a] p < 0.01
Transcript level relative to Actin
0.7
0.6
0.5
0.4
0.3
0.2
0.1
0.0

S3 Fig

```
                                                
```

S4 Fig

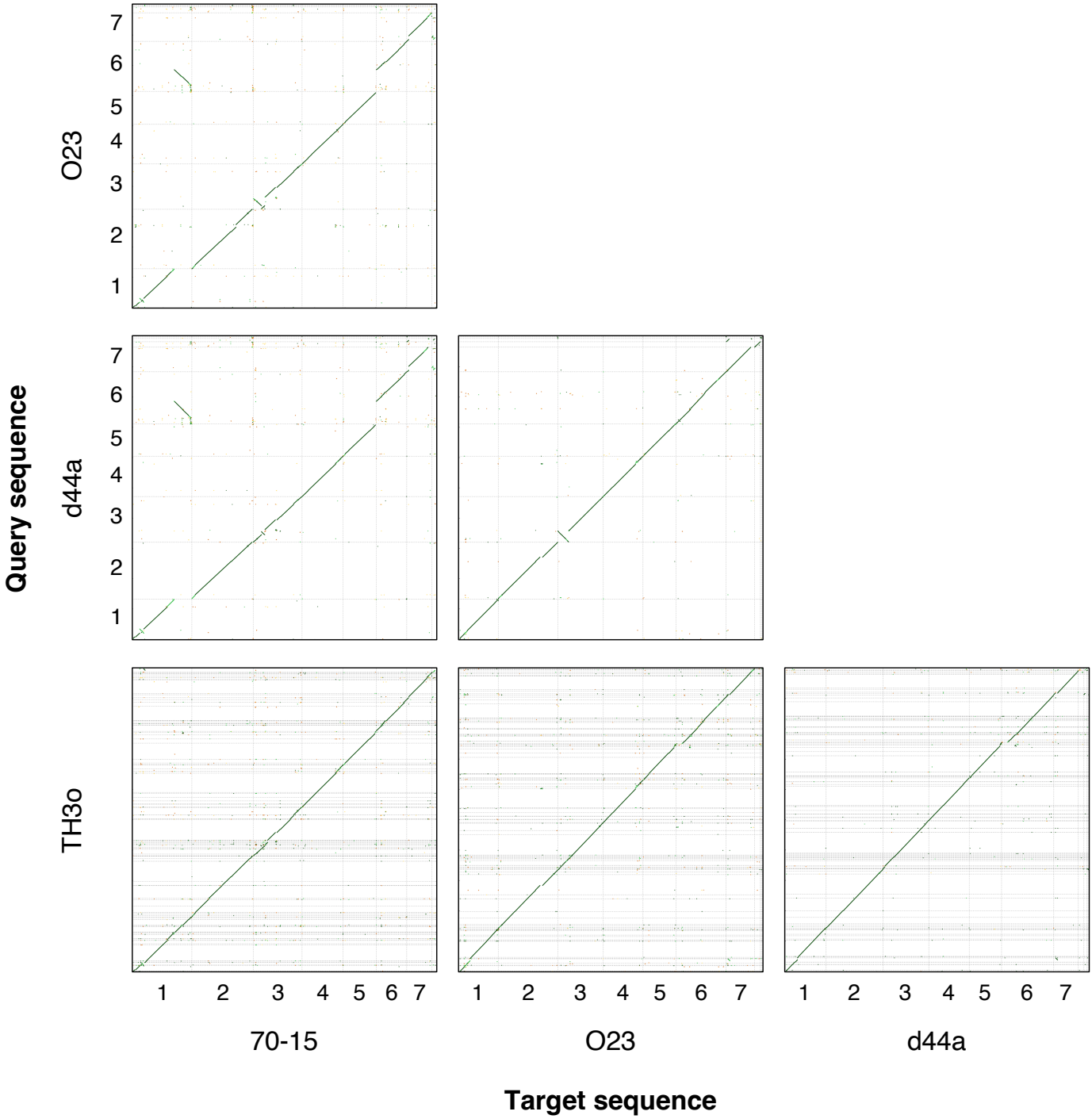
Query sequence
O23
d44a
TH3o
1
2
3
4
5
6
7
70-15
O23
d44a
Target sequence

S5 Fig

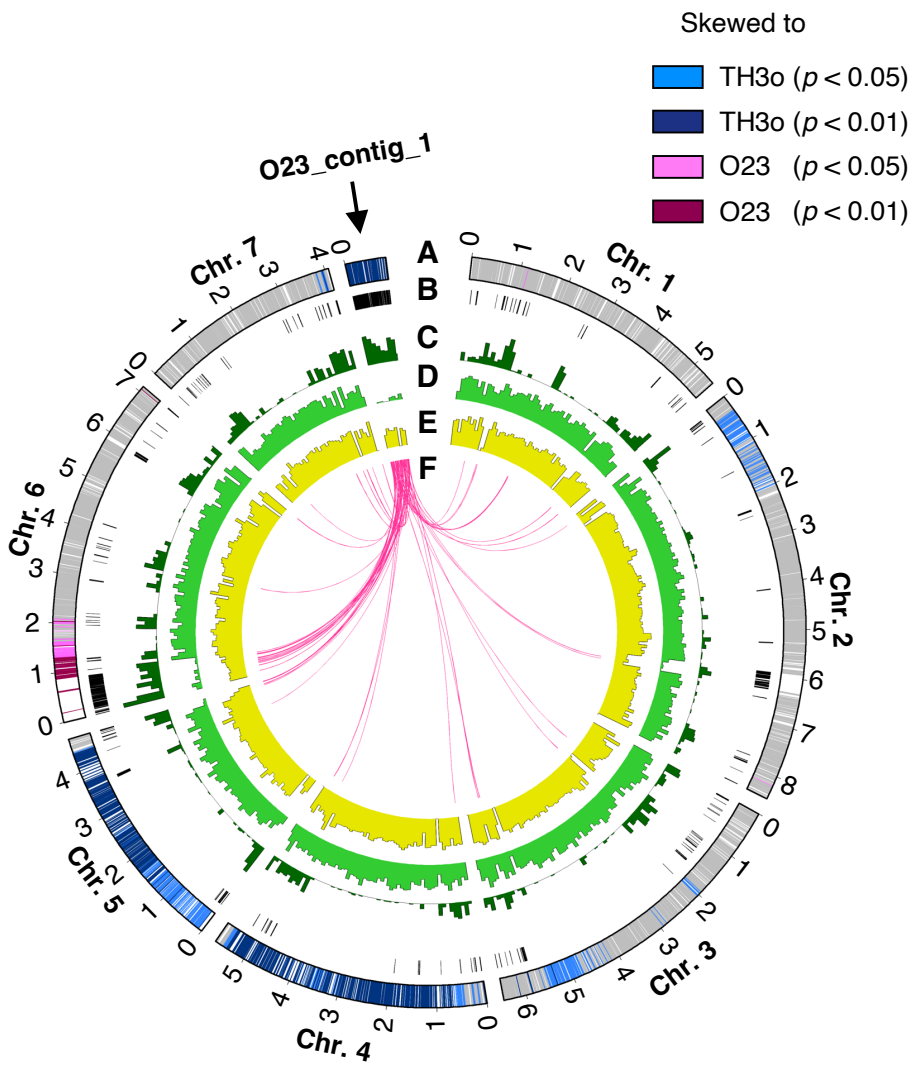
Skewed to
TH3o ($p < 0.05$)
TH3o ($p < 0.01$)
O23 ($p < 0.05$)
O23 ($p < 0.01$)
O23_contig_1
A
B
C
D
E
F
Chr. 1
Chr. 2
Chr. 3
Chr. 4
Chr. 5
Chr. 6
Chr. 7

S6 Fig

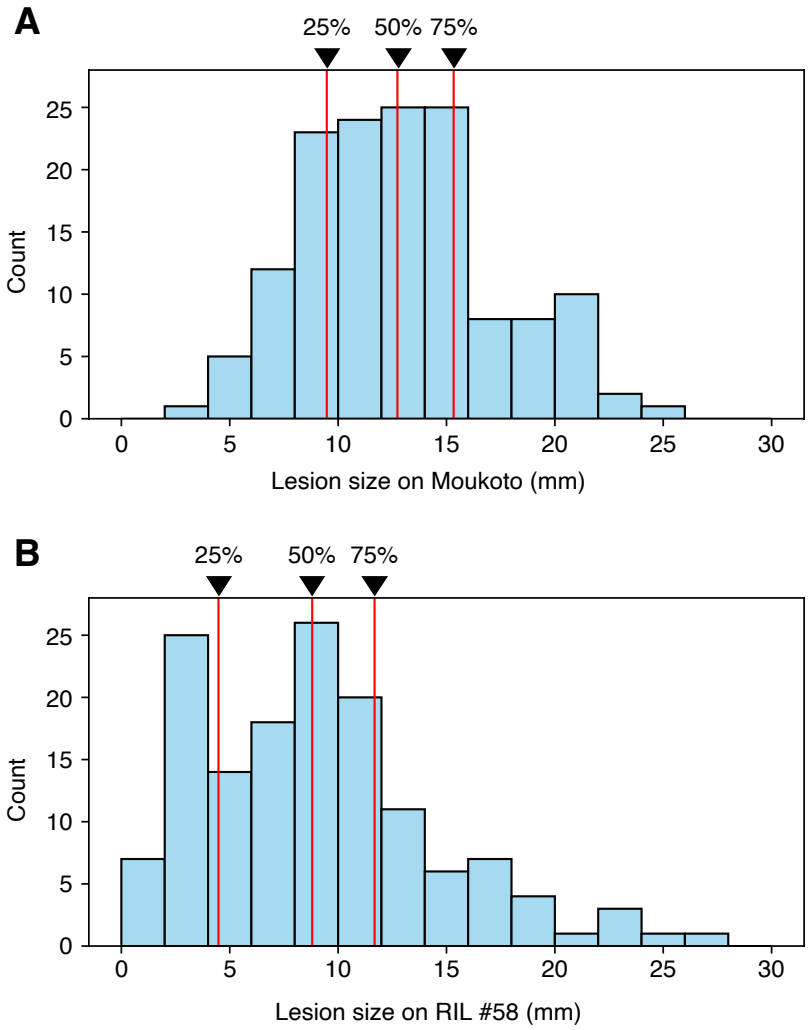
A
25%
50%
75%
Count
0
5
10
15
20
25
0
5
10
15
20
25
30
Lesion size on Moukoto (mm)
B
25%
50%
75%
Count
0
5
10
15
20
25
0
5
10
15
20
25
30
Lesion size on RIL #58 (mm)

S7 Fig

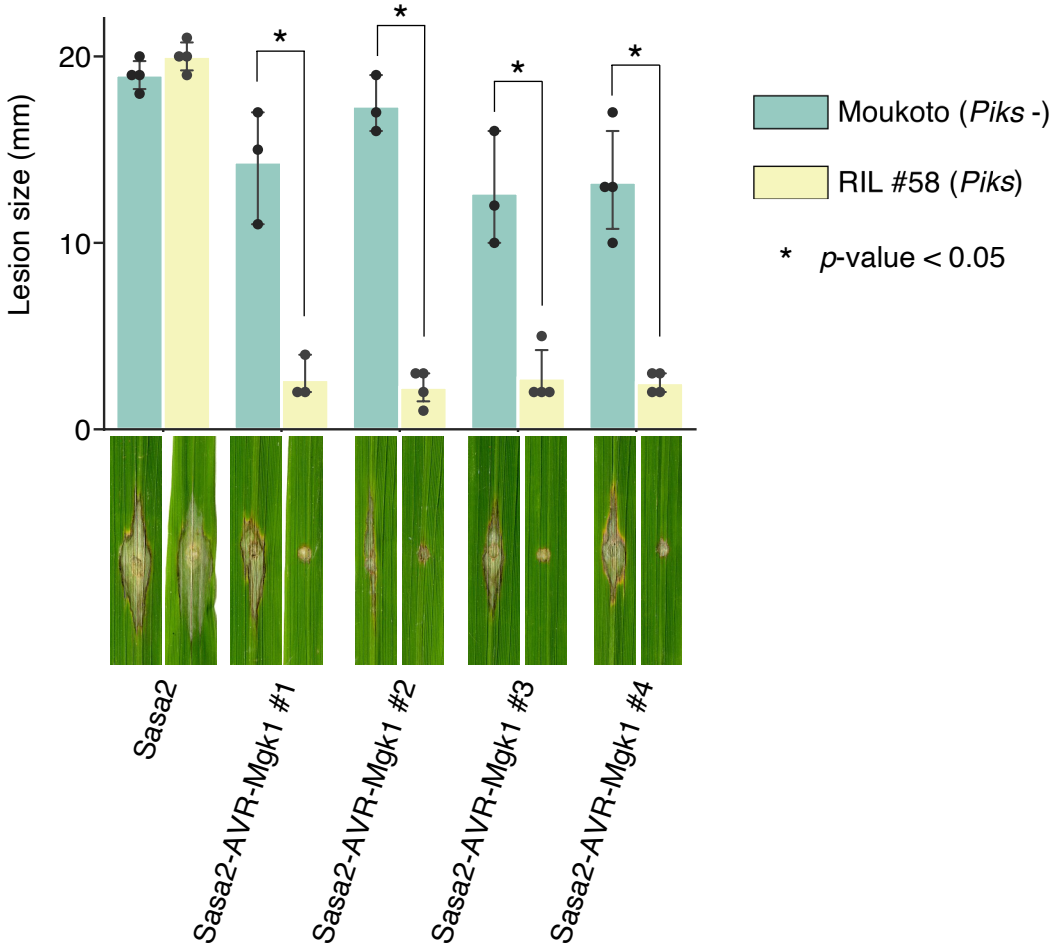
Lesion size (mm)
20
10
0
*
*
*
*
Moukoto (Piks -)
RIL #58 (Piks)
* p-value < 0.05
Sasa2
Sasa2-AVR-Mgk1 #1
Sasa2-AVR-Mgk1 #2
Sasa2-AVR-Mgk1 #3
Sasa2-AVR-Mgk1 #4

S8 Fig

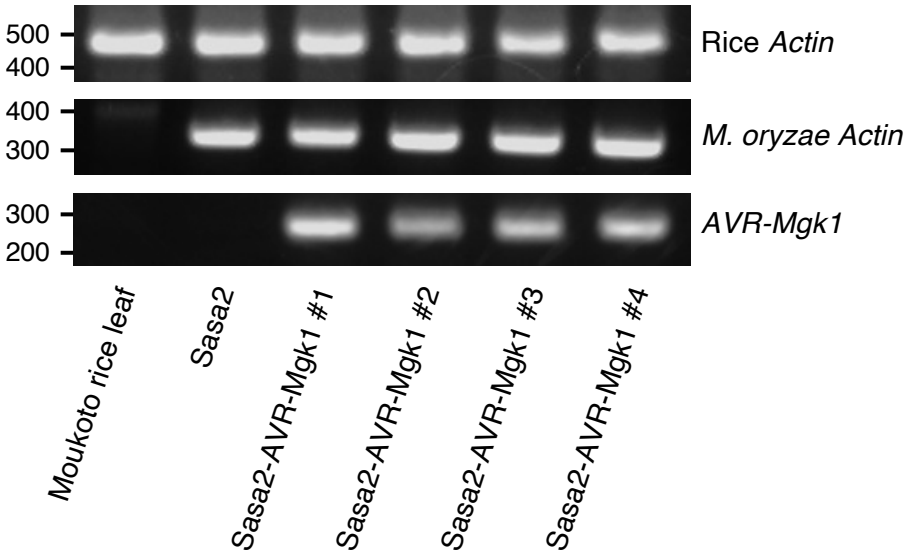
500
400
Rice Actin
400
300
M. oryzae Actin
300
200
AVR-Mgk1
Moukoto rice leaf
Sasa2
Sasa2-AVR-Mgk1 #1
Sasa2-AVR-Mgk1 #2
Sasa2-AVR-Mgk1 #3
Sasa2-AVR-Mgk1 #4

S9 Fig

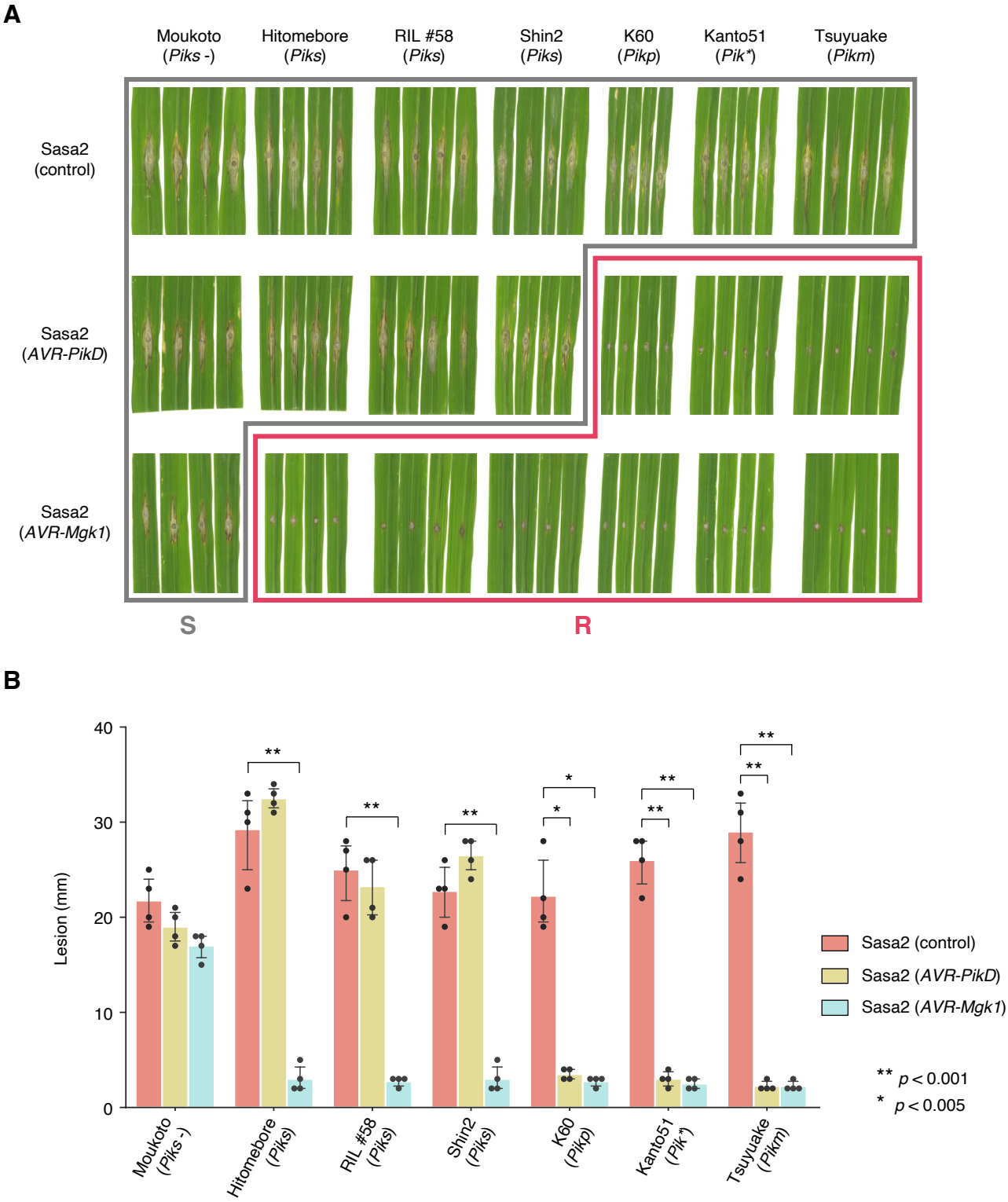
A
Moukoto (Piks -)
Hitomebore (Piks)
RIL #58 (Piks)
Shin2 (Piks)
K60 (Pikp)
Kanto51 (Pik*)
Tsuyuake (Pikm)
Sasa2 (control)
Sasa2 (AVR-PikD)
Sasa2 (AVR-Mgk1)
S
R
B
Lesion (mm)
40
30
20
10
0
**
*
Sasa2 (control)
Sasa2 (AVR-PikD)
Sasa2 (AVR-Mgk1)
** p < 0.001
* p < 0.005
Moukoto (Piks -)
Hitomebore (Piks)
RIL #58 (Piks)
Shin2 (Piks)
K60 (Pikp)
Kanto51 (Pik*)
Tsuyuake (Pikm)

S10 Fig

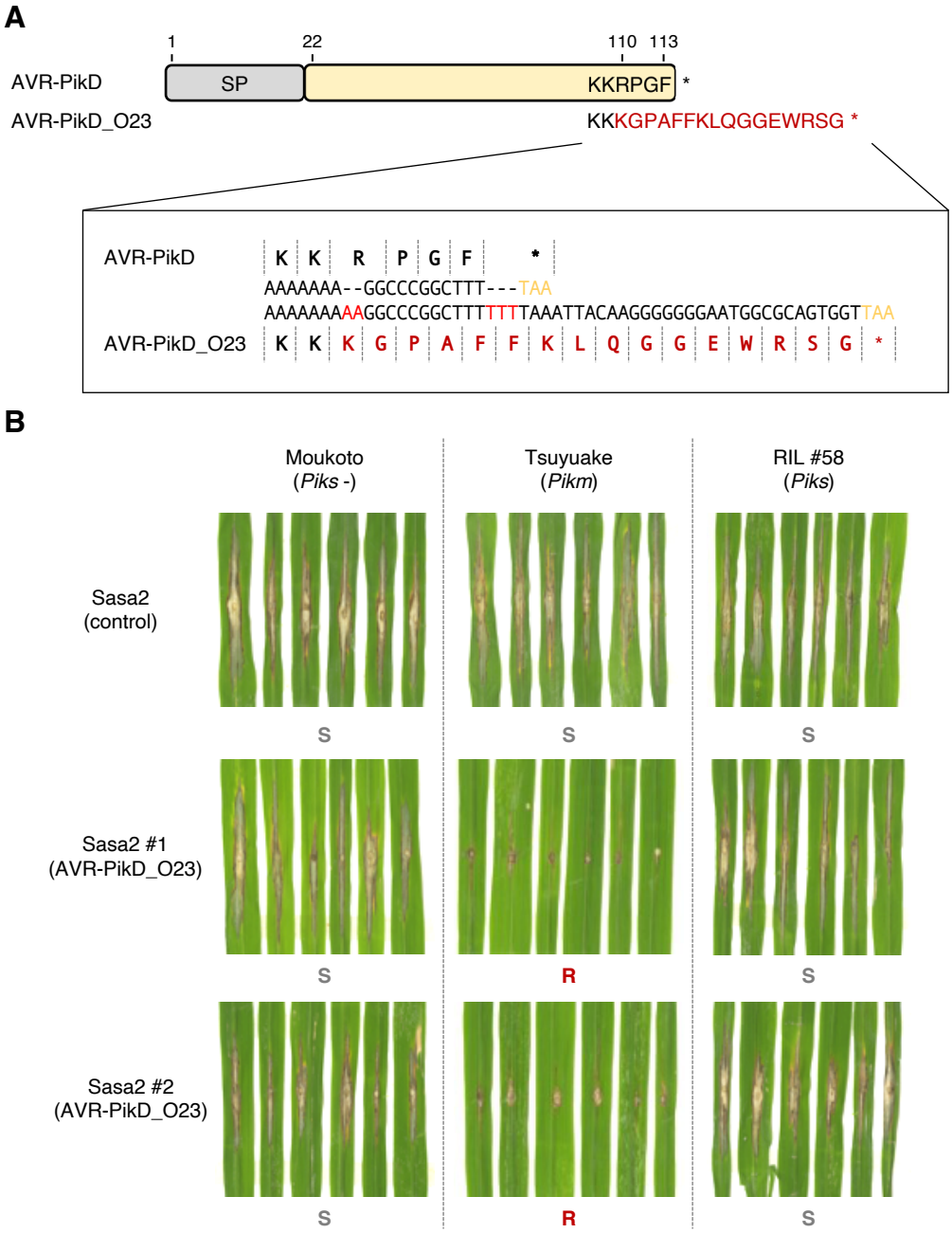
A
1
22
110
113
AVR-PikD
SP
KKRPGF *
AVR-PikD_O23
KKKGPAFFKLQGGEWRSG *
AVR-PikD
K K R P G F *
AAAAAAA--GGCCCGGCTTT---TAA
AAAAAAAAAGGCCCGGCTTTTTTTAAATTACAAGGGGGGGAATGGCGCAGTGGTTAA
AVR-PikD_O23
K K K G P A F F K L Q G G E W R S G *
B
Moukoto
(Piks -)
Tsuyuake
(Pikm)
RIL #58
(Piks)
Sasa2
(control)
S
S
S
Sasa2 #1
(AVR-PikD_O23)
S
R
S
Sasa2 #2
(AVR-PikD_O23)
S
R
S

S11 Fig

```
            1                                                                                                                  85
            |                                                                                                                  |
AVR-Mgk1    MWSKSTIVTSAALLLFNQAALVAARNCRIWQDMGSV---------WQEVVVVTPPVTVDIITKR---------HGAFSLFVPVGCG---IRDTGGALRATETDDPW
            M           LL     A V A                             P       K                  VG     I              W
AVR-PikD    M---RVTTFNTFLLTLGTVAVVNAETGNKYIEKRAIDLSRERDPNFFDHPGIPVPECFWFMFKNNVRQDAGTCYSSWKMDMKVGPNWVHIKSDDNCNLSGDFPPGWIVLGKKRPGF
            |                                                                                                                  |
            1                                                                                                                  113
```

S12 Fig

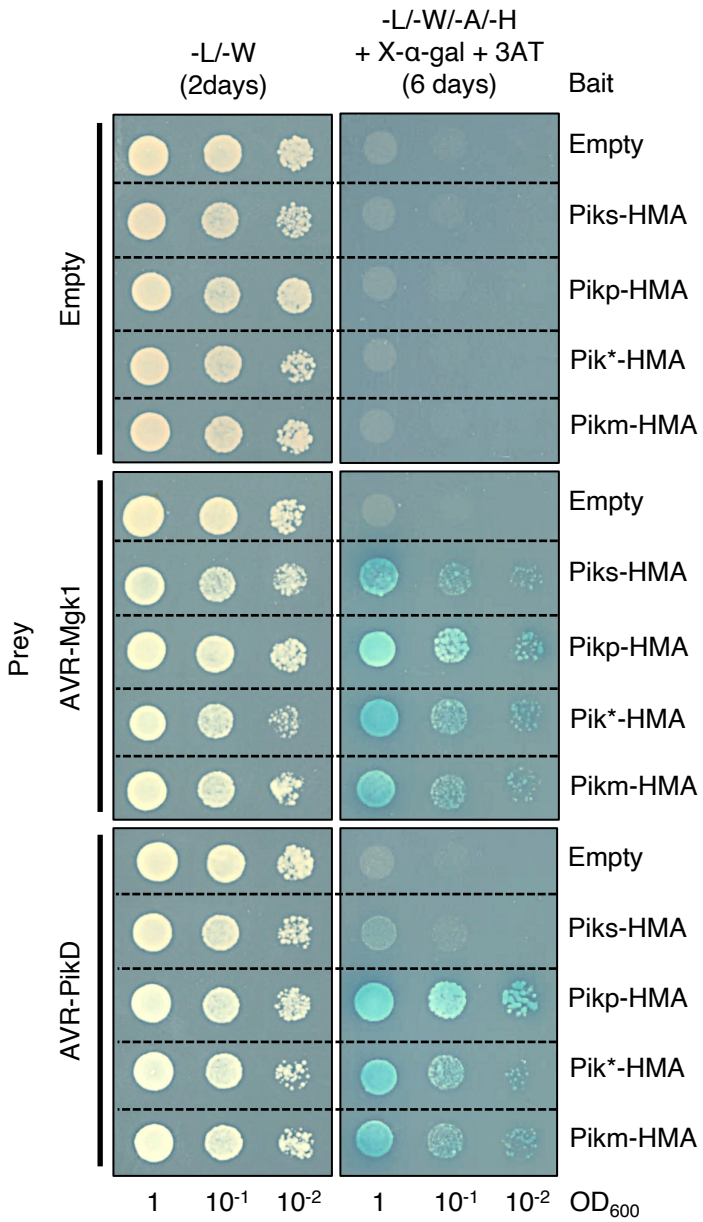
-L/-W
(2days)
-L/-W/-A/-H
+ X-α-gal + 3AT
(6 days)
Bait
Prey
Empty
AVR-Mgk1
AVR-PikD
Empty
Piks-HMA
Pikp-HMA
Pik*-HMA
Pikm-HMA
1
10-1
10-2
OD600

S13 Fig

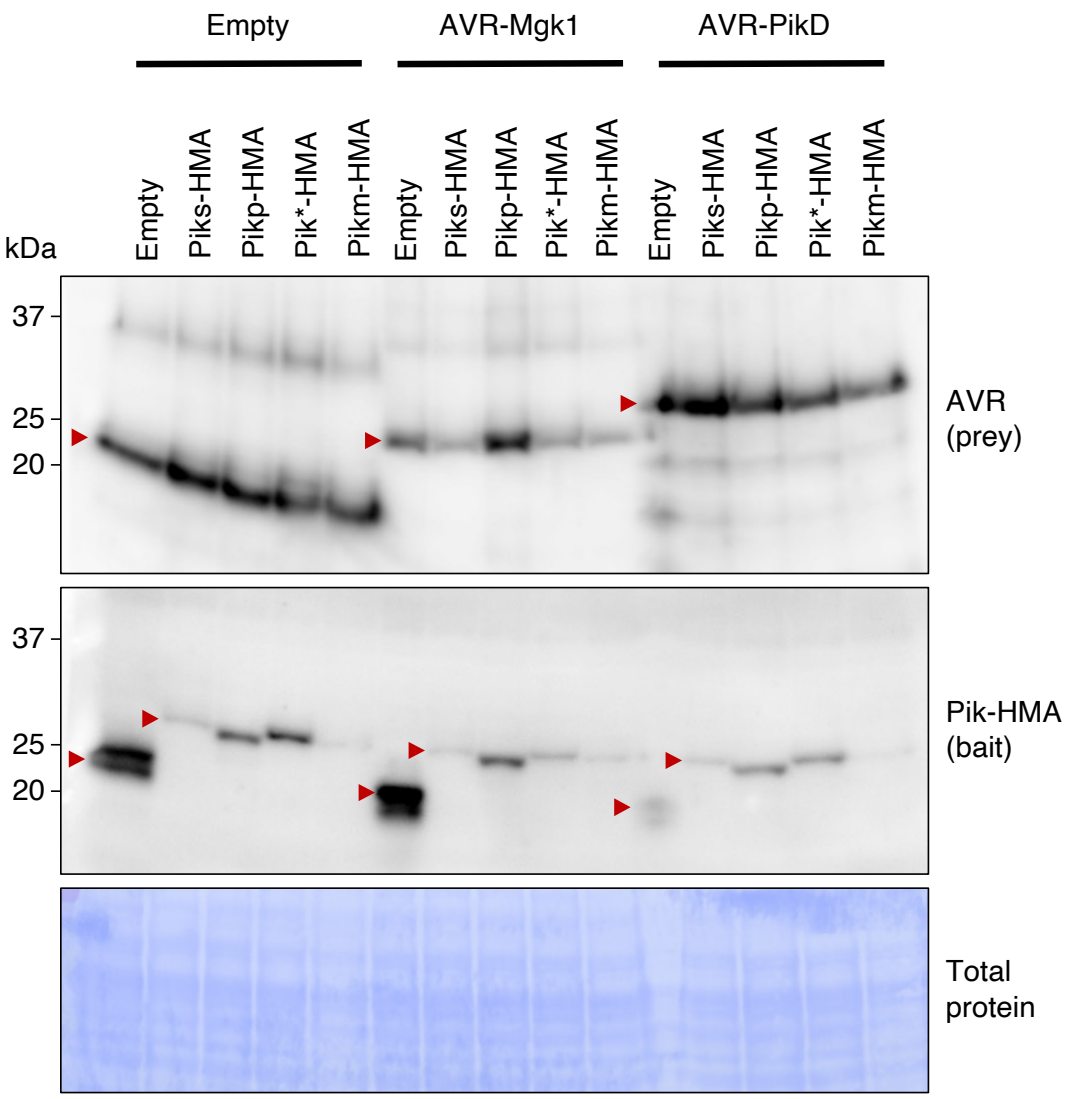
Empty
AVR-Mgk1
AVR-PikD
Empty
Piks-HMA
Pikp-HMA
Pik*-HMA
Pikm-HMA
Empty
Piks-HMA
Pikp-HMA
Pik*-HMA
Pikm-HMA
Empty
Piks-HMA
Pikp-HMA
Pik*-HMA
Pikm-HMA
kDa
37
25
20
AVR
(prey)
37
25
20
Pik-HMA
(bait)
Total
protein

S14 Fig

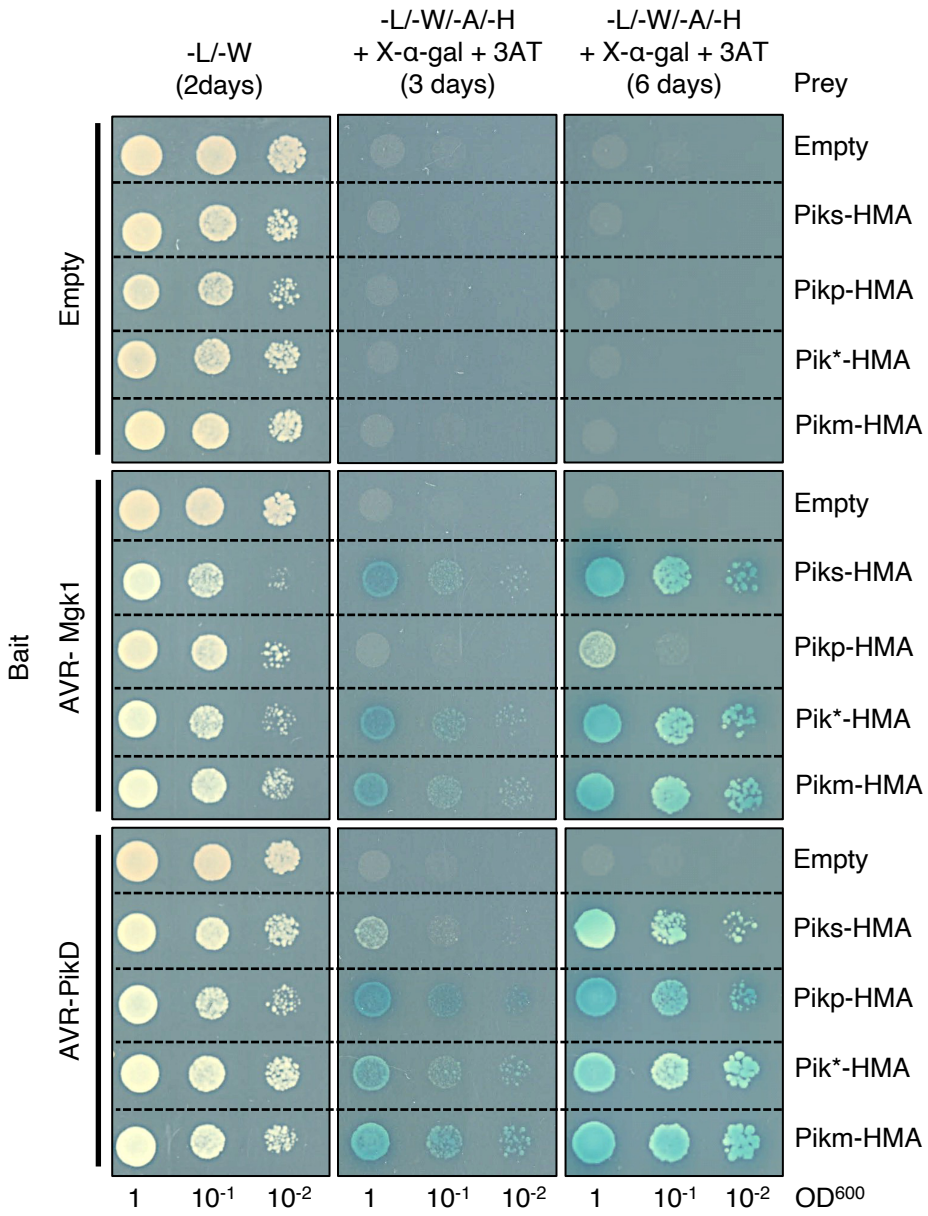
-L/-W
(2days)
-L/-W/-A/-H
+ X-α-gal + 3AT
(3 days)
-L/-W/-A/-H
+ X-α-gal + 3AT
(6 days)
Prey
Bait
Empty
AVR- Mgk1
AVR-PikD
Empty
Piks-HMA
Pikp-HMA
Pik*-HMA
Pikm-HMA
1
10-1
10-2
OD600

S15 Fig

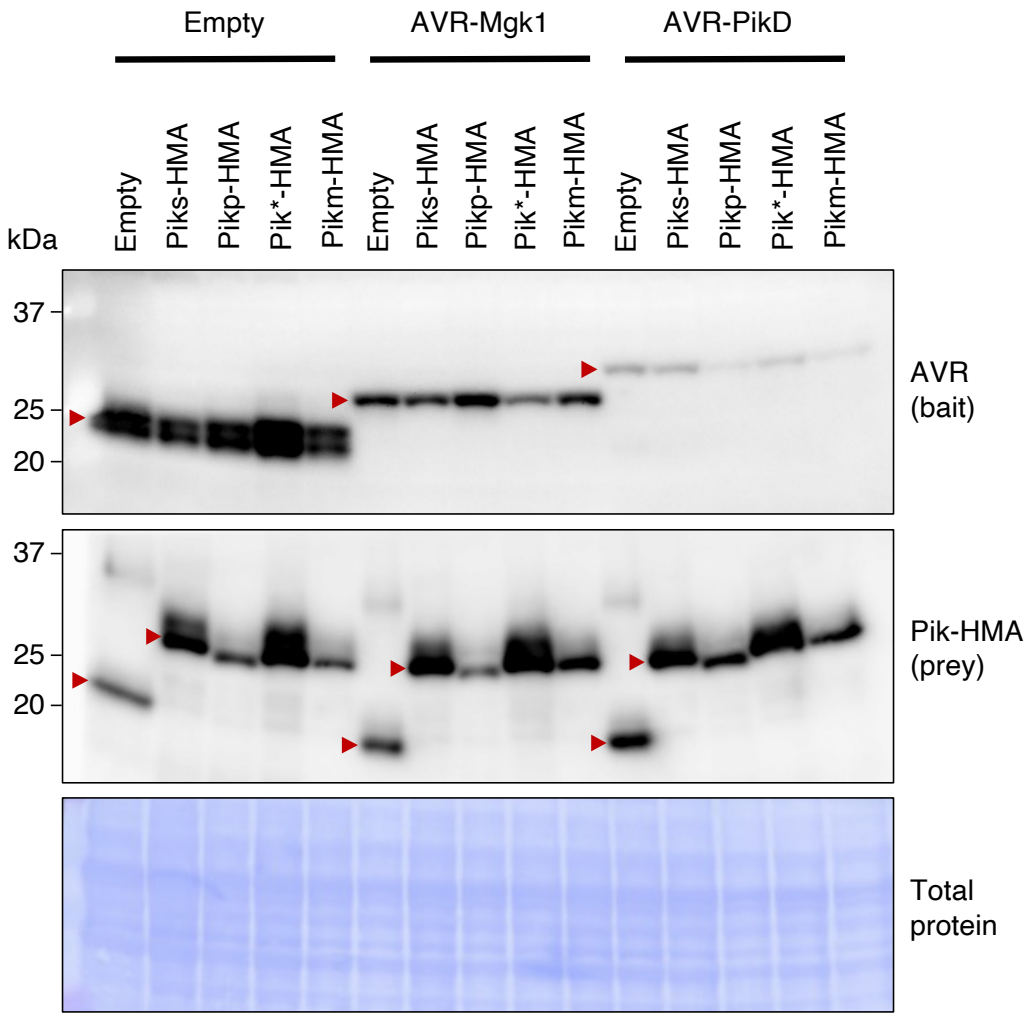
Empty
AVR-Mgk1
AVR-PikD
kDa
Empty
Piks-HMA
Pikp-HMA
Pik*-HMA
Pikm-HMA
Empty
Piks-HMA
Pikp-HMA
Pik*-HMA
Pikm-HMA
Empty
Piks-HMA
Pikp-HMA
Pik*-HMA
Pikm-HMA
37
25
20
AVR
(bait)
37
25
20
Pik-HMA
(prey)
Total
protein

S16 Fig

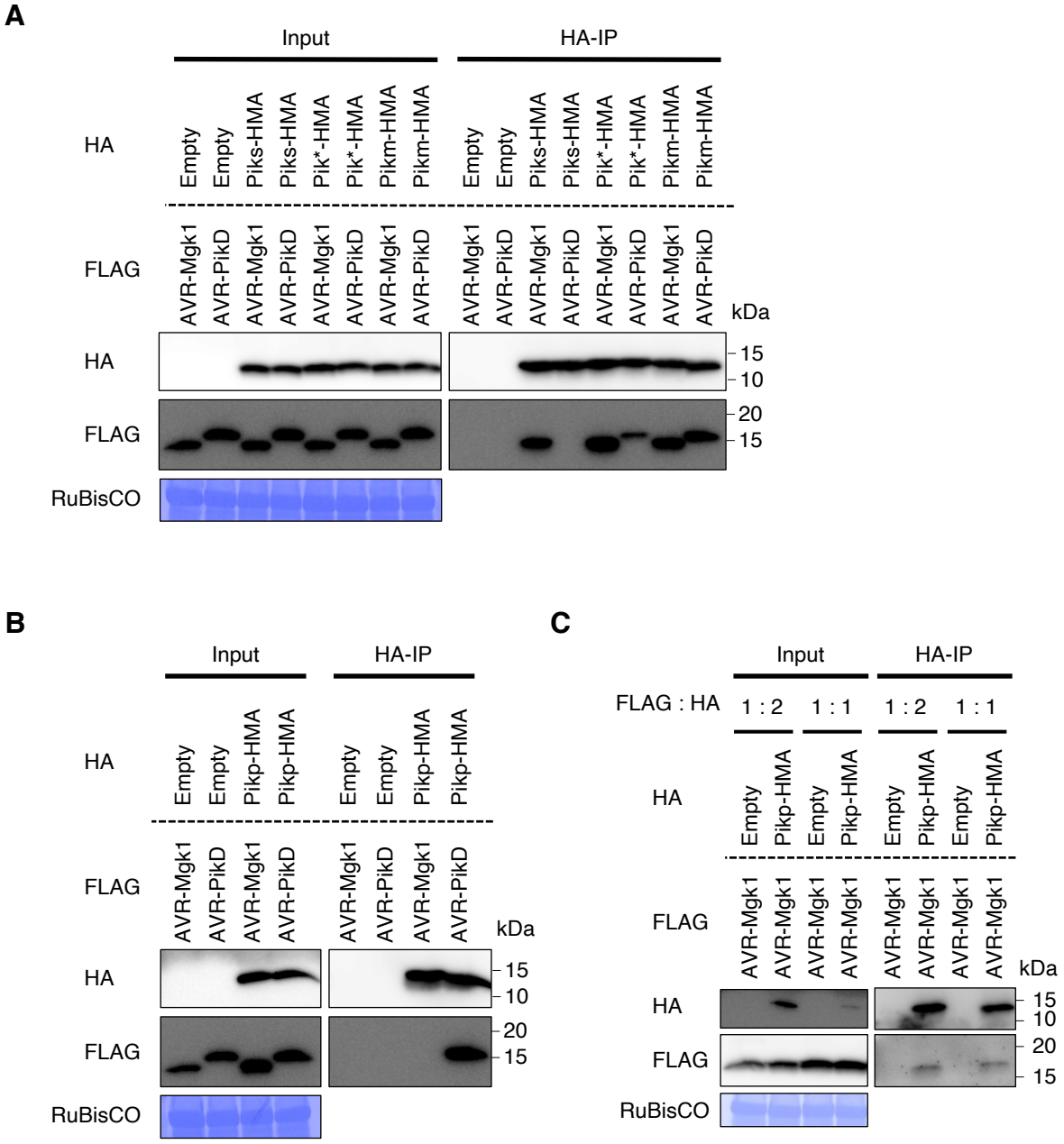
A
Input
HA-IP
HA
Empty
Empty
Piks-HMA
Piks-HMA
Pik*-HMA
Pik*-HMA
Pikm-HMA
Pikm-HMA
FLAG
AVR-Mgk1
AVR-PikD
kDa
15
10
20
RuBisCO
B
C
FLAG : HA
1 : 2
1 : 1
Pikp-HMA

S17 Fig

A

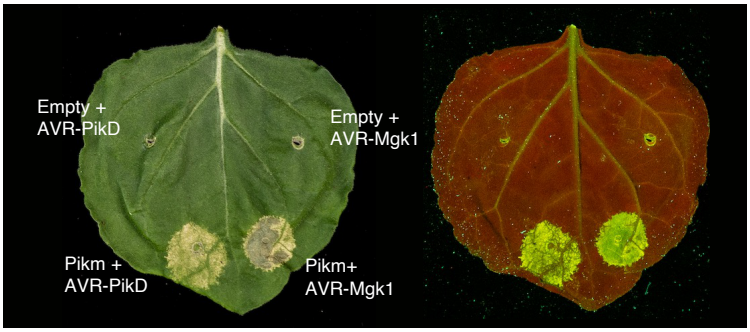
Empty +
AVR-PikD
Empty +
AVR-Mgk1
Pikm +
AVR-PikD
Pikm+
AVR-Mgk1

B

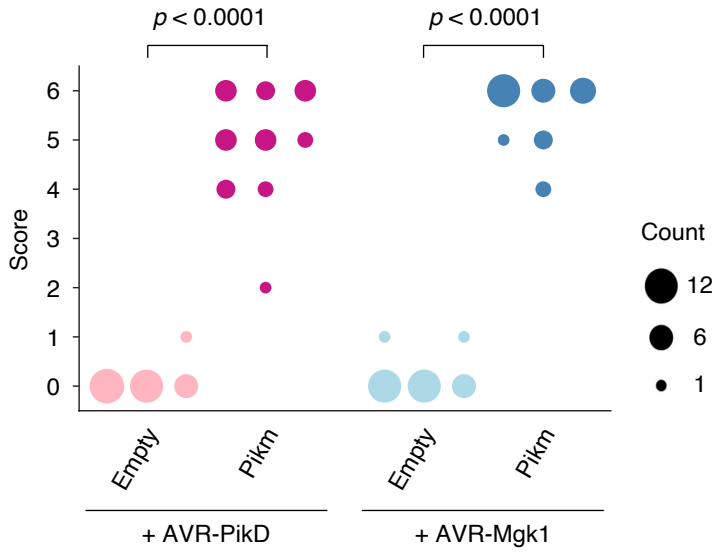
p < 0.0001
p < 0.0001
Score
6
5
4
3
2
1
0
Empty
Pikm
Empty
Pikm
+ AVR-PikD
+ AVR-Mgk1
Count
12
6
1

S18 Fig

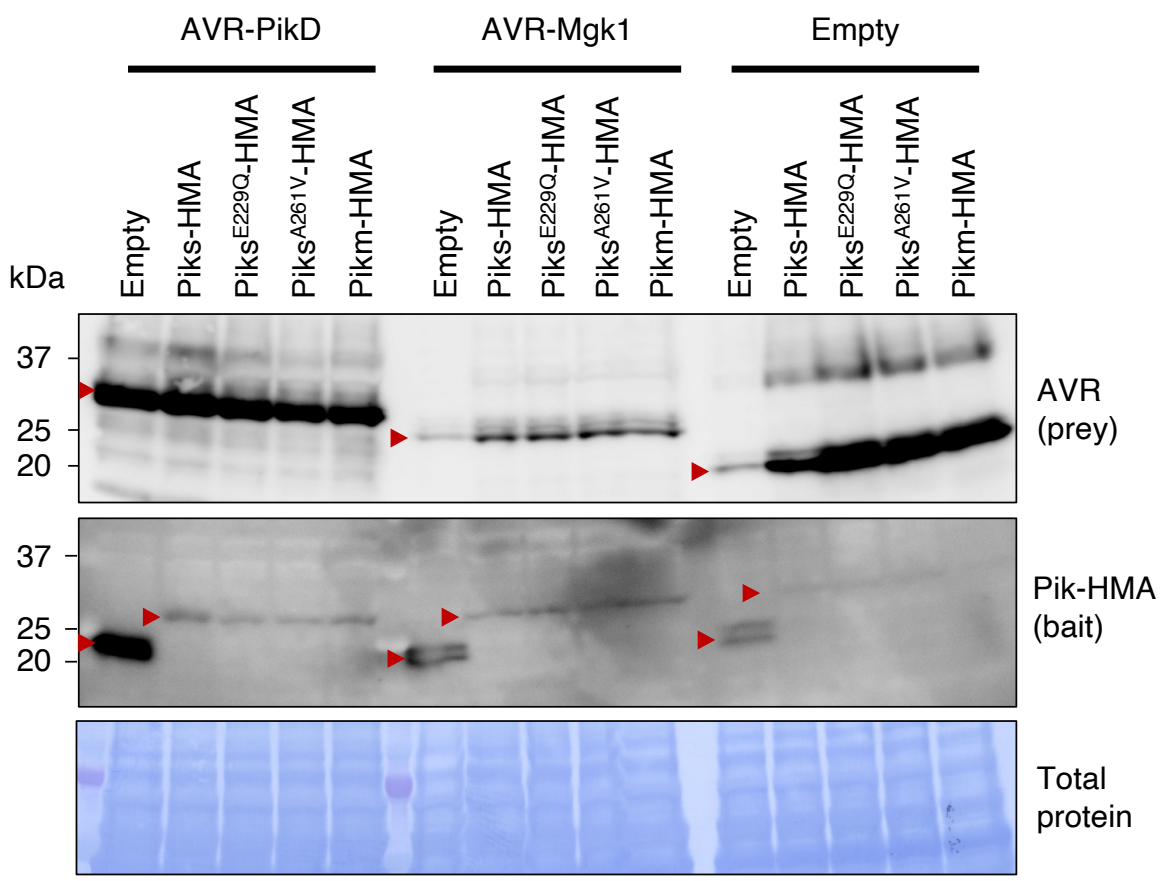
AVR-PikD
AVR-Mgk1
Empty
kDa
Empty
Piks-HMA
PiksE229Q-HMA
PiksA261V-HMA
Pikm-HMA
Empty
Piks-HMA
PiksE229Q-HMA
PiksA261V-HMA
Pikm-HMA
Empty
Piks-HMA
PiksE229Q-HMA
PiksA261V-HMA
Pikm-HMA
37
25
20
AVR
(prey)
37
25
20
Pik-HMA
(bait)
Total
protein

S19 Fig

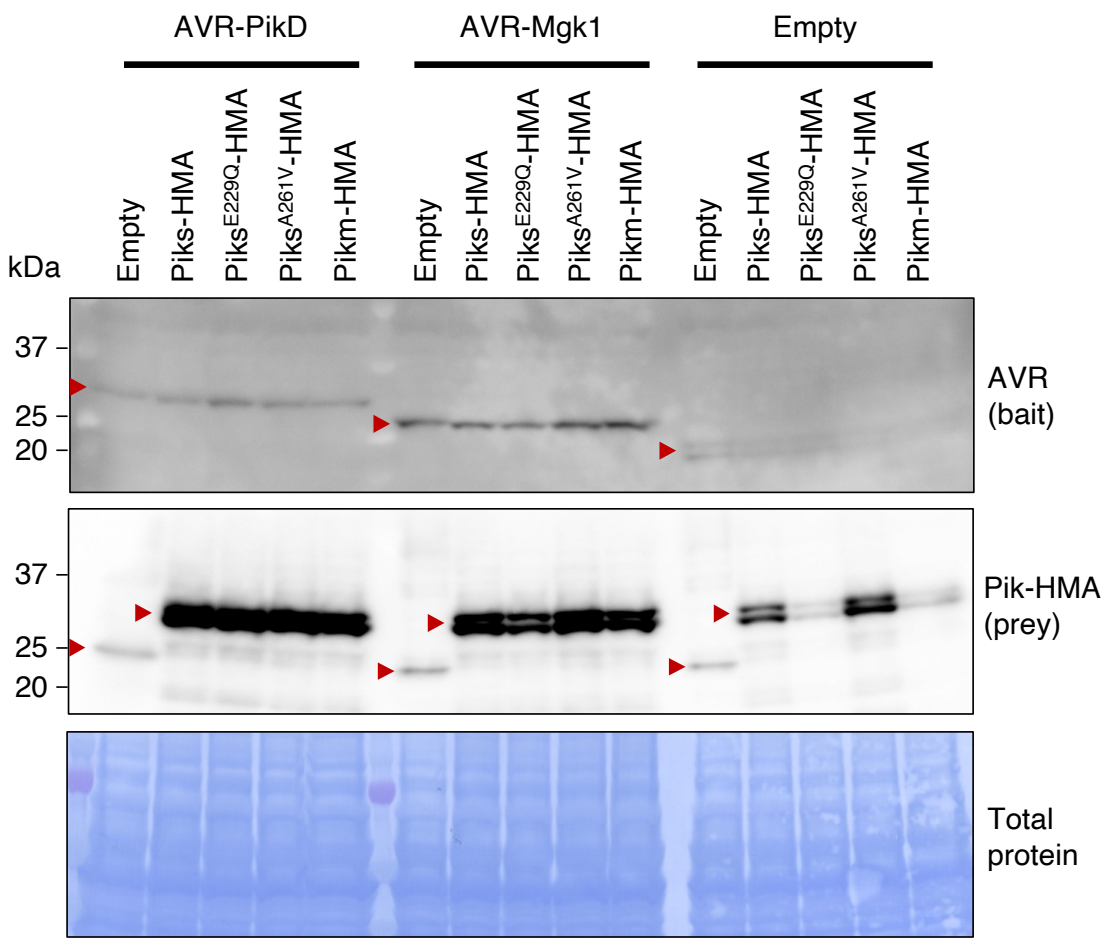
AVR-PikD
AVR-Mgk1
Empty
Empty
Piks-HMA
PiksE229Q-HMA
PiksA261V-HMA
Pikm-HMA
Empty
Piks-HMA
PiksE229Q-HMA
PiksA261V-HMA
Pikm-HMA
Empty
Piks-HMA
PiksE229Q-HMA
PiksA261V-HMA
Pikm-HMA
kDa
37
25
20
AVR
(bait)
37
25
20
Pik-HMA
(prey)
Total
protein